University of Warwick

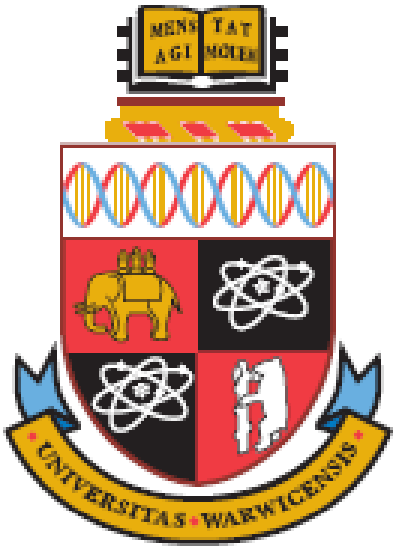

Energy Saving Through Voltage Optimisation & Non-intrusive Load Monitoring in Domestic House

by

Hao Liu

Thesis

Submitted to the University of Warwick

for the degree of

Doctor of Philosophy

School of Engineering

May 2015

Table of Contents

List of Figures

List of Tables

List of Symbols and Abbreviations

THD	Total Harmonic Distortion
MOSFET	Metal–Oxide–Semiconductor Field-Effect Transistor
IGBT	Insulated-Gate Bipolar Transistor
LQR	Linear Quadratic Regulator
DAQ	Data Acquisition
PA	Power Analyser
$A \oplus B$	Addition of load signature A and B
$A \Theta B$	Subtraction of signature A and B
HFR	Harmonic to fundamental ratio
FAD	Fundamental angle difference

Acknowledgements

First and foremost, I would like to thank my supervisor, Professor Jihong Wang, for her valuable advices and constant support during the whole period of my study. Her dedicated and thorough supervision have massively improved my research work and the quality of this thesis. I will cherish the guidance she gave on not only academic research, but also science work in general.

Secondly, I would also like to give thanks to my colleague Dr Oleh Kiselychnyk for his help on my experimental work and advices on control theory, and Dr Stephen Mangan for his kind help on electronics circuit design and programming. I learned quite a lot during the time spent with them and their precious suggestions definitely improved this research work in various aspects.

Thirdly, I would like to thank my lab colleagues, Marker Dooner, Shen Guo, Chirstopher Krupke, Kamyar Mehran, Ashwin Rajan, Yue Wang, Xing Luo and Jacek Wojcik, for their companionship and coffee time stories. I wouldn't enjoy my time as much without being a member of this team.

Finally, I would also like to give my thanks to my family for the financial support and encouragement in every step of my work, and for putting up with my ever changing moods throughout these years.

Declaration

This thesis is submitted in partial fulfilment for the degree of Doctor of Philosophy under the regulations set out by the Graduate School at the University of Warwick. This thesis is solely composed of research completed by Hao Liu, except where stated, under the supervision of Professor Jihong Wang between the dates of February 2011 and May 2015. No part of this work has been previously submitted to any other institution for a higher degree.

Hao Liu

May 2015

Publication

Part of this work has been published as:

Liu, H. & Wang, J., 2012. Analysis and control of a single phase AC chopper in series connection with an auto-transformer. *Automation and Computing (ICAC), 2012 18th*, (September), pp.2–7.

Abstract

Energy consumption worldwide in domestic domain accounts for almost one third of the total energy consumption so it is important to reduce energy usage in this sector for energy sustainability. The project aims to investigate two domestic energy saving methodologies in domestic sector, namely voltage optimisation and non-intrusive load monitoring. The first method is to address the issues of unnecessarily extra usage of electrical energy caused by excessively high mains voltage. It is achieved via a voltage optimiser to maintain the voltage at a desired constant level. The second method is to make electrical energy usage information more transparent to consumers and identify the potential energy waste caused by misusing energy of devices. This is to be achieved via the methodology of load disaggregation.

The mains voltage delivered to individual houses varies constantly depending on the location of the house, the load condition and other factors. The method of installing voltage optimiser in domestic houses to optimise the voltage and reduce energy consumption started from last decade. Most of the existing voltage optimisers do not have very precise voltage control and there is very limit report on the theoretical analysis of them. Therefore, a power electronic based voltage stabiliser for voltage optimisation in domestic house is proposed in this project and an intensive study of proposed voltage stabiliser is carried out in terms of the topology, mathematical modelling and control strategy design. The simulation and experiment results are also presented to verify the proposed voltage stabiliser in this thesis.

The current method adopted for analysing energy saving is via comparing the electricity bill of a house before and after the installation of a voltage optimiser. But it is impossible to ensure that the user behaviour and energy usage pattern are exact same in these two cases.

The lack of quantitative analysis on energy saving has become a major obstacle to convince people and promote the voltage optimisation in domestic house. This project investigated a method for estimating the energy saving of installing a voltage optimiser in real time. An energy saving algorithm is presented and implemented. A test rig hosting different types of electric loads is established to verify the robustness of this algorithm. The experiment results demonstrate that the presented algorithm can estimate the energy saving achieved by a voltage optimiser in real time with very high accuracy.

Non-intrusive load monitoring is to disaggregate the total electricity consumption into individual appliances based on the voltage and current measurement at premise level. Most of the existing approaches require massive training and pre-known dataset to obtain the disaggregated energy breakdown of a house and there is no well accepted approach to monitor the home appliances operation in real time. The project is to explore a new method by which the operations of individual appliances can be monitored in real-time simultaneously. A new load signature is proposed to describe the features of appliances and an event based algorithm is developed in this project. The algorithm is then implemented onto a test rig with 6 different appliances and 11 working modes. The evaluation results demonstrate that the proposed algorithm is able to monitor the operations of individual appliances and feedback the information in real time.

Chapter 1 Introduction

This chapter introduces the background of the research project and the research challenges presented. It explains the motivations of conducting the research clearly. Then, the structure of this thesis is given, which is a brief overview to the thesis and the project work.

1.1 Background

Although the energy demand of the UK has been declining since 2008, the demand of the world has been rising up dramatically since last century due to increased world population and economic development, which brought great impact on energy reserve and environment globally. In order to maintain a sustainable energy supply and prevent irretrievable climate change, many countries have set up different goals on reduction of greenhouse-gas emissions. As for the UK, it requires a 34% cut in 1990 greenhouse gas emissions by 2020 and at least an 80% cut in emission by 2050 (Climate Change Act 2008). To meet these relative goals, varieties of research projects have been introduced to reduce energy demand and improve energy efficiency within the UK, which includes projects relevant to renewable energy, energy demand reduction and automotive industries.

The total energy consumption of the UK in 2012, including transportation, industry, domestic housing, commercial and public administration, reaches 1724 TWh, in which the energy used in homes accounts for more than a quarter (29.11%) (Department of Energy & Climate Change 2013). Intriguingly, domestic housing consumes more energy than either road transport or industry. It indicates that a significant portion of total energy usage is composed of domestic electricity consumption in the UK. In order to reduce the energy consumption and maintain a sustainable energy supply in long run, many energy saving technologies and

efficiency improvements have been or are being discussed and investigated in different sectors.

In terms of the road transportation sector, most of the methods to enhance the energy efficiency and reduce the energy demand are all based on the designing aspects of vehicles. The improvement of aerodynamics can minimise the drag and make most of the traction to increase fuel economy. Introducing new material, such as aluminium and carbon fibre, can reduce the weight of the vehicle without losing the stiffness and hence increase both the performance and fuel efficiency. Advanced LED lighting system requires less electricity but provide better illumination compared with conventional lights. High performance tyres can decrease the friction between tyres and road as well as rolling resistance itself. Applying regenerative breaking is able to recapture the energy which would lose on normal cars. Compared with the efficiency improvement mentioned, the rise of electrical vehicles and hybrid vehicles realise a significant progress on energy saving since electrical motors have much high efficiency over combustion engines. Using electrical motors, especially on start-up and low speed running, can effectively avoid engine working at low efficiency conditions. Apart from technical improvements, driving with energy conservative manners helps saving energy as well.

Industrial sector also consumes massive amount of energy to conduct different types of manufacturing and processing works. It requires large amount of heat, mechanical power and electricity to accomplish various tasks. So there is also a great diversity of energy efficiency improvement opportunity in this sector. Electrical motors are undoubtedly the most widely used load in industry and accounts most of the electricity consumption. With the development of power electronic-based motor drives, the operation speed of motors can be easily controlled by installing variable speed drive to match the different loads. It increases the not

only flexibility of operation but also the efficiency of motors. Also, the motor coil with superconducting material can decrease the copper losses dramatically. What's more, the operation of motors can be also improved by voltage optimisation, better process control and maintenance work.

The efficiency improvement of power generation and transmission is also very important. Although the generating electricity from thermal energy has been put into practices hundreds year ago, different technologies can be still applied to increase the efficiency and make most of the fuel. For example, supercritical coal fired power plant, as the leading option, can reach cycle efficiency up to 46%, which is around 10% higher than the current power plant. Combined heat and power (CHP) plant cogenerate usable heat and electricity in one single process while the conventional power plant simply wastes the heat when generating electricity. The heat is captured as a by-product and then used for processing steam, heating or other industry applications in CHP plant. The cogeneration of both heat and electricity makes most of fuels and achieves over 80% efficiency. The electricity is transported through power grids after it is generated. The loss on transmission system also accounts for a large amount of energy waste and the global average loss is 12%. The most straightforward technology to reduce the transmission loss is to apply high voltage AC transmission lines, which would require massive investment and advanced control strategy. With increasingly more wind and solar power generation installed into the power grid, high voltage DC transmission becomes a possible solution for consideration since it requires less cost over long distance (100 km) compared with AC transmission. The transmission loss can be also reduced to 3-4% per 1000 km, which is also lower than AC transmission at same distance.

There are also various approaches aiming at saving energy in domestic house as well. Replacing old appliances with high efficiency appliances, for instance, LED lighting,

refrigerators and air-conditioners with variable speed drive, leads to massive saving on particular appliances. Some research also proposes DC distribution system to serve the DC powered appliances and renewable energy in residential house since it has centralized AC/DC conversion in the mains rather than separate conversion made by different appliances. Installing voltage stabiliser for voltage optimisation is also a practical way to reduce excessive voltage. The voltage stabiliser can help appliances operate under a good condition, reach better efficiency and hence make energy saving. In addition, a domestic load monitoring system can be installed to provide the operating states of individual appliances. Therefore people can benefit from the system to change user behaviour and operate appliances in an energy conservative way.

Energy saving technologies in domestic sector are very essential and worthy being investigated as it accounts for around one third of the whole energy consumption. Using advanced tyres with correct tyre pressure can saving around 3% fuel, replacing AC transmission with high voltage DC reduced the loss around 8% (from global average 12% to 4%), using supercritical coal fired power plant increases the around 10% efficiency. Installing a voltage stabilizer in domestic house is claimed to make 7% to 10% energy saving. Given energy disaggregation feedback to consumers can help people using energy conservatively and make saving from 3.8%-12.0% reported in (Ehrhardt-martinez & Donnelly 2010). Considering various approaches in domestic sector, the energy saving could be estimated over 20% as stated in (World Energy Council 2013). In summary, the energy saving technologies in domestic sector is very promising to achieve large saving and make contribution to greenhouse gas emission reduction due to the following features:

- Large proportion. This sector accounts for one third of total energy and ranks first as single sector.

- Massive potential. The amount of energy saving could be potential made in this sector is estimated over 20%.

Therefore, an overview of various energy saving technologies in domestic houses is presented in the following section.

1.2 Energy Saving Technologies in Domestic Houses

1.2.1 High Efficiency Appliances

Apart from installing renewable energy generation, replacing the low efficiency appliances with the high efficiency equivalent ones can also make energy savings as well. One typical example is the lighting system in a house. Incandescent light bulb, as the traditional lighting, is used in many houses and rated as 40W to 120W. Both light and heat are generated when it lit up, which means some energy is wasted and dissipated as heat. Alternatively, compact fluorescent lamps can be applied in houses for lighting and it is rated less than an incandescent light bulb (9W-30W). A 9W CFL has the roughly same lumen equivalent as a 40W incandescent light bulb, which makes it very competitive for energy saving purposes. LED lighting is also other candidate for lighting up a house. It not only provides massive lumens with less power rating but also has extremely long lift time. Three lighting products from GE are compared in Table 1-1 to evaluate the energy saving made by replacing traditional incandescent light bulb.

Table 1-1 Comparison of incandescent light bulb, CFL and LED

Parameters	GE 19946 Incandescent	GE 88696 CFL	GE 98725 LED
Power Rating (W)	40	9	6
Nominal Lumens (lm)	410	470	410
Rated life time (hour)	1000	10000	45000
Rated efficacy (lm/W)	10.25	52.22	68.33
Price (£)	1.54	4.50	15.92

As shown in Table 1-1, three light bulbs have roughly same lumens while traditional incandescent light consumes at least three times of energy compared with CFL and LED. What's more, the life time of incandescent light bulb is the worst among three options. CFL can run 10 times longer than it and LED can do 45 times longer. Although the CFL and LED have higher prices, it is no doubt that large savings can be done by replacing incandescent light bulb. Moreover, intelligent control system of lighting can be also introduced into household as discussed in (Byun et al. 2013). This control system takes advantage of multiple sensors and wireless communication to detect the movement and activities of people and then control the on-off and the light intensity of the lighting system. Therefore less energy would be wasted when there is no people present within the houses.

Apart from lighting system, the motor-based and compressor-based home appliances, for instance, refrigerator, washer and air-conditioner, also has some potential for energy saving due to the development of high efficiency motor drive. (Yabe et al. 2005) explains a high efficient motor drive for refrigerator manufactured by Mitsubishi. It mentions that this technology is able to increase the driving efficiency around 6% and achieve low noise at 17dB. It has been applied on refrigerator, air conditioner produced by Mitsubishi since 2003 and can be extended to fan motor and pump motor for energy saving purposes as well.

Apparently, the approach would benefit the houses with lots of old and traditional appliances. As long as the old appliance are replaced gradually, there is less saving can be made through this method.

1.2.2 Residential DC Distribution System

Due to the increase of DC powered home appliances and the integration renewable energy generation, establishing small scale DC micro-gird in domestic house is a very promising

approach to increase the energy efficiency and make energy savings (Figure 1.1). DC power can be directly used by consumer electronics (PC, laptop, Laptop, LED light) and motor based appliances with motor drive (refrigerator, washer, air conditioner), therefore less conversion is required and hence less losses is involved during conversion. Instead of having rectifiers on each appliance individually, a large rectifier with high efficiency can be installed in DC distribution system. It is also more friendly and compatible with renewable generation and potential energy storage system since they are directly connected with DC voltage. Additionally, DC distribution system has considerable reduction on cable losses due to the absence of reactive power compared with AC system. Some study in residential DC distribution system are conducted in (Engelen et al. 2006)(Oliveria et al. 2014) and a typical DC distribution system in domestic house is illustrated as follows:

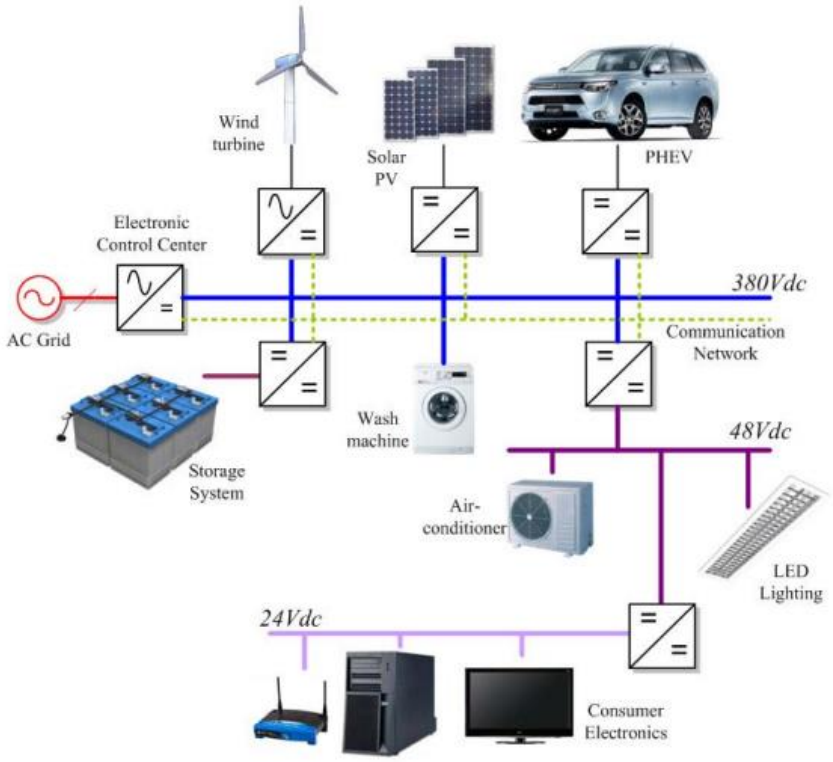

Figure 1.1 Diagram of a residential DC distribution system presented in (Oliveria et al. 2014)

It is reported in (Garbesi et al. 2011) that switching to DC distribution system can save the total house electricity consumption around 7%-13% compared to house with no DC system. More saving can be potentially made if more DC-related resource involved into houses, such as electrical vehicle and energy storage system.

Although it can bring in significant benefits, DC distribution system still has its drawbacks when applying in domestic houses. The standardisation of DC system is still under investigation. The protection against overloads and short-circuit and grounding also need to be looked into and designed carefully to ensure a safe operation. The cost and investment of installing a DC system into a house is massive since it involves new converters, cables and sockets. Once a DC distribution system is put into practice into a house, the plugs for DC based appliances also have to be changed, which would increase the investment again. Taking the above barriers into consideration, DC distribution system is still far away from widely adoption.

1.2.3 Voltage Optimisation

In order to push forward the harmonisation of voltage level within European Countries, harmonisation Document 472 (HD 472) was implemented in the UK on 1 January 1995, when the nominal voltage in the UK was changed to 230V ranging within +10% to -6% from the previous nominal voltage of 240% ±6% (Cook 2002). Theoretically, the mains voltage out from a wall socket may ranges from 216.2V and 253V depending on local condition, loads connected and other reasons. In practical, the mains voltage in a promise is very likely to be much over the nominal voltage 230V. Figure 1.2 illustrates the mains voltage in a typical house and office on 25/06/2013.

It can be noticed that the real voltage is higher than the nominal voltage 230 V in these cases. Meanwhile, some places in different countries, mostly developing countries, also suffer from under-voltage problem. Therefore, optimising the voltage in domestic house is necessary and it is beneficial for the following reasons. Firstly, overrated voltage may result in various issues such as lighting dimming, loss of heat control and loss of motor control (Felce et al. 2004). Secondly, it not only decreases the efficiency of the equipment but also lead to unwanted extra electrical energy consumption. Finally, the excessive high or low voltage level of power supply may cause failure in operation and even harm the devices, such as personal computer (Djokić et al. 2005). As a result, voltage optimisation starts to be investigated and applied in decades ago (Preiss & Warnock 1978). It was well-established for commercial sector in the very beginning and is now increasing being promoted in domestic market (Hunt 2013).

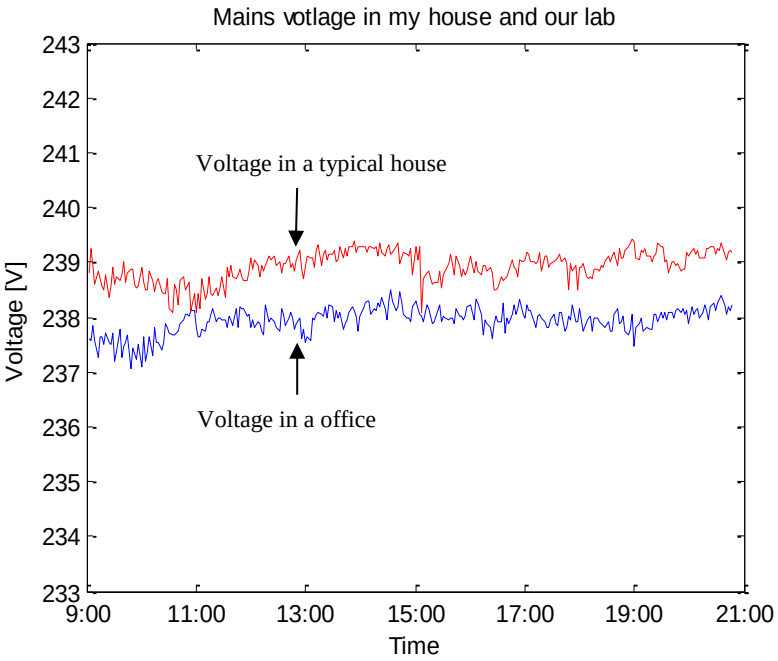

Figure 1.2 Mains voltage in a typical house and office on 25/06/2013

The adoption of voltage optimisation in residential house is to install a voltage optimisation equipment/unit in series with the main power supply in the house. The voltage supplied on

the home appliances is then affected by the unit and optimised. Since different types of load may behave differently with voltage optimisation, it is estimated that most domestic house should save 8-13 percent electricity depending on the user profile. Considering the average electricity consumption of a house in the UK is 4648 KWh and the average electricity price is 0.14 £/ kWh, the amount of saving of one year is around £65. The price of such equipment/unit for domestic house normally ranges from £200-£500 hence the return of investment is roughly three to five years. Moreover, the potential benefit, such as extended lifetime of appliances, makes it more competitive to be introduced in residential houses.

1.2.4 Energy Feedback Information Enhanced Energy Management

There is a strong relationship between the electricity consumption of a house and the behaviour of the occupiers. Generally, using electricity conservatively, for instances turning off unused appliances and avoid energy peaks, makes a lot of contribution on reduction of electricity consumption. One of the practical and effective ways is to provide energy feedback information to the consumers in order to increase the energy awareness, encourage people managing their electricity conservatively. Depending on the types of energy feedback, the average household electricity savings can vary from 3.8%-12.0% reported in (Ehrhardt-martinez & Donnelly 2010) as shown in Figure 1.3. The most saving can be achieved by real-time information down to appliances level while the least saving is made when only web based energy audits provided.

In order to provide energy feedback in appliance level, a load monitoring system is required to be installed in the house. It points out the working modes of appliances and that information can be utilized to offer specific suggestions to operate the appliances. The monitoring system can detect if any appliances work in poor energy efficiency and give advices to switch them into a more energy efficiency mode.

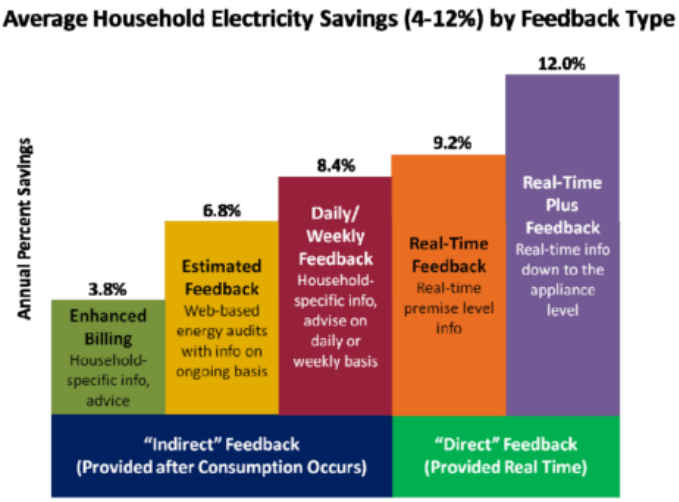

Figure 1.3 Electricity saving by applying feedback of electricity usage

Normally the appliances with economy or stand-by mode will benefit from the energy disaggregation feedback in this way. The load monitoring system helps people understand the energy usage of different appliances and increase them the awareness of using energy conservatively. For example, the usage of some unnecessary appliances can be deferred until low electricity price applied in off peak time. The load monitoring system also detects the appliances which consume abnormal electricity due to fault or ageing (Laughman et al. 2003) and occupants could either repair or replace the faulty or aged appliances and avoid from wasting energy on them.

The most straightforward method is to perform intrusive load monitoring and its basic idea is to install a meter for each appliance and transmit the information of individual appliance energy consumption to a central server. In (Ito et al. 2004; Kato et al. 2009), different measurement systems are introduced into wiring system to acquire the voltage, current and power values of individual appliance, identify the appliance and finally feedback the operation state of it into a central hub through different communication approaches. However, deploying one meter for each appliance is extremely time-consuming and costly. The whole

wiring system in the premise will become much more complex with all those meters included. It not only reduces the reliability of the wiring system but also causes inconvenience to the occupants in the premise. Additionally, more meters would be required when new appliances are purchased and connected into the house. Above all, the intrusive monitoring system is not realistic to be generalized in household unless the cost of meter drops down to an acceptable level(Carmel et al. 2013).

Alternatively, non-intrusive load monitoring system can be adopted to provide the disaggregated energy feedback. It is first introduced in (Hart 1992) and defined as determining the energy consumption of individual appliances turning on and off in an electric load, based on detailed analysis of current and voltage of the total load, as measured in premise-level. This system requires sensors and data acquisition system installed at main breaker level to gather the electrical information of all appliances within the premise as a whole. Then, the data is transferred, processed and analysed by the algorithm. Finally, the disaggregated energy information is feedback to the costumers. Considering the easy installation feature, applying non-intrusive load monitoring system into residential house is very promising to help people understanding the electricity consumption of the house and change their behaviour of using electricity in a conservative way.

1.3 Research Objectives

With all the above introduced potential energy saving technologies for domestic consumers, the project focuses on voltage optimisation and non-intrusive load monitoring approach.

1.3.1 Challenges Presented in Voltage Optimisation

The voltage optimisation unit can be realised in two techniques: multi tap transformer and power electronic-based AC converter. The voltage adjustment of multi-tap transformer is not

continuous and has to be step changes, which means the optimised voltage is not guaranteed to be reached with the voltage variation from gird, such as the product from EMS UK (https://vo4.co.uk/single-phase/). Power electronic based AC voltage regulator can achieve the smooth voltage regulation, for example, VPhase (http://www.bdelectrical.co.uk/new-page). Due to the advances of high speed power electronic switching devices, various topologies of power converters are proposed/developed to achieve controlled AC/AC conversion (Jie et al. 2008; Kwon et al. 1996; Kim et al. 1998) and they can be used as voltage stabiliser for voltage optimisation in house hold as well. Unlike full range AC/AC converters, the voltage stabiliser in domestic house is only required to stabilise input voltage within a certain range. Taking the advantage of the smaller range of regulation, the auto-transformer based switching AC voltage regulator was placed onto market, which has relatively low cost compared with the full voltage range AC-AC converters.

Although a number of voltage regulators/stabilisers are popular in the market, very few reports are found on the theoretical analysis and modelling of the voltage stabiliser. So it is unclear whether the current products are in their best design and whether the dynamic responses can be improved. In practice, it is often found that the voltage took a few minutes to stabilise at the desired value. There is much scope for further investigation in the area.

Although installing voltage optimiser/stabiliser is deemed to make energy saving in residential houses, there is no widely-accepted approach to quantify and verify the exact amount of energy saving through installing a voltage stabiliser. Some cases are studied by comparing the electricity bills of several houses before and after installation of a voltage optimiser to estimate the savings. However, it is impossible to guarantee that the energy usage pattern and the user behaviour are exactly same before and after the installation. The customers frequently challenge the voltage optimiser providers with doubts on energy saving

and this has become a major obstacle to promote the energy saving technology. Therefore, it is a foremost important task to develop an effective and convincing method in estimation of the energy saving.

1.3.2 Challenges presented in Non-Intrusive Loading Monitoring

It is relatively easy to obtain the aggregated power consumption figures but it is extremely challenge to gain the disaggregated load information. However, the disaggregated information is the foundation for understanding user behaviours and loopholes of energy waste. A specific and unique signature for appliance needs to be properly selected for load disaggregation. Researchers in (Norford & Leeb 1996; Farinaccio & Zmeureany 1999; Marceau & Zmeureanu 2000; Bijker et al. 2009) use change of active power and reactive power as signatures to distinguish appliances. It works for appliances with large power consumption but doesn't have good performance for appliance having similar power pattern. Researchers in (Liang et al. 2010; Cole & Albicki 2000; Ruzzelli et al. 2010; Li et al. 2012) try to analyse the current and voltage waveform to obtain unique features. It requires high sampling frequency but demonstrate better performance than the methods using power values as single signature.

Moreover, real time implementation of non-intrusive load monitoring system is another technical challenge in this research area. Many approaches take advantage of pubic dataset reported in (Kolter & Johnson 2011; Anderson et al. 2012; Makonin et al. 2013) to build appliance models, train the system and then conduct load disaggregation. Those approaches require massive pre-known data or information of appliances and are still not able to disaggregate the total energy usage in real time. Even after training, the algorithms normally utilise the power consumption of a relatively long time, for instance one day, to figure out the breakdown of energy usage in this long time period, which means the energy auditing can be

obtained after a while but the approaches of providing instant load monitoring information still need to be investigated.

1.3.3 Research Objectives

The project focuses on voltage optimisation and load monitoring approach with the following objectives:

- *The project is to conduct intensive modelling study and theoretic study of a step up/down AC/AC voltage stabiliser used in domestic houses, and investigates control strategy to achieve improved performance in terms of response speed and robustness.*
- *The project is to investigate the solutions for real time estimation of energy saving with various operation modes and load conditions.*
- *This project is to explore new methods by which the total power consumption of a house can be disaggregated into individual appliances and monitor the operation of individual appliances in real time to provide energy feedback instantly and achieve more potential saving.*

1.4 Research Contributions

The contributions of this research work towards to these objectives are summarised as follows:

1. A topology of step up/down AC/AC voltage stabiliser is developed to extend the current voltage stabiliser's functions. This topology takes advantage of multi-winding transformer and conventional AC/AC converter to implement both step-up and step-down functionality. The nonlinear mathematical model of this topology is established firstly, and then it is transformed to rotating d-q reference frame and linearize the

model. What's more, a LQR controller is designed for the linearized model to maintain the voltage level under disturbance from input voltage and load current. The simulation and experiment results demonstrate the performances of the controller in terms of response speed and robustness.

2. In order to demonstrate the energy saving achieved by voltage optimiser, an energy saving estimation algorithm is presented to estimate the power saving made in real time which was originally proposed by (Jihong Wang, Pub.No.: Wo/2014/027198). The algorithm is implemented in both LabVIEW and microprocessor to work with voltage optimiser in parallel and display the estimated power saving instantaneously. A verification system is designed to demonstrate the accuracy of the algorithm, the results shows that the errors of the algorithm for all types of load within the tests are below 1%.
3. As for research on non-intrusive load monitoring system, a brand new signature of appliance load is defined and investigated. The mathematical operations of the signature are introduced and a novel real time disaggregation algorithm is developed based those operations. The algorithm is implemented in both hardware and software and evaluated in an established test environment including 6 appliances with 12 working states in total. The results shows that the overall accuracy of identifying appliances is over 94.1%

1.5 Thesis Structure

The remaining chapters of this thesis are structured as follows:

Chapter 2 gives a description of introduction and literature review of voltage optimisation and non-intrusive load monitoring. To start with, it provides the detailed review of voltage optimisation including fixed ratio transformer and power electronic based AC converters.

Then, the different approaches on establishing mathematical model and control methods are discussed. Meanwhile, a background study of non-intrusive load monitoring, including the adopted load signatures and disaggregation algorithm, is provided in this chapter.

Chapter 3 proposes a topology of step up/down voltage stabiliser. It starts with the introduction of the circuit description and working principle and then the mathematical modelling of it is derived. The mathematical model is then validated with the circuit model through simulation. Despite of the nonlinear involved in the model, a PI controller is designed for the proposed voltage stabiliser. The performance of the control is investigated through simulation.

Chapter 4 presents a d-q transformation with fictive axis for the mathematical model in order to linearize the model and design control strategy analytically. Based on the transformed model, this chapter introduces the LQR controller adopted to maintain the voltage against disturbances form input and load. The simulation results are finally provided to demonstrate the performance of the proposed control strategy.

Chapter 5 introduces the power saving algorithm for estimating the savings achieved by installing a voltage optimiser. First, this algorithm is described and proven theoretically and then implemented in LabVIEW along with the data acquisition hardware. Second, a verification system, including precise power analyser and load bank, used to evaluate the algorithm is described into detail. Lastly, the experiments results with different types of load

Chapter 6 presents the proposed signature for load disaggregation. It gives a brief introduction on load features and then explains the definition as well as the derivation of the proposed signature. Next, the mathematical operations of signature are defined and explained. Based on the proposed signatures, a load classification mechanism is explained at last.

Chapter 7 describes a novel approach of non-intrusive load monitoring using the proposed signature in Chapter 6. Firstly, the algorithm is divided into three parts and each part is fully explained. Secondly, the hardware for data acquisition is introduced and the software implementation in LabVIEW is also presented. Thirdly, the algorithm is evaluated within lab environment including multiple appliances and the evaluation results are provided and discussed to demonstrate the performance of the proposed approach.

Chapter 8 summarizes the research work presented in this thesis and makes conclusions of all the chapters. The limitations of both voltage optimisation and load monitoring work in this project are discussed. Suggestions for potential future extension of this research work is provided, emphasising on the control strategy of proposed step up/down voltage stabiliser and different algorithm of non-intrusive load monitoring with proposed signature.

Chapter 2 Literature Review

This chapter introduces the background and review on both voltage optimisation and non-intrusive load monitoring research area. To start with, the transformer-based voltage optimiser is discussed. Next, the previous work on power electronics based AC voltage converter is then investigated in terms of topology, modelling and control design. Furthermore, the existing approaches in non-intrusive load monitoring are reviewed. The load signatures and disaggregation algorithms used in different methods are discussed and investigated.

2.1 Literature Review on Voltage Optimisation

2.1.1 Transformer Based Voltage Optimiser

Transformer based voltage optimiser is the most straightforward and simplest way to realise voltage optimisation. The basic principle is to introduce a transformer in series connection with the mains power supply. The mains voltage is fully applied on the primary winding while the secondary winding is in series connection with the home appliances. The basic circuit diagram of transformer based voltage optimiser is shown as follows:

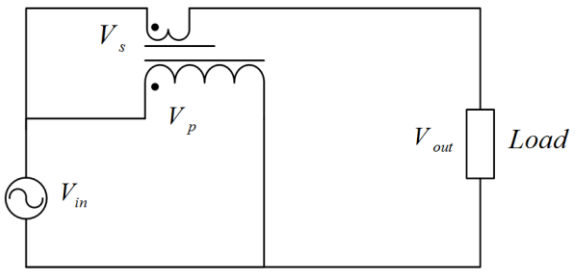

Figure 2.1 Basic circuit diagram of transformer based voltage optimiser

The voltage applied on the load is the deduction of secondary winding voltage from input voltage since secondary winding is in series with the load. Note that the secondary winding voltage is literally a fraction of input voltage and it depend on the ratio of the transformer. Overall, it results in that the output voltage is slightly lower than the input voltage. The voltage reduction then contributes to an amount of energy saving on the load connected in the circuits.

The advantages of this circuit are simple configuration and low cost. Obviously, few components are required in the circuit and the costs of them are quite low. But the functionality of this circuit are very limited. The conversion ratio is fixed and it would be problematic for different locations with different incoming voltages from the grid. For example, if the circuit is designed for reducing input voltage 230V down to optimised level, the house with 240V input voltage is not able to reach optimised level after installing this particular. It also cannot compensate the voltage variation resulted from input voltage and load conditions. Therefore, it is not guaranteed that the optimised level can be achieved constantly.

The product 'Volties Home' (http://www.marshalltufflexenergy.com/voltis/voltis-home/) from Marshall Tufflex is designed based on this configuration. To make sure the proper voltage reduction is applied, the product has two versions, namely HD version and LD version. The HD version is suitable for voltage between 230V and 253V while the LD version is suitable for voltage between 225V and 243V. Furthermore, the input current is also measured and compared with a threshold value 0.5A. A relay is then controlled based on comparison to decide if the transformer is engaged. If the current is lower than 0.5A, the transformer wastes more energy than it can save so it is not engaged and the unit is in bypass

mode. Despite of this, the output voltage is still not regulated and the maximum saving is not achieved in all circumstances.

Likewise, the product 'VO4HOME' from EMS (https://vo4.co.uk/single-phase/) is also a transformer-based voltage optimiser but it has multiple taps to change voltage reduction. The basic circuit diagram is shown as follows:

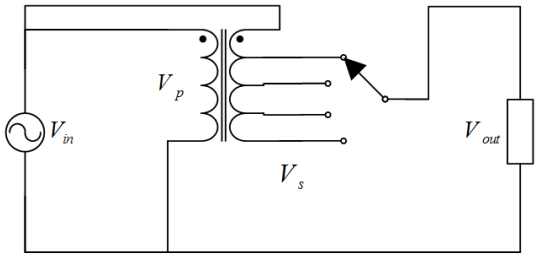

Figure 2.2 Circuit diagram of transformer based voltage optimiser with multiple taps

It is required to check the input voltage of a primes before installation and then determine which tap should be connected. The taps are marked with voltage reduction it can made, for instance, '5V', '10V' and '15V'. Once it is selected, the tap cannot be changed during operation. It has to be changed when the power is switched off. Although it provides different taps to optimise the output voltage, the adjustment of voltage level is step change rather than continuous change. Meanwhile, there is also no control mechanism during the operation, which mean the output voltage is not regulated.

2.1.2 Power Electronic Based Voltage Optimiser

Another type of voltage optimiser is based on power electronic technology. More specifically, the conversion between input and output is by means of controlled power switches, for instance, MOSFET and IGBT, and it covers DC/DC conversion, AC/AC conversion, DC/AC conversion and AC/DC conversion. Since it is supposed to be installed in domestic house, the

voltage optimiser is often inspired by single phase AC/AC converter technology, which is also known as single phase voltage regulator or line conditioner. The basic objective of a single phase AC/AC converter is to convert and control AC power based on the requirements and hence it is very suitable to apply for voltage optimisation purpose.

The investigation of single phase AC/AC converter consists of three aspects, namely topology, mathematical modelling and control strategy. The topology refers to how the power switches, passive components and other items are connected together to form the circuit. It not only determines the working principle and efficiency of a single phase AC/AC converter but also directly links with the manufacturing cost of it. A good topology aims to achieve the design requirement within a simple and efficient configuration for the particular applications.

The mathematical modelling is to present the behaviours and characteristics mathematically. It can be used to verify the feasibility of a new topology and to design a control strategy for controlling the AC/AC converter meeting the control requirements. What's more, it also help people analysing the characteristics of an AC/AC converter and selecting the suitable component value based on theoretical calculations. A control algorithm needs to be designed for an AC/AC converter to meet the requirements and specifications. Generally, an AC/AC converter is required to have good behaviour under different circumstances and disturbances, for instance, different types of loads and/or varying input voltage. Therefore, it is essential that a good controller works alongside with the converter to make sure it is well controlled all the time.

2.1.2.1 Topology

(Khoei, A; Yuvarajan 1988) and (Enjeti & Choi 1993) introduce the basic topology of single phase AC/AC converter at later 80s and early 90s. At that time, they were still using

MOSFET as the power switches for conducting current. In (Khoei, A; Yuvarajan 1988), a very basic AC/AC converter with two bidirectional switches is proposed. However, there is no passive filter designed in the circuit and the switching frequency discussed in paper is as low as 90 Hz. Therefore, some certain harmonic frequencies in such circuit is extremely high, stated by the author. In order to solve this problem, the work in (Enjeti & Choi 1993), as an extension of (Khoei, A; Yuvarajan 1988), proposes a buck type single phase AC chopper topology, which is shown as Figure 2.3

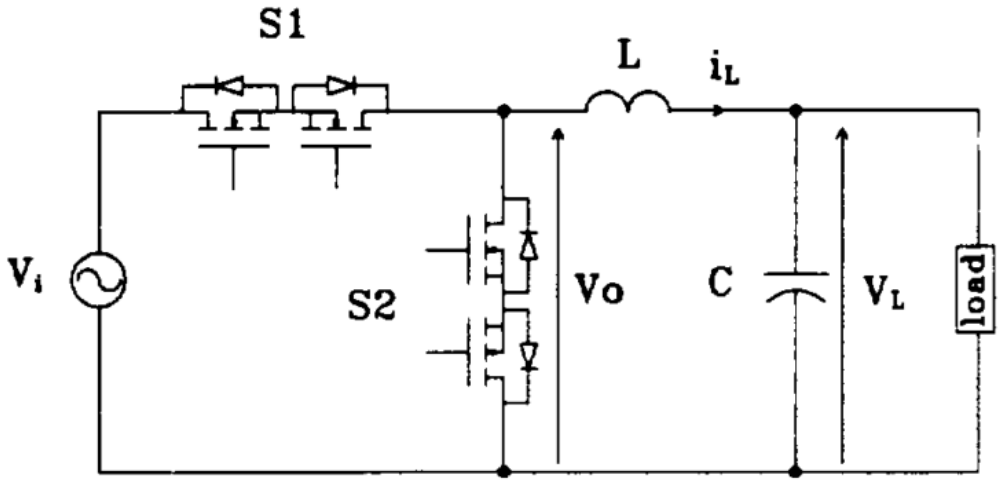

Figure 2.3 Basic buck type single phase AC chopper (Enjeti & Choi 1993)

Since an LC passive filter is built into the circuit, the high frequency harmonics are largely reduced. The working principle of four working states and switching technique is introduced and explained in this paper. Some experiments are conducted to validate the operation of the circuits in this paper.

Kwon proposes some topologies of AC chopper in (Kwon et al. 1996) based on Figure 2.3. Not only buck type AC chopper is introduced, but also the boost type of AC chopper is described in his work. The structure is still quite similar with previous work in (Enjeti & Choi 1993), which using only passive components and bi-directional switches (IGBT rather than MOSFET) to compose the AC choppers. Some analysis of buck type AC chopper including

output voltage range, total harmonic distortion (THD) and power factor is provided in this work as well. The experiment work of proposed single phase buck AC chopper is presented to demonstrate the feasibility of this topology.

Different from previous work, (Jang & Choe 1998) introduces a transformer with thyristors-controlled tap changer into the basic AC chopper circuit. The proposed circuit diagram is shown as Figure 2.4. This topology has isolation from the input due to tap changer transformer and it is able to work both in step-up and step-down mode to regulate voltage based on the requirements. However, the drawbacks are as follows: no passive filter to cancel out the harmonics and high manufacturing cost due to more components involved. What's more, the thyristors in the transformer not only increase the complexity of the operation but also have poor transient behaviour, which would slow down the response time of the whole system.

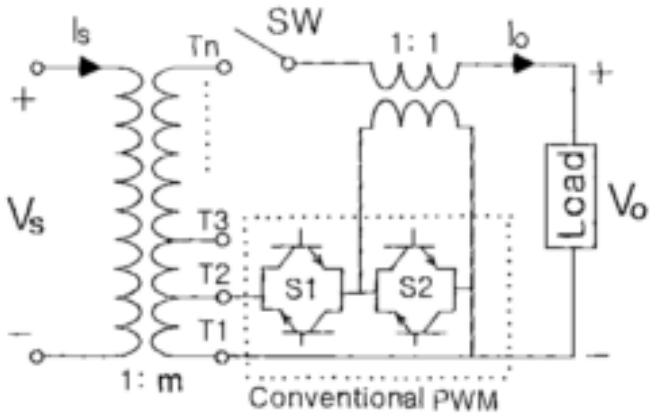

Figure 2.4 Proposed topology AC voltage regulator in (Jang & Choe 1998)

In order to get rid of the thyristors and regulate the voltage sag, (Hietpas & Naden 2000) simplifies the topology in (Jang & Choe 1998) and replaces the tap change transformer with a normal transformer. The proposed model block diagram is shown as Figure 2.5:

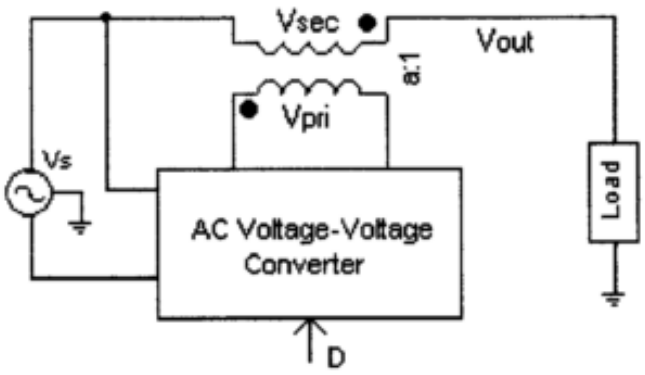

Figure 2.5 Model block diagram of the AC/AC converter system in (Hietpas & Naden 2000)

The primary winding of a transformer is directly connected with a basic AC chopper and secondary winding is then connected with the load. The voltage drops on secondary winding will build up the load voltage to compensate voltage sag.. Although the proposed topology looks promising, this work is verified by simulation only and no hardware implementation work is presented to demonstrate the feasibility of the proposed topologies.

The work in (Kwon et al. 2002) provide another approach to implement an AC/AC converter, which is shown in Figure 2.6. Instead of chopping the input voltage waveform, the topology described in this work has two completely different stages.

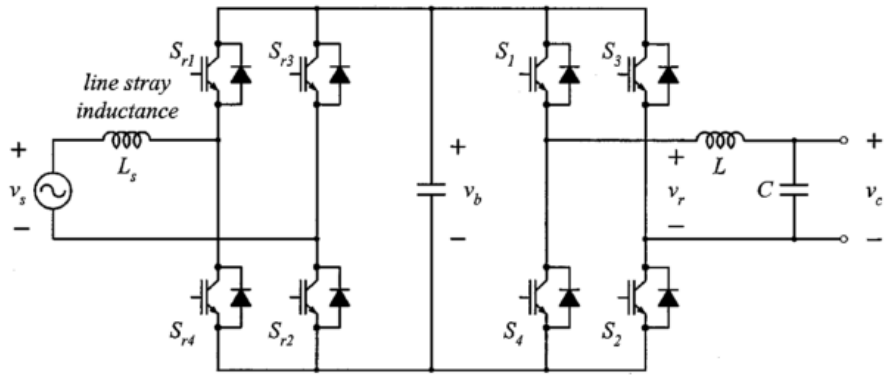

Figure 2.6 Power circuit of proposed AC chopper in (Kwon et al. 2002)

The first stage is to use 4 power switches converting single phase AC to DC and then use another 4 power switches converting DC back to AC again with voltage level regulation. A leakage transformer can be also added at the load side to provide isolation and regulation. This AC chopper has been analysed and implemented with a controller in this paper. It concludes that the presented topology gives good both dynamic and steady-state behaviour.

As an extension of Kwon's work, Soeiro discusses a topology which combines transformer and the two stages AC/AC converter together in (Soeiro et al. 2012). This paper proposes several high efficiency topologies by changing the position of the AC/AC converter and/or rearranging the passive filter and transformer. The advantage of those topologies is that they only process the part of the power so gives better performance on efficiencies. The analysis of different topologies and modelling work is also described in this wok. A small signal model is established and the associated control strategy is designed to track the voltage reference. One topology along with control strategy is implemented as an example (shown in Figure 2.7) and the experiment results are presented to validate the proposed study mentioned in this work.

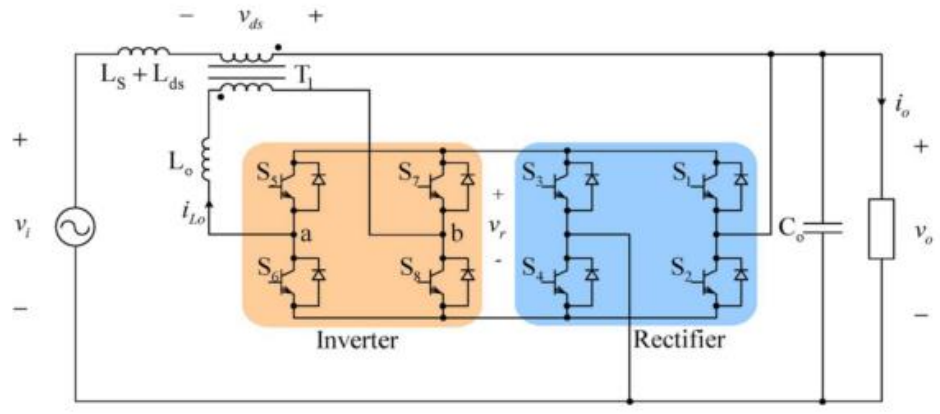

Figure 2.7 Proposed topology in (Soeiro et al. 2012)

Apparently, those topologies in (Kwon et al. 2002) and (Soeiro et al. 2012) has full control on the output including both amplitude and phase compared with previous topology which only has 4 power switches in total. However, the cost of 8 switches along with the passive components made this type of topology less competitive. Meanwhile, the control strategy is also more complicated to make sure 8 switches being turn on-off in a correct sequence and meet the control objectives.

(Ryoo et al. 2003) describes a study on an AC voltage regulator using AC chopper with a transformer, which is similar as the proposed work in (Hietpas & Naden 2000) and shown as Figure 2.8. The authors extends Hietpas's work with adding passive filter and RC snubber circuit and a similar three phase application is also proposed. The experiment of both single phase AC regulator and three phase application has been also done in this paper. Although the output voltage has a little phase shift compared with input voltage, the results shows that this topology works perfectly in order to compensate the voltage higher than reference value. However this topology shows no ability to increase the output voltage.

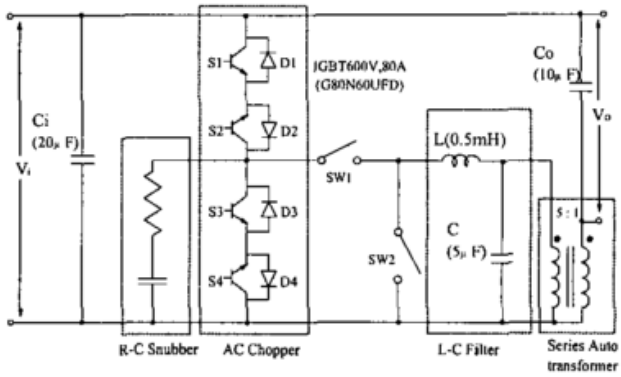

Figure 2.8 Voltage regulator using single phase buck AC chopper proposed in (Ryoo et al. 2003)

Having discussed the topologies of AC/AC converter in previous research, the following section will introduce some techniques on modelling and control strategy of single phase AC/AC converter

2.1.2.2 Control Strategies

PI control

As one of the most popular control strategies, PI control is also widely used for controlling AC/AC converter. (Polmai & Sugprajun 2007) provides the detailed study of modelling work and the control design of the basic single phase AC chopper topology, which is shown as Figure 2.9

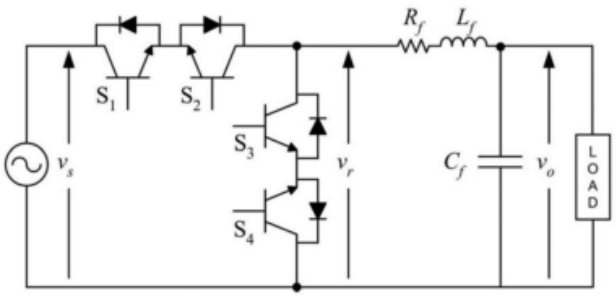

Figure 2.9 Configuration of single-phase AC chopper in (Polmai & Sugprajun 2007)

The working principle of this basic topology is firstly introduced based on previous research and then authors pay more attention on the modelling and control work of this topology. First, the voltage after chopping the input voltage is derived as the multiplication of the input voltage and duty ratio based on averaging method. Next, components of the passive LC filter are modelled based on their own differential equations. Therefore, the block diagram of AC chopper model can be shown as Figure 2.10:

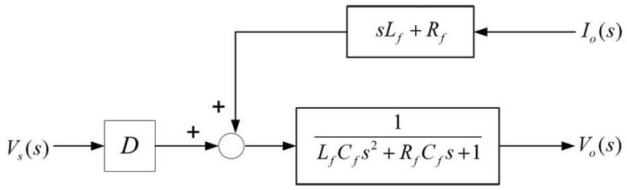

Figure 2.10 Black diagram of single phase AC chopper in (Polmai & Sugprajun 2007)

The open loop system explains the relationship between input voltage, duty ratio, output voltage and load current in a basic single phase AC chopper. Based on this model, a PI controller can be easily applied to regulate the output voltage and maintain it at reference level. In this work, the basic single phase AC chopper with the control strategy is implemented to verify the proposed modelling and control design. The experiment results demonstrate that the proposed closed loop control system can provides fast step change response and good quality waveform with non-linear load.

This modelling method establish the foundation for modelling AC/AC converter and it is suitable for different topology based on basic ac chopper with other passive components or transformers. Meanwhile, PI controller is also widely used in voltage and current control for converters due to its simplicity and effectiveness. Similar modelling work and PI controller design can be also found in (Jie et al. 2008; Jin et al. 2009), which has slightly different topologies compared with basic single phase AC chopper.

In pervious feedback PI controller, the input voltage is assumed to be constant and the control unit, which is duty ratio, is adjusted to eliminate the error. However, in real application, the input voltage may vary within a certain range and it would help if a better control mechanism other than feedback control can be introduced. The working presented in (Nan et al. 2010; Jin et al. 2012; Liu & Wang 2012) is using the same way to set up the mathematical model of different single phase AC choppers but propose a slightly different control strategy to

improve the performance of the controller. Basically, a feedforward control unit is calculated based on the mathematical relationship of the input and output voltage and then a normal feedback PI controller is added into the close loop to eliminate the difference between output and reference voltage. The benefit of involving this feedforward control is that the duty ratio can be brought to the required level very quickly when input voltage varies and steady state error is then compensated by a feedback PI control. The block diagram of this feedforward and feedback controller is shown as Figure 2.11.

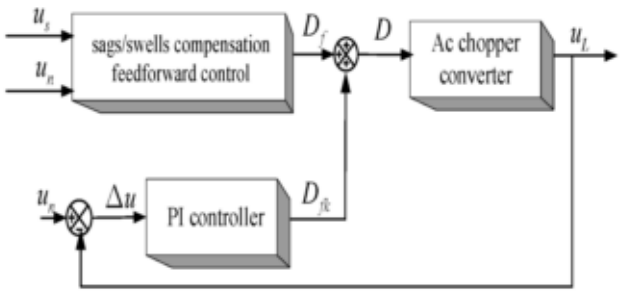

Figure 2.11 Block diagram of feedforward and feedback control proposed in (Jin et al. 2012)

Overall, this modelling method of converters is widely applied in this research area due to its simplicity and it can be easily extended to other topologies for different control strategy design. However, all the variables are literally RMS values of the AC voltage and currents so the instantaneous behaviour of the AC/AC converter cannot be described by this method. The calculation of RMS value also requires additional circuits and it may affect the performances of controller. F, both duty ratio and input voltage can vary and be considered as inputs so the multiplication of both introduces nonlinearity into the system. Therefore, other modelling or control approaches are also discussed and applied for controlling power converters.

Model Predictive Control

The previous control method for AC/AC converter is using duty ratio as control input. When the duty ratio is determined, the switching sequences of different switches are generated to control the output of the AC/AC converter. Model predictive control takes advantage of the discrete nature of converters and figure out the best switching state to minimise the given cost function as the next control action. Since the combination of on-off switch states is limited, the optimization problem can be simplified and reduced to prediction of the system behaviour for those possible switching states (Kouro et al. 2009). Therefore, this method is known as Finite Control Set MPC (FCS-MPC). The block diagram of a typical FCS-MPC is shown as Figure 2.10 and it is explained in the following part.

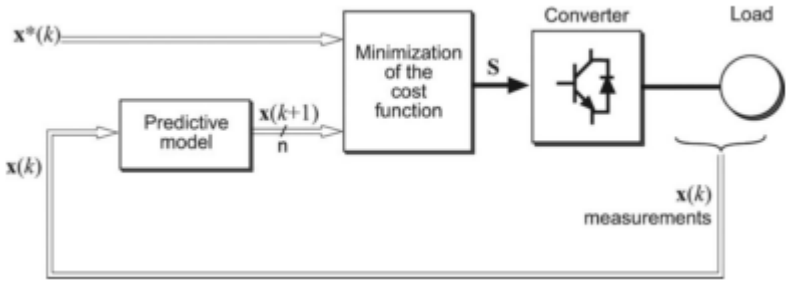

Figure 2.12 Block diagram of FCS-MPC (Cortes et al. 2008)

Firstly, the number of switching states needs to be determined. Basically, there are only two states, on and off, for a single switch. The total number of switching states is equal to the number of different combinations. However, some combination are not possible due to the working principle of the converters, the number of possible switching states, defined as n, can be reduced further. For example, the basic single phase AC chopper shown in Figure 2.9 consists of 2 bi-direction switches; the total number of combination is $2^2 = 4$. Since the two bi-directional switches cannot be either turn-on or turn-off at the same time, the possible number of possible switching states is reduced to 2. Secondly, the n predictive models are established for all possible switching states. When the states variables $x(k)$ are measured or

estimated, the n set of predicted values $x(k+1)$ can be calculated based on n predictive models. Thirdly, a cost function should be defined based on the control objectives of the application. The n set of predict value $x(k+1)$ are then evaluated with the cost function. The switching state S with minimum cost is selected and applied as the next control input.

With different cost functions defined, this approach has been applied for different applications within power conversion research area, for instance, current control of inverter in (Rodríguez et al. 2004), power control of rectifier in (Antoniewicz & Kazmierkowski 2006), torque control of induction machine in (Miranda et al. 2009) and voltage control of power converter in (Yusoff & Lillo 2012; Perez et al. 2012; Tomlinson et al. 2011).

One of the major problems of FCS-MPC is that it results in a variable switching frequency of power switches, which is not preferred for commercial products. The voltage and current with variable switches frequency contains a large ranges of harmonics, which would be problematic for EMI filter design and power switch protection. Meanwhile, the sampling frequency of the controller is required to be twice higher than the required switching frequency; otherwise the switching frequency can be never achieved.

Vector Control

In terms of designing control strategy with AC voltage and current involved, one challenge is that the sinusoidal waveform brings nonlinearity into the system. Therefore, the linear control analysis cannot be directly applied into such system. Typically, a system as three phase converter is transformed from stationary frame to dq rotating frame with a certain frequency and then simple PI controller can be designed to meet the control requirements. However, dq transformation requires at least two orthogonal variables while the single phase application apparently has only one phase.

In order to generate another orthogonal phase from an existing single phase AC/AC converter, (Zhang et al. 2002) introduces a concept called imaginary orthogonal circuit. It assumes the imaginary orthogonal circuit has exact same components and parameters, including switches and passive components, as the original circuit. The state variables and control reference are 90 degree shifted with respect to their corresponding counterparts in the original circuit. Although the imaginary circuit doesn't physically exist, the state variables of both real and imaginary circuit are able to form two orthogonal phases for dq transformation. In real implementation work, the imaginary state variables can be obtained by phase shifting the measured signals by a quarter of the fundamental period through applying a filter as introduced in (Miranda et al. 2005; Golestan et al. 2011). The block diagram of proposed method is shown as Figure 2.13.

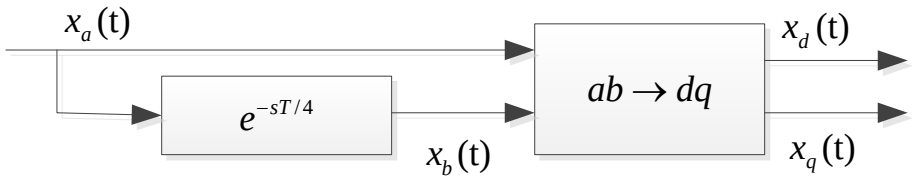

Figure 2.13 Construction of imaginary circuit by applying filter (Miranda et al. 2005)

Another method to generate the imaginary state by using observer is also discussed in (Saritha & Jankiraman 2006). The authors measure the load current through Hall sensor and directly feed the measured value into a curve-fitting observer to get orthogonal values. The block diagram of this method with observer is shown as Figure 2.12.

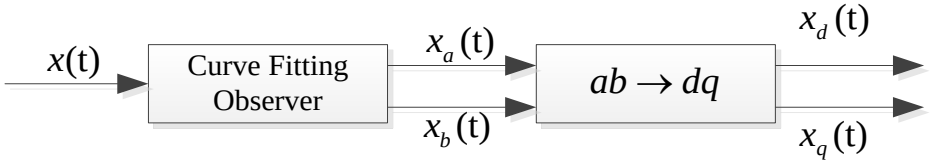

Figure 2.14 Construction of imaginary circuit by applying observer (Saritha & Jankiraman 2006)

As long as the system is transformed into dq rotating frame, a PI controller can easily be applied to make the output tracking the reference value. Since the output of the PI controller is still in dq reference frame, a transformation from dq frame to stationary frame is required and then the switch sequence can be generated by power width modulation. The simplified block diagram of current control described in (Miranda et al. 2005)is shown as Figure 2.15.

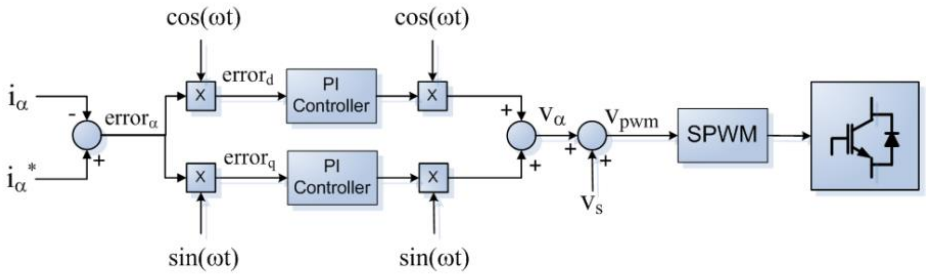

Figure 2.15 Simplified Single phase dq current control block diagram in (Miranda et al. 2005)

2.1.3 Summary

The transformer based voltage optimiser is not a good choice since it is very difficult to control the output voltage. It normally reduce the output at a predetermined ratio therefore there is no regulation as the input voltage varies. On the contrary, power electronic based single phase AC/AC converter is very promising to realise a voltage optimiser/stabiliser for domestic use.

The basic AC chopper with passive filters in (Enjeti & Choi 1993) has the simplest topology and works quite well for compensating overvoltage issue compared to the AC/AC converter with 8 power switches in (Kwon et al. 2002), but it suffers from two major problems for regulating voltage in domestic house. First, the full range of voltage is not necessary for voltage optimisation in residential house. Second, this topology can only provide voltage

reduction, which limits the functionality of this topology as a voltage optimiser/stabiliser in domestic house.

The topology with a transformer connected in series as mentioned previous is a good choice for decreasing the current flow in the power switches, since only a friction of load current flows through the switches. For building an AC/AC converter with same power rating, this type of topology can save tremendous costs on switches with fitting in a transformer only. In addition, some improvement of circuit connection is required to be made for realising a voltage optimiser/stabiliser in household for both step up and step down purposes.

In terms of modelling and control of AC/AC converter, the averaging method will bring sinusoidal variables and nonlinearity into the model as discussed previously. It increases the difficulty of applying linear control method and designing controller analytically. Meanwhile, a peak detector or RMS calculator is required in the close control loop, which may slow down the behaviour of controller and increase the cost as well. What's more, the dynamic behaviour of the system is not well represented by applying averaging method for modelling since only RMS values of voltage and current are involved in averaging method.

Model predictive control appears to be advantageous over simple PI controller with averaging model because it uses multiple predictive models to describe a power converter and each model only presents a single working state with a certain switching state, so the predictive model are more precise compared with averaging model. However, it is not computational efficient compared with other approaches due to more calculation needed. Next, the sampling frequency of the control system is required to be much higher than switching frequency, which would increase the cost of implementation work. Lastly, this method still cannot guarantee a fixed switching frequency in some applications.

In order to deal with the sinusoidal variables in AC converters, dq transformation is a good choice to be applied for linearizing the model. With an imaginary circuit introduced, the single phase AC converter can be also transformed into dq rotating frame and linearized. After linearization, it would be fairly easy to apply linear control methods for the purposes of optimising the voltage level.

2.2 Literature Review on Non-intrusive Load Monitoring

2.2.1 Introduction

Generally, two of the most essential elements in non-intrusive load monitoring system are the appliance signature and the disaggregation algorithm. With those two parts selected and defined, the implementation of a non-intrusive load monitoring system begins with data acquisition system, and then the appliance signatures are extracted from the acquired signals, finally the signatures are analysed by applying the algorithm and the appliances are recognised and identified. The typical process of a non-intrusive load monitoring system described in (Wong et al. 2013) is shown as follows:

Figure 2.16 Three stages of a typical non-intrusive monitoring process

Have introduced the general idea of non-intrusive load monitoring, the overview of the approaches investigated in this research area is given in the following section and it is divided into three parts, namely load signatures, event detection and appliance recognition.

2.2.2 Load Signatures

Various load signatures are acquired and used to conduct load disaggregation algorithms in previous work. It could be any electrical characteristics as long as it can be applied to distinguish different appliances. Generally, we consider sampling frequency less than 1 Hz for low frequency sampling. The data acquired with low frequency sampling is relatively limited, for instance, voltage and current, power and power factor. The advantage of low frequency sampling is that it can be achieved easily through the most existing methods, for instance, normal energy meter, plug-in energy monitor, smart meter in (Park et al. 2010). However, instantaneous value voltage and currentcan be acquired at high frequency sampling rate with advanced equipment installed. It increases the possibility to manipulate more complicated signatures such as harmonics, V-I curves.

2.2.2.1 Signatures with Low Frequency Sampling

The most common signature is the power consumption of an appliance, which is first introduced in (Hart 1992). A digital AC monitor described in (Hart et al. 1985) is installed and set to capture the power and voltage RMS values at1Hz sampling frequency. In order to increase the robustness and reduce the influences from the voltage variation, the powers values is then normalised by using the equation as follows (Hart 1992):

$$P_{norm}(t) = \left[\frac{120}{V(t)}\right]^2 P(t) \qquad (2.1)$$

where V is the voltage and P is the power.

The value 120 refers to the nominal voltage in US power distribution system. The edge detector is applied through constantly monitoring the changes of steady-state power values.

Once an edge is detected, the change of real and reactive power ($\Delta P - \Delta Q$ plane) is then extracted and put into a two-dimensional signature space shown as follows:

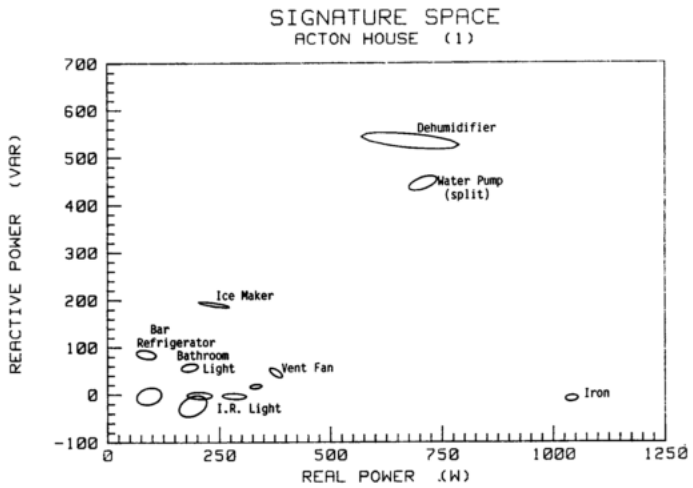

Figure 2.17 Normalized complex power signature space (Hart 1992)

Next, the events are paired or associated with known clusters through a best likelihood algorithm. Last, the operating state of the appliance is determined by comparison with the power consumption. Power plot is shown to demonstrate the approach described in Hart's work as follows:

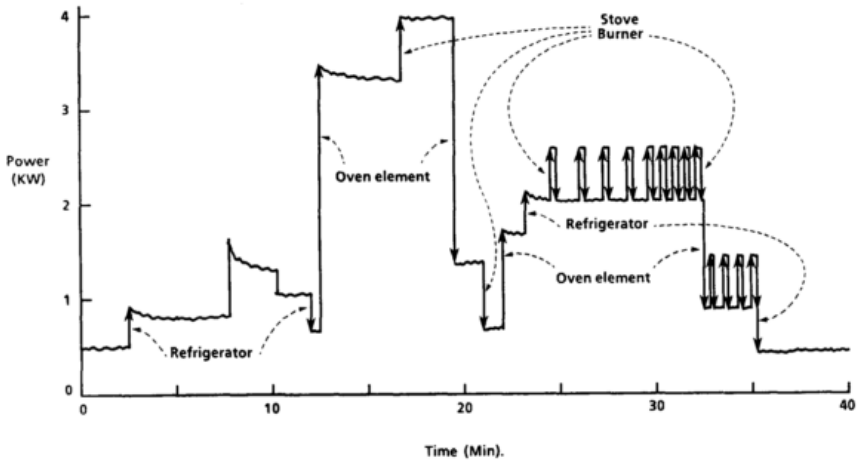

Figure 2.18 Power versus time shows step changes due to individual appliance events (Hart 1992)

As Figure 5.3 illustrates, the method is able to detect the appliance with same turn-on and turn-off behaviours easily, but it has some obvious shortcomings. Firstly, the real power consumption has significant noise which is not taken into consideration in this method. Secondly, some appliances consumes very similar real power and reactive power (see Figure 2.18), which are very difficult be separated by simply relying on the change of power values (Laughman et al. 2003). Thirdly, the method is very difficult to cope with the appliances with multiple working states or variable power consumption. Lastly, the matching mechanism assumes the turn-off characteristic is as same as turn-on, which is not applicable to all appliances. The error of mismatch due to this reason is reported as 10% in (Sultanem 1991). Despite of all this drawbacks, this approach points out the essential elements and classic infrastructure of a typical non-intrusive load monitoring system.

As an extension of Hart's work, the approach mentioned in (Norford & Leeb 1996) applies a median filter to remove the narrow spikes in the power plot, which makes it easier to determine the magnitude of the changes in power and somehow reduce the effect of electrical noise. In addition, the start-up transient of motor-driven appliances is investigated. A v-section normally exists when such appliance starts as Figure 5.4 illustrates.

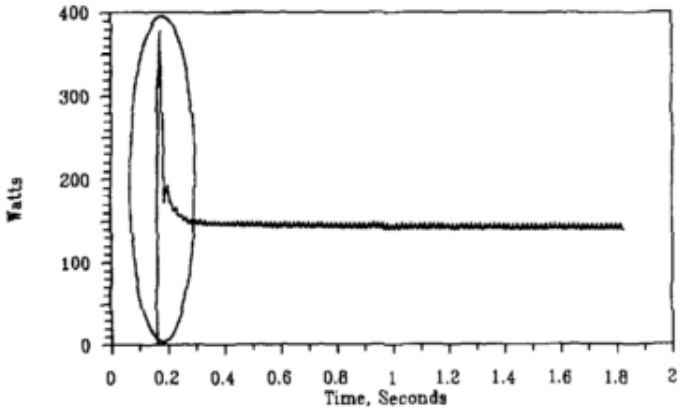

Figure 2.19 Measured instant-start lamp-bank real power transient, with v-section noted (Norford & Leeb 1996)

The appliances can be identified through matching the v-section in transient as long as each of the v-section doesn't overlap with others. Although the whole monitoring improves with filter and transient identification, the authors mentioned the poor repeatability and consistency of the v-section as well as the overlap problem happening in practice.

Based on real power consumption, another feature is defined and extracted for some appliances in (Cole & Albicki 1998b), specifically for the appliance with start-up power spike, varying power draw or different working states, such as heat hump compressor and washing machine. Both the edges and slopes of real power value within one operation cycle are investigated and the feature is extracted from them shown in Figure 5.5.

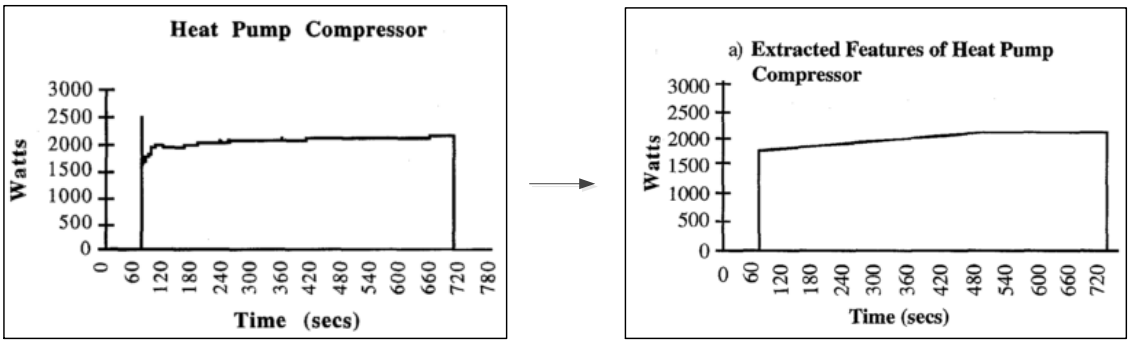

Figure 2.20 Feature extraction based on 'edges' and 'slopes' in (Cole & Albicki 1998b)

This feature works with the algorithm proposed in (Cole & Albicki 1998a). In this work, the algorithm identifies the abrupt changes in power level as edges firstly and then matches the nearest and smallest collection of edges which sum to zero to form a loop. A repeated loop is deemed to be an event of operating a load. After clustering and mapping, the load is finally identified.

Apart from the methods using both active power and reactive power aforementioned, some approaches use the change of real power only to disaggregate the total load, for instance, the algorithm discussed in (Powers et al. 1991). Given a known dataset of premise level with

sampled at every 15 min, it records all the occurrence, timing and magnitude of all large changes (spikes) in the total power consumption and then matches this spikes with the end-use appliances. Some adjustment is also made according to consistency check before the disaggregated load profile produced. The method requires massive information of individual appliances to infer the behaviour of them and train the algorithm for matching. Also, the appliance with less power consumption is very likely to be ignored by this method due to the long sampling interval (15 min). Therefore, it is not very realistic to be the right choice of load disaggregation.

The approach introduced in (Marceau & Zmeureanu 2000) is somehow similar to the one introduced in (Powers et al. 1991). Although it samples and calculate the real power at 16s intervals, it also takes account of the appliance operating time when identifying the appliances. To start with, it acquires the change of real power as signal and filters the signal through 7 steps to get distinct rectangular shapes which are likely to represent on-off events of the appliances. Next, those rectangular shapes are attributed to corresponding appliance based on the magnitude of real power change. Then, a number of subroutine are applied to check if the shapes matches the attributed operation of appliances, based on average duration, maximum duration, zero demand and other factors. Finally, the power consumption of different appliance is calculated and derived as output. This method is reported to detect the major appliances with accuracy over 90%. However, it is still hardly applicable for real installation in domestic houses since it only disaggregates the appliances with significant power consumption and requires excessive training data which includes at least one week record.

Baranski and Voss have proposed a measuring system using an additional optical sensor to measure the real power every 1s continuously in (Baranski & Voss 2003). Based on this

system, they create an algorithm which focuses on the frequent power changes only and then matches a large number of on-off events with such power changes to the appliances in time as reported in (Baranski & Voss 2004b). Furthermore, another method is described in (Baranski & Voss 2004a) to handle the appliance with multiple states (finite state machine) through dynamic programming and finally it can infer state transitions of such appliances.

2.2.2.2 Signatures with High Frequency Sampling

Mostly, only active power and reactive power are used in the methods to disaggregate appliances mentioned in last part. The information of operating appliances is very limited with low frequency sampling. Therefore, researchers also try to deploy high sampling frequency equipment to achieve more accurate detection based on the signatures which are hidden under low frequency sampling.

The most straightforward feature which can be only observed with high frequency sampling is harmonics. The Nyquist-Shannon sampling theorem explained in (Matthews et al. 2008) states that to capture the highest frequency component of interest in a signal, one much sample at more than twice that frequency. Hence, in order to look into the 10^{th} harmonic, the required sampling frequency should be higher than 1 kHz since the fundamental frequency in the UK is 50 Hz.

However, the high frequency sampling may suffer from data transmission and storage problem. To solve these problems, the original data is normally processed locally and then transferred to the next stage for analysis or storage. Alternatively, the advanced data acquisition system is able to program and handle the original data in really high sampling rate and then record the significant information.

As it mentioned previously, the harmonics are discussed in (Laughman et al. 2003) as an additional features to distinguish some appliances. Specifically, the third harmonic can be used to tell the difference between personal computers and a bank of incandescent lamps whereas the real power and reactive power in two dimension space of them are extremely close and hardly distinguishable. Although it doesn't give a full description on using harmonics to disaggregate all types of appliances, this work points out the possibility of involving harmonics in non-intrusive load monitoring.

Other work proposed in (Leeb et al. 1995) also take advantages of harmonics to monitor the operations of appliances. Differently, it introduces a novel concept of 'spectral envelope', which is formed of the magnitudes of first several harmonic components. In another words, more information of harmonics are involved compared with (Laughman et al. 2003). Based on spectral envelope as a load signature, a multi-scale prototype is developed for detecting transient of appliances, which also includes variable-load appliances. Since the approaches with low sampling rate is very poor when identifying variable-load appliances, this method prove that the spectral envelope based on harmonics would benefit appliances identification.

As an extension of the work proposed in (Leeb et al. 1995), Shaw introduces a method in (Shaw et al. 2008) which also make use of spectral envelope to classify different appliances. However, the classification of those approaches is completely different. The work in (Shaw et al. 2008) formulas the classification as the least squares problem and then select the exemplar which gives the least residual. If the residual is still larger than a set threshold, the event is regarded as unclassified. This method shows that the least square procedure is simple and powerful once the signature is transformed into a numerical form.

The approaches mentioned above are all based on transient harmonic signatures which are sampled at high frequency. The most significant drawback of using such signatures is that the

transient is not consistent and the detection of a transient is not guaranteed. Therefore, some researchers also pay attention to use steady state signatures captured at high frequency sampling rate to identify appliances.

(Srinivasan et al. 2006) proposed a neural network based signature recognition based on harmonics as signatures. The implemented system introduced in this work includes 8 appliances, current sensors, power harmonics analyser and a trained neural network. The current value is measured by the sensors and processed to extract the features by the power harmonic analyser. In order to detect these 8 appliances, the authors train the neural network with 256 all possible combination of on-off states. Moreover, different neural network based models are evaluated and the one with best performance yields accuracy around 80% to 90%. Although the experiment results look promising, this approach is very difficult to extend a real domestic house with 20-30 appliances, which requires 2^{20} to 2^{30} combinations to train the system.

Akbar and Kham also investigate the harmonics of different appliances, especially on non-linear appliances in (Akbar & Khan 2007). This paper firstly introduces taxonomy of household appliances and then looks into the current waveform of several appliances in both time domain and frequency domain to illustrate the difference among them. One example of a fan dimmer is shown as Figure 5.6:

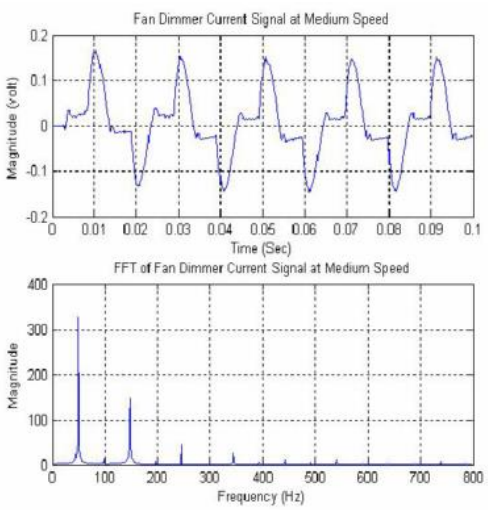

Figure 2.21 Fan dimmer current signal plot in time and frequency domain when fan is medium speed (Akbar & Khan 2007)

It shows that different non-linear appliances, such as fluorescent lamp, lamp dimmer and fan dimmer, do have different pattern of harmonics between each other. Even for a single appliance, the harmonics changes dramatically when it operates at different mode or speed. However, the identification algorithm is not explained clearly and no experiment result is given to demonstrate it although the analysis of measurement and signature looks promising.

The approaches with high sampling rate introduced previously are based on the harmonics as signatures. However, the work in (Patel et al. 2007) describes a complete different method which takes advantage of the noise during either on-off transient or steady state. One example of the noise is illustrated as Figure 5.7.

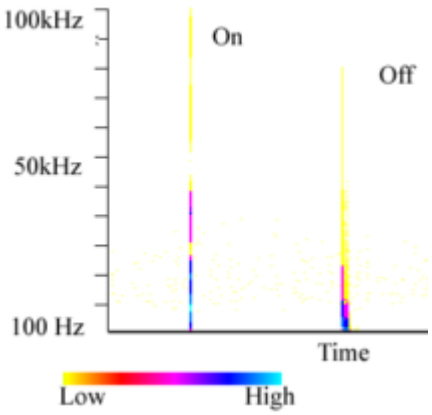

Figure 2.22 Frequency spectrum of a particular light switch being toggled (Patel et al. 2007)

The noises are processed by applying Fast Fourier Transform to obtain the amplitude values of the frequency components in vector form. Once a transient isolated, the vector serves as the feature for the particular transient. Next, the machine learning technique, specifically support vector machine, is used to recognize the noisy events. Both the hardware and software are implemented and the results show that the approach can identify appliances with good performance with accuracy above 85%. However, the authors of (Gupta et al. 2010) point out that the transient event is not consistent and may not be surely captured every time. What's more, this transient noise-based method is not suitable for identifying mobile devices, since the transient of the same appliance may change when they connected to sockets at different location.

The work in (Gupta et al. 2010) introduces another approach for recognizing switch mode power supplies (SMPS). This type of loads is widely installed in domestic house nowadays and generates very high frequency electromagnetic interference (EMI) constantly due to the high frequency switching of the power supply. This feature is then captured and analysed by utilizing Fourier Transform in the range of 36-500 kHz. As it shown in Figure 5.8, the left subplot shows the spectrum when no appliances switched on. After a device turns on, more component with different frequency are shown in the middle subplot. The new feature is then extracted through Gaussian fit and its features including amplitude (A), mean (μ), and variance (σ) are illustrated as right subplot.

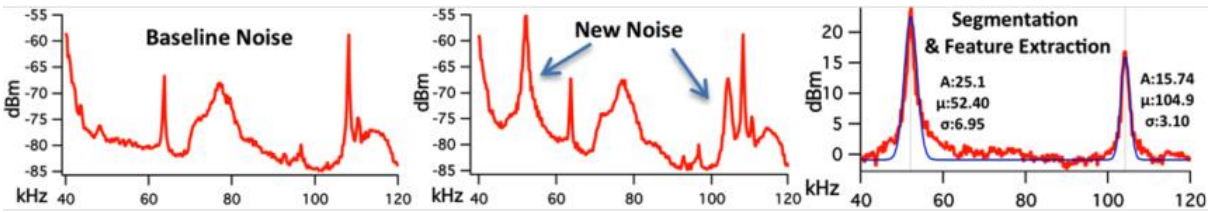

Figure 2.23 The noise of base line (left), new device turn-on (centre), extracted feature (right) (Gupta et al. 2010)

A feature vector is then created based on those features and the centre frequency. The event detection algorithm scans the vectors and alert an event when any value greater than predefined threshold. Finally, the K-Nearest Neighbour and Euclidean distance metric are applied to match the events with an appliance. The evaluation results report an accuracy around 93.8%. Even though this approach seems to be promising, some problems are also addressed. Firstly, the EMI for external or neighbourhood is uncertain, which means the EMI from different homes under a same wiring system may affect the detection. Secondly, the detection based on EMI is only suitable for SMPS devices and other appliances, for instance, resistive appliance, don't show significant EMI, therefore EMI cannot be the signature for detecting appliances other than SMPS device. Thirdly, this method can only accomplish the task of detection, the power consumption of individual appliances still remain unknown without other specific measurement.

Apart from Fourier Transform, the authors of (Chan et al. 2000) propose another technique to extract features of an appliance current waveform, which is called wavelet decomposition. They states that wavelet analysis is based on the decomposition of a signal according to scale rather than frequency, using basis functions with adaptable scaling properties. A current waveform can be decomposed by wavelet analysis with five level as Figure 5.9shows.

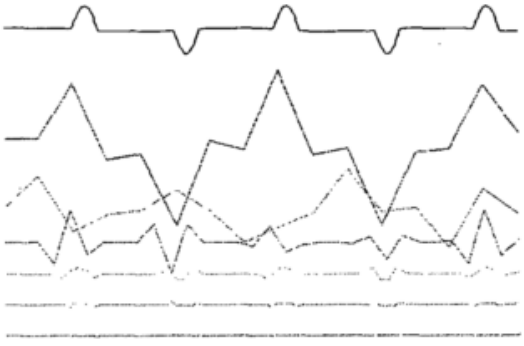

Figure 2.24 Wavelet Decomposition of PC current waveform(Chan et al. 2000)

Other appliance are also investigated and the results demonstrate that the wavelet features are very distinguishable. However, those features of multiple appliances are not strongly linked with individual appliances. What' more, this paper doesn't explain how to make most of the wavelet to conduct load disaggregation.

V-I Curve, which is actually the mutual curve of voltage and current instantaneous value, has also been investigated as a feature in (Lee et al. 2004) and (Lam et al. 2007). They demonstrate that this feature are quit distinctive for different appliances and a novel taxonomy is established based on it. (Hassan et al. 2014) extend the research on this wave shape based method. Several metrics are defined to describe a wave-shape and then form a feature vector for identification. One example of V-I trajectory is shown as follows:

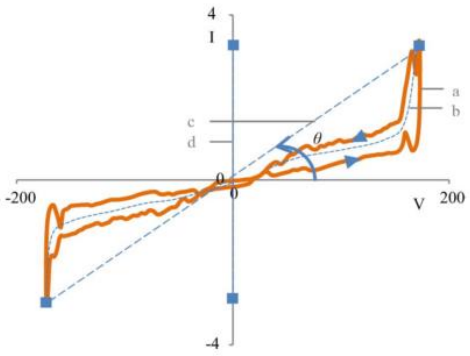

Figure 2.25 A graphical illustration of wave-shape metrics: (a) V-I trajectory (b) mean curve (c) reference line joining points of highest and lowest I-coordinate in the V-I plane (Hassan et al. 2014)

In this work, the wave shape features are compared with other features, such as real and reactive power, harmonics with different disaggregation algorithms based on the public dataset provided in (Kolter & Johnson 2011). Although the wave shape features gives the most outstanding results, this work is purely based on previous data and simulation and no hardware implementation work has been done to prove the robustness and reliability of this method.

Having reviewed various signatures used in previous research work, the following part introduces the comparison of event-based methods and non-event based methods in non-intrusive load monitoring and the algorithms associated.

2.2.3 Event Detection & Disaggregation Algorithms

When the load signature is properly selected, the non-intrusive load monitoring system normally requires an event detection mechanism and a disaggregation algorithm to process and analyse the sampled signatures and then figure out the exact on-off states of each individual appliances.

Generally, most of the existing non-intrusive monitoring approaches can be grouped as event based and non-event based. The event based method monitors the adopted signatures continuously and assumes the operations of loads remain unchanged if no event is detected. Normally, an edge detection algorithm or a threshold of signature is applied in this type of method. Once an event is detected, the change of signature is captured and treated as operation change of a certain appliance. Finally, this change of signature is classified through different approaches, for instance, support vector machine, K-Nearest Neighbour and Euclidean distance metric, with the database including the signatures of all appliances. The appliance with closest signature is found and regarded as the one changing its operation (turn on-off, mode changes). Some examples of previous work based on event detection are listed in Table 2-1:

Table 2-1 Examples of event based approaches

Approaches	Signature(s)	Algorithm(s)
(Patel et al. 2007)	Transient noise FFT	Euclidean distance metric
(Gupta et al. 2010)	Steady noise FFT	K-Nearest Neighbour

(Figueiredo et al. 2011)	Real and reactive power, power factor	K-Nearest Neighbour, Support vector machine
(Wang & Zheng 2012)	Real power	Clustering, Euclidean distance metric
(Wang et al. 2013)	Current Envelope	Euclidean distance metric
(Hassan et al. 2014)	Wave shape	Support vector method

Different from the above methods, non-event based method doesn't have a stage detecting events. All the samples of measurement are considered and processed for load disaggregation. This type of method pays more attention on the relationship of signature over a relative long time period and highly relies on the inference algorithm with high accuracy and robustness rather than the diversity of signatures. One of the most popular approaches is to model the appliances by using a single probabilistic framework, for instance Hidden Markov Model. In this method, the following elements are defined to describe the behaviour of an appliance:

- **States**: indicate the operation state of an appliance. It could be on-off states or operating modes.
- **Transition probability**: indicate the probability of an appliance transit from one state to another. It is normally in matrix form and requires training to get it accurate.
- **Observations**: indicate the observation or measurement of an appliance; normally it is real power value. Each state is deemed to emit observation varying with a certain range.
- **Emission probability**: indicate the probability of a state emit a certain observation and is described by a Gaussian distribution. It is in matrix form and requires pre-known data for training.

For example, a kettle has two states, namely on and off. The probabilities of transition between two states actually reflect how often it is switched between on & off and how long it

is switched on for one working cycle. The observations are the power value apparently; on-state emits large power observation within a small range while off-state emits almost zero power. With a known sequence of observed real power value, the states of the kettle can be inferred by apply an inference algorithm, for instances, Viterbi Algorithm introduced in (H. Kim et al. 2011).

Kotler provide a public dataset for load disaggregation research and firstly apply this method on non-intrusive monitoring method in (Kolter & Johnson 2011). Different extension of Hidden Markov model are then proposed and investigated in (Zia et al. 2011; Zoha et al. 2013; Mueller et al. 2014). However, those methods are evaluated by using public dataset and not real implementation is achieved.

Compared with non-event based methods, event based methods requires less computation and analysis since only detected events is focused for inference and identification. Furthermore, event based methods have the potential to give the feedback of the operation of appliances instantly while non-event based methods have to take advantage of the data over a long time period. Therefore, event based methods is much more suitable for developing an online non-intrusive load monitoring system which monitors the on-off states of each individual appliances continuously.

2.2.4 Summary

It is noticed that the major difference of existing non-intrusive load monitoring methods are the load signature they used. The disaggregation algorithms of different methods are all among those several choices. Therefore, developing a new signature is essential for non-intrusive load monitoring system. Based on the reviews of load signatures identified by different approaches, the potential of investigating signatures with low sampling frequency,

such as real and reactive power, is very limited. Therefore, signature captured with high sampling rate is preferred to be investigated in this project.

Considering computation efficiency of the disaggregation algorithm, event based method is apparently the preferred choice over non-event based method in this project. The event detection is performed on every sample but the inference and identification are only conducted when an event is detected.

The ideal algorithm is required to be simple, computational efficient, robust and accurate. Generally, processing signatures in numerical form, such as power and harmonics, requires less computation compared with processing signatures in graphical or geometrical form, such as envelope and trajectory. Built upon previously published work as reviewed in the chapter, the project aims to develop a distinctive load signature in numerical form and propose a simple and efficient algorithm to accomplish non-intrusive load monitoring in real time for certain types of load.

Chapter 3 Step-up/down voltage Stabiliser for Voltage Optimisation

This chapter introduces the proposed step-up/down voltage stabiliser on its different aspects. The topology and the working principle are described in the beginning. The mathematical model is then established and a control strategy based on PI controller is introduced to regulate voltage in the presence of disturbances. The simulation results and implementation work are also presented at the last part of this chapter.

3.1 Topology & Operation Principle

The circuit diagram of the proposed voltage stabiliser consisting of four power electronic switches (S_1-S_4), one relay switch S_0, a multi-winding transformer and LC filter is shown in Figure 3.1. The transformer has two secondary windings which have the same number of turns but different connected with the circuit in opposite polarity. When the proposed voltage stabiliser is in operation, only one winding can be connected in series with the circuit at a time. The controlled switch S_0 determines which winding is connected to the circuit, therefore determining whether the stabilizer is working in step-up or step-down mode.

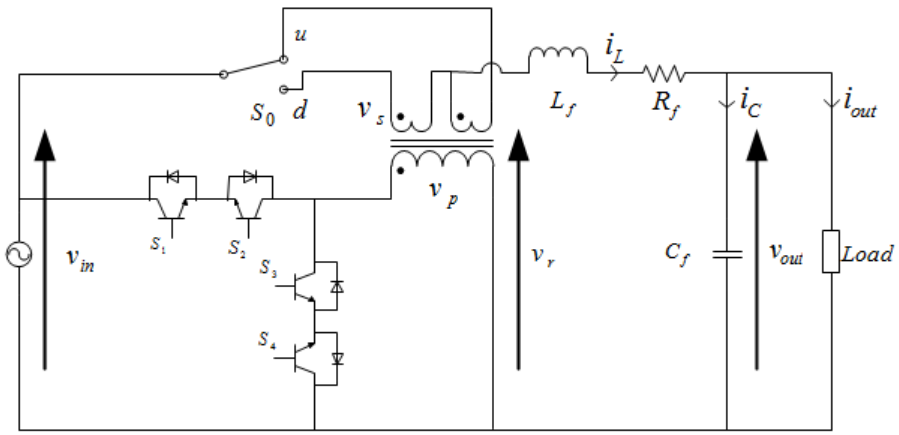

Figure 3.1 Topology of proposed step up/down voltage stabiliser

In each mode, the IGBT switches with reversed diode S_1-S_4 are always switching on-off in a certain pattern with duty ratio D to achieve the voltage regulation. Moreover, an LC filer is applied to the circuit to cancel out the high frequency harmonics components resulting from the fast switching process.

3.1.1 Step-down Mode

In this mode, S_0 is switched to position 'd' and the proposed voltage stabiliser has two working states, namely active state and freewheeling state, based on different on-off states of bi-directional switches. The current flows of different states in this mode are shown in Figure 3.2 and Figure 3.3.

Active State

In this state, S_1 and S_2 are conducting while both S_3 and S_4 are off. The transformer is engaged in and the second winding voltage will be reduced proportional to the transformer winding ratio k. With the arrangement of the secondary winding polarity, the output voltage to the load is the subtraction of the input voltage and the secondary winding voltage as shown in Figure 3.2.

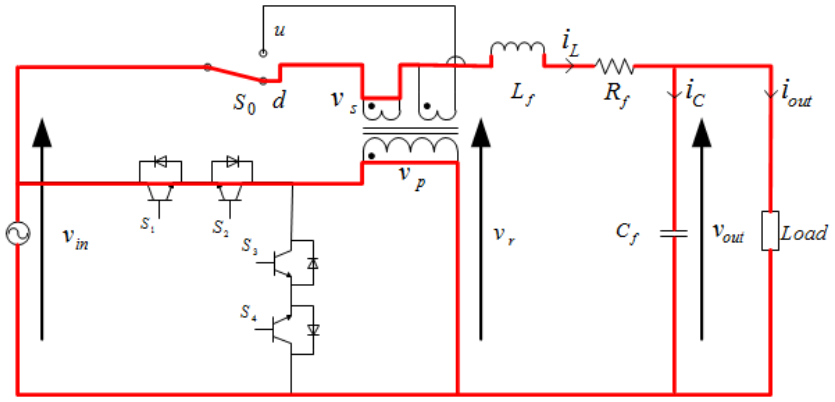

Figure 3.2 Current flow of active state in step down mode

Freewheeling State

When S_3 and S_4 are conducting, both S_1 and S_2 must be off. The circuit works in its freewheeling state and the current flows are shown as Figure 3.3. Since the transformer is not engaged in, the output voltage is equal to the source voltage with the difference caused from the inductance in the loop.

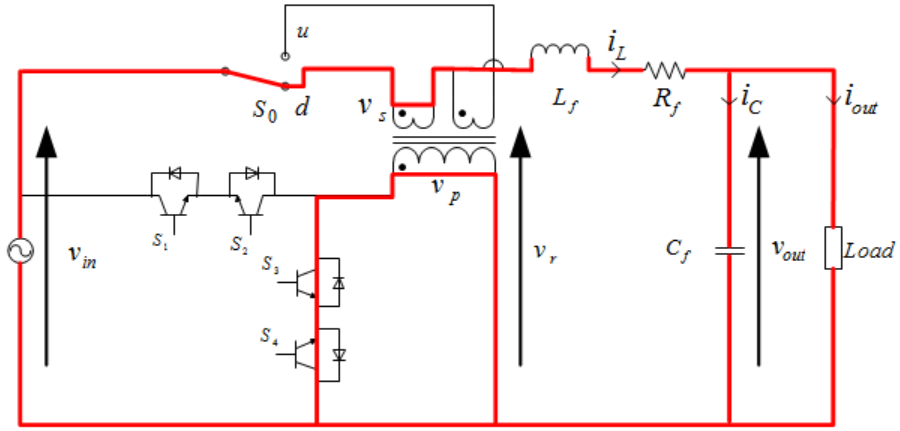

Figure 3.3 Current flow of active state in step down mode

Generally, the state, which the stabilier is in, depends on the current switching pattern of the bi-directional switches in the circuit. The original output voltage without filtering is equal to either input voltage in free-wheeling state or input voltage subtracting a minor voltage increase on the seconding winding in active state as it demonstrated in Figure 3.4 with $D = 0.5$ and $f_s = 1kHz$ ..

The output voltage after applying an LC filter to the original output is a sinusoidal waveform with significantly decreased harmonics. Its amplitude is always slightly lower than the input voltage and is determined by both the duty ratio D and the turn ratio k. As turn ratio is regarded as fixed in operation, the output voltage control is accomplished by controlling the duty ratio D.

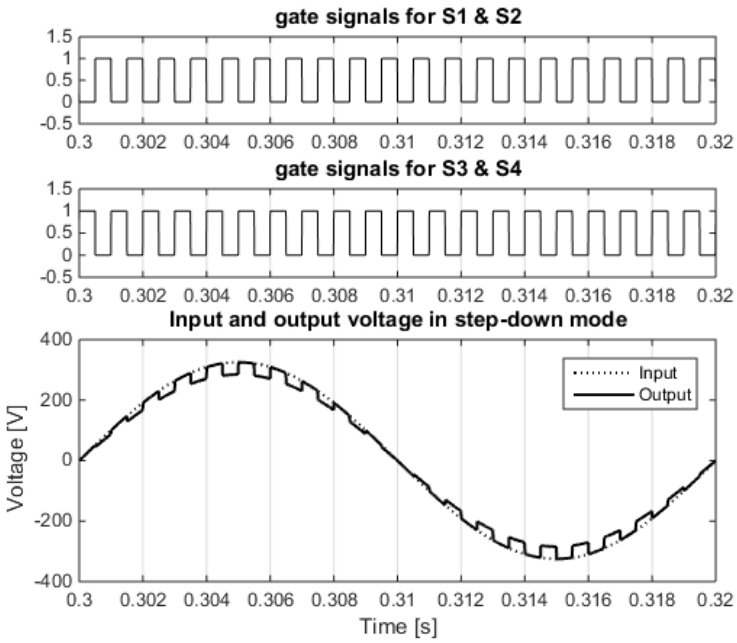

Figure 3.4 Input and original output voltage without filtering comparison in step down mode (duty ratio $D = 0.5$, switching frequency $f_s = 1kHz$)

3.1.2 Step-up Mode

When S_0 is switched to "u" position, the output voltage is the source voltage plus the secondary winding voltage with the transformer polarity arrangement to realise its step-up function. The switching sequences of S_1-S_4 in this mode are quite similar as step down mode.

Active State

In this state, S_1 and S_2 are switched on while both S_3 and S_4 are off. The transformer is engaged in and second winding voltage will be reduced proportional to the transformer winding ratio *k*. Since the polarity in this mode is opposite as it is in step-down mode, the output voltage to the load is the addition of the input voltage and the secondary winding voltage and the current flows in this state are as shown in Figure 3.5.

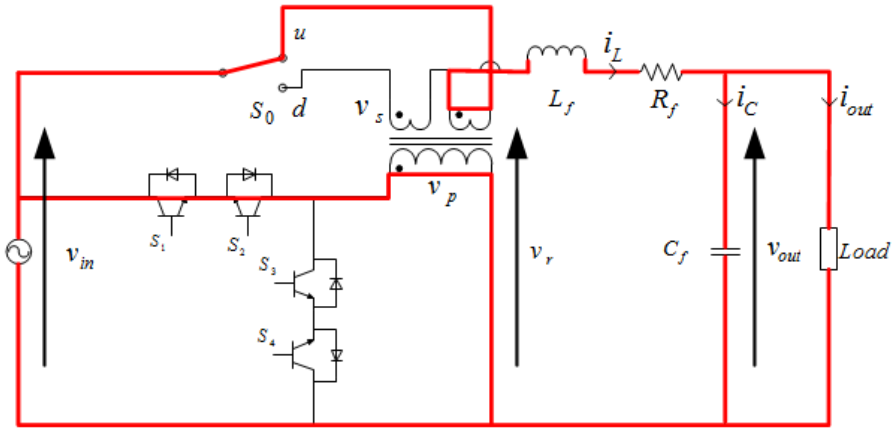

Figure 3.5 Current flow of active state in step up mode

Freewheeling State

The proposed AC voltage stabiliser in step up mode works exactly same as it does in step down mode. When S_3 and S_4 are conducting, both S_1 and S_2 must be switched off. The circuit works in its freewheeling state as shown in Figure 3.6. The transformer is not engaged in so the output voltage is equal to the source voltage with the difference caused from the inductance in the loop.

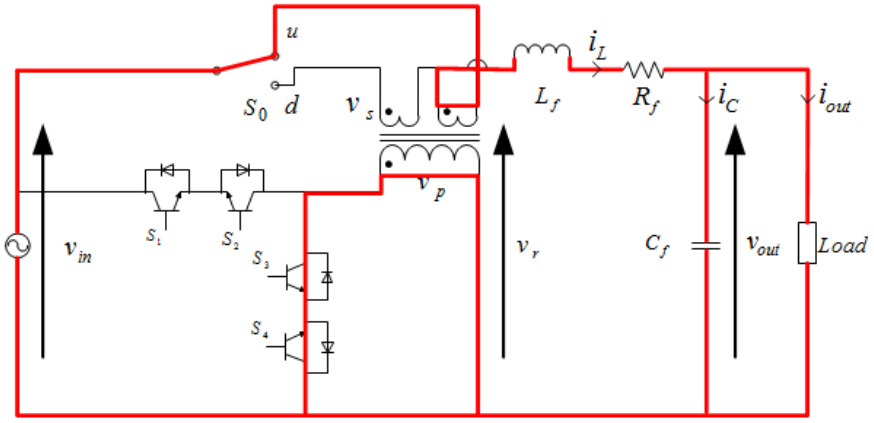

Figure 3.6 Current flow of freewheeling state in step up mode

The relationship between original output voltage without filtering and input voltage in step-up mode is illustrated in Figure 3.7

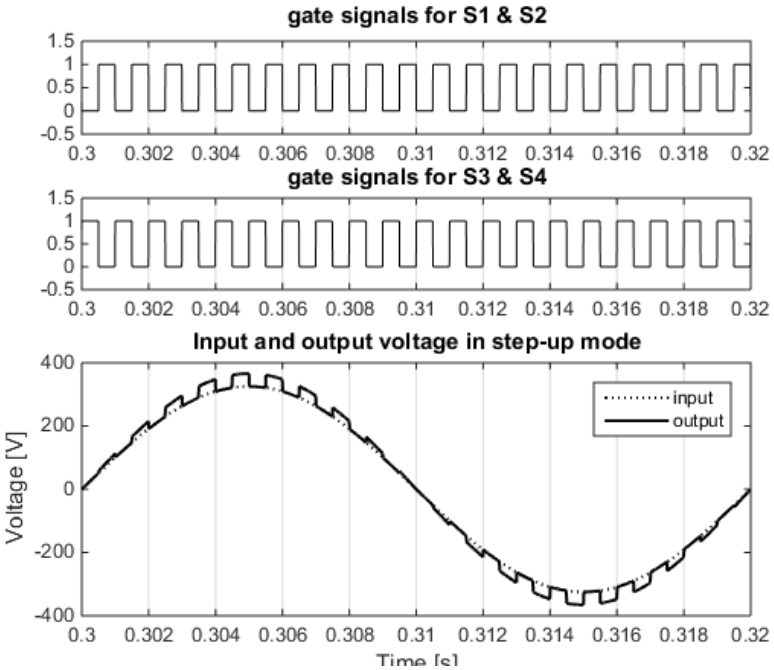

Figure 3.7 Input and original output voltage without filtering comparison in step up mode (duty ratio D , switching frequency $f_s = 1kHz$)

The output voltage without filtering is either slightly higher than or equal to the input voltage. Compared with step down mode, the only difference is the direction of connecting secondary winding into the main loop. With the same LC filter, the majority of high frequency harmonic components can be filtered out and it results in an output voltage in an excellent sinusoidal shape with amplitude slightly higher than the input voltage. Likewise, the RMS value of output voltage is determined by duty ratio D as well as turn ratio k .

3.2 Mathematical Modelling

3.2.1 Model of the Proposed Voltage Stabiliser

Modelling the AC voltage stabiliser covers the AC chopper, transformer and filter. The four PWM controlled switches S_1-S_4 with duty ratio D act as an AC chopper. The corresponding AC voltage on the primary winding of the transformer is described by

$$v_p(t) = v_{in}(t)g(t) \qquad (3.1)$$

where

v_p is the primary winding voltage.

v_{in} is the input voltage.

g is switching sequence.

S0 determines how the secondary winding connects with the circuit. Therefore, the relationship between primary winding voltage and secondary winding voltage can be described as:

$$\frac{v_s(t)}{v_p(t)} = \begin{cases} 1/k & step-up \\ -1/k & step-down \end{cases} \qquad (3.2)$$

where

k is the turn ratio of the transformer.

v_s is the secondary winding voltage.

The voltage before the filter v_r is

$$v_r(t) = v_{in}(t) + v_s(t) \qquad (3.3)$$

Considering the voltage drop on the inductor of filter, the output voltage can be expressed as follows:

$$v_{out}(t) = v_r(t) - (L_f \frac{di_L(t)}{dt} + i_L(t)R_f) \qquad (3.4)$$

where

v_{out} is the output voltage.

i_L is the inductor current.

L_f and R_f are inductance and resistance of the inductor respectively.

The inductor current is described as:

$$i_L(t) = i_C(t) + i_{out}(t) = C_f \frac{dv_{out}(t)}{dt} + i_{out}(t) \qquad (3.5)$$

where

i_C is the capacitor current.

C_f is the capacitance of the filter capacitor.

i_{out} is the load current.

Substituting (3.1)-(3.3) into (3.4), it can be obtained that:

$$v_{out}(t) = v_r(t) - (L_f C_f \frac{d^2 v_{out}(t)}{dt^2} + L_f \frac{di_{out}(t)}{dt} + R_f C_f \frac{dv_{out}(t)}{dt} + R_f i_{out}(t)) \quad (3.6)$$

Substituting equation (3. 1), (3.2) and (3.3) into equation (3.6), it can be obtained that:

$$v_{out}(t) = v_{in}(t)(1 \pm \frac{g(t)}{k}) - (L_f C_f \frac{dv_{out}(t)}{dt} + L_f \frac{di_{out}(t)}{dt} + R_f C_f \frac{dv_{out}(t)}{dt} + R_f i_{out}(t)) \quad (3.7)$$

Assume that the duty ratio $D(t)$ is fixed in a single switching period. Then the gate switching function $g(t)$ can be expressed as:

$$g(t) = \begin{cases} 1 & nT_s < t < (n + D(t))T_s \\ 0 & (n + D(t))T_s < t < (n+1)T_s \end{cases} \quad (3.8)$$

where

$n = 0, 1, 2, 3...$

Applying Fourier series to decompose equation (3.8), it can be obtained as follows:

$$g(t) = D(t) + \sum_{n=1}^{\infty} \frac{2\sin(nD(t)\pi)}{n\pi} \cos(n\omega_s t) \quad (3.9)$$

As it is shown in equation (3.9), the switching function consists of the duty ratio and high frequency harmonic components with small amplitude. Since the harmonic is filtered out afterward, switching function *g(t)* can be replaced by *D(t)* approximately. Therefore, equation (3.7) is rewritten as:

$$v_{out}(t) = v_{in}(t)(1 \pm \frac{D(t)}{k}) - (L_f C_f \frac{d^2 v_{out}}{dt^2} + L_f \frac{di_{out}(t)}{dt} + R_f C_f \frac{dv_{out}(t)}{dt} + R_f i_{out}(t)) \quad (3.10)$$

Transform equation (3.10) into s-domain and rearrange it, the input and output relationship can be expressed as follows:

$$(s^2L_fC_f + sR_fC_f + 1)V_{out}(s) = V_{in}(s)(1 \pm \frac{D(s)}{k}) - (sL_f + R_f)I_{out}(s) \quad (3.11)$$

Based on equation (3.11), it can be noticed that the output voltage V_{out} is influenced not only by input voltage V_{in} but also duty ratio D and output current I_{out}. The block diagram of the system is illustrated in Figure 3.8. The relationship between the output voltage and three inputs, namely the input voltage, the duty ratio and output current, in s-domain is shown as follows:

$$V_{out}(s) = G_1(s)V_{in}(s) - G_2(s)I_{out}(s) + G_3(s)V_{in}(s)D(s) \quad (3.12)$$

where

$G_1(s)$, $G_2(s)$ and $G_3(s)$ can be represented as:

$$G_1(s) = \frac{1}{s^2L_fC_f + sR_fC_f + 1} \quad (3.13)$$

$$G_2(s) = \frac{sL_f + R_f}{s^2L_fC_f + sR_fC_f + 1} \quad (3.14)$$

$$G_3(s) = \begin{cases} \dfrac{1/k}{s^2L_fC_f + sR_fC_f + 1} & step-up \\ \dfrac{-1/k}{s^2L_fC_f + sR_fC_f + 1} & step-dwon \end{cases} \quad (3.15)$$

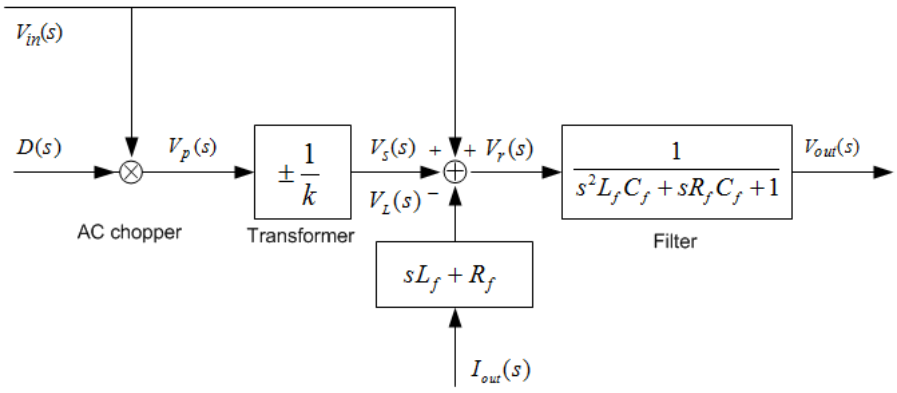

Figure 3.8 Block diagram of open loop model

Since the LC filter applied is a second order system, the nature frequency of it is described as:

$$\omega_n = \sqrt{\frac{1}{L_f C_f}} \qquad (3.16)$$

where

ω_n is the nature frequency of the system.

Therefore, the voltage with frequency less than ω_n is likely to keep its own magnitude whiles the voltage with frequency higher than ω_n starts damping as the frequency increases. The purpose of adding filter is to get rid of the high frequency component caused by fast switching and keep the voltage of original frequency as it is. Therefore, the range of ω_n can be described as:

$$2\pi f < \omega_n = \sqrt{\frac{1}{L_f C_f}} < 2\pi f_s \qquad (3.17)$$

Where

f is the fundamental frequency of input voltage.

f_s is the switching frequency.

In general, the frequency of input voltage is 50/60Hz and switching frequency is higher than 10 kHz. The natural frequency of the filter is set to at least less than 1/3 of the switching frequency to filter most of the high frequency harmonics in the output voltage. To investigate the dynamic response of the proposed voltage stabiliser, the load is assumed as resistive load and ranges from 0A to 20A. With proper components value selected, the Bode diagram of the system is shown in Figure 3.9.

As it shown in Figure 3.9, the gain of system stays at 0dB at supply voltage frequency 50/60Hz and drops to -20 dB at switching frequency 10 kHz for resistive loads from 1A-20A. Therefore, the fundamental component of voltage can be fully passed on to the output whilst the high frequency harmonics with frequency higher than 10 kHz are filtered out by the LC filter.

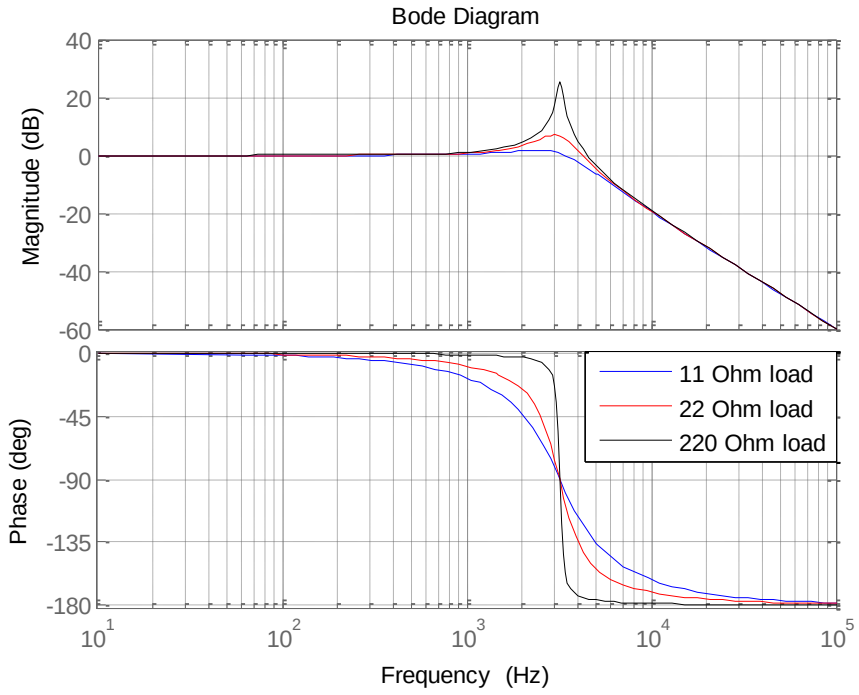

Figure 3.9 Bode diagram of the system with resistive load

3.2.2 Control Strategy

As it is shown in equation (3.12), both the input voltage and the duty ratio are considered as inputs and affect the level of output voltage. However, the input voltage is determined by the power supplier and may vary in a certain range while the duty ratio can be adjusted programmatically. Based on the above, the main objective of the control strategy is to compensate the input voltage sags and swells with fast response and small steady state error

by controlling the switches S_0-S_5. The proposed control strategy with circuit diagram is illustrated as Figure 3.10.

First of all, the operation mode is determined by comparing the input voltage and reference voltage v_{ref} . The comparison generates a logic signal which not only decides the switching state of S_0 but also the sign determiner in the feedback loop. Secondly, the output voltage is measured and then compared with reference voltage as well to obtain the voltage error.

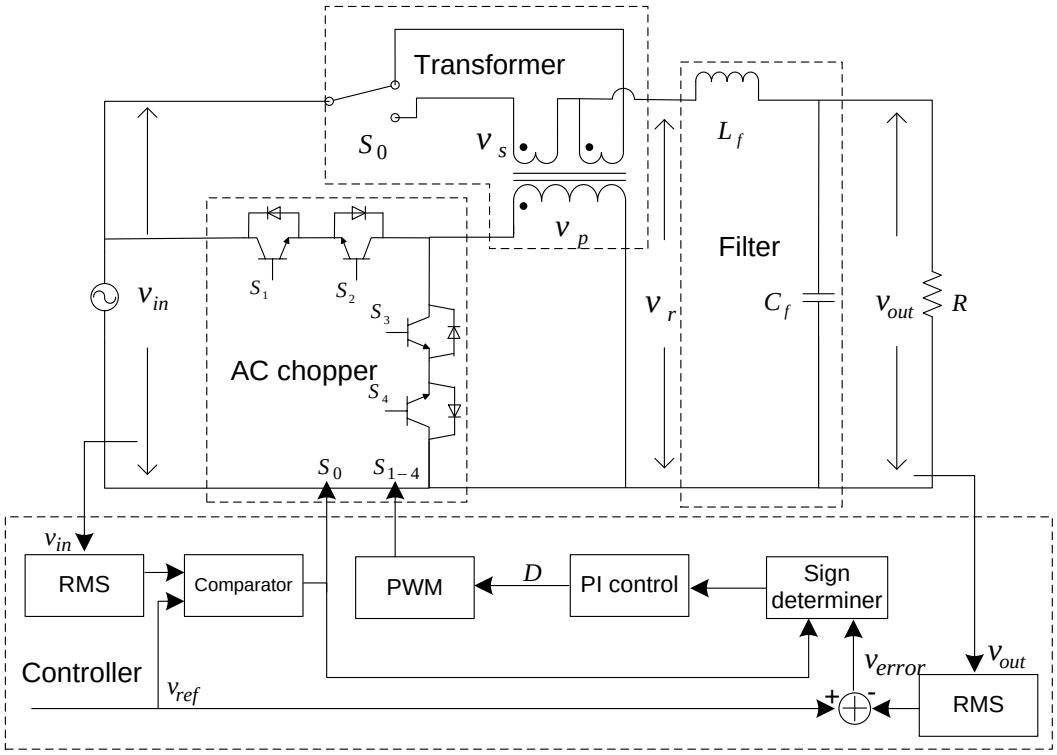

Figure 3.10 Proposed step up/down voltage stabiliser with PI control

Before being fed into the PI controller, the sign of voltage error is determined by sign determiner in different modes. In step- up mode, an increase of duty ratio is required if the voltage error is positive while the duty ratio should be reduced when error is positive in step-down mode. Therefore, the sign of gain is apparently different for different modes due to the

working principle mentioned in section II. Hence, the gain of sign determiner in s-domain can be expressed as follows:

$$K_A = \begin{cases} 1 & step\ \ up \\ -1 & step\ down \end{cases} \quad (3.18)$$

The error after sign determiner represents the absolute voltage level required to be compensated by the proposed voltage stabiliser and then this error signal is fed into a PI controller to obtain the corresponding duty ratio D. The expression of the PI controller in s-domain is represented as:

$$G_p(s) = K_p + \frac{1}{s} K_i \quad (3.19)$$

where

K_p is the proportional gain of the PI controller.

K_i is the integral gain of the PI controller.

Finally, gate signals for switches S1-S4 are generated with duty ratio D through pulse width modulation (PWM). To guarantee a good performance with rapid response and small overshoot, the best parameters of PI controller are obtained as $K_p = 9.09 * 10^{-3}$ and $K_i = 0.68$ after the tuning and trials with the closed loop model in MATLAB/Simulink, given parameters from Table 3-1.

Table 3-1 Circuit Parameters

Parameter	**Name**	**Value**	**Unit**
Turn Ratio	K	8	-
Filter capacitance	C_f	1	μF
Filter inductance	L_f	3.9	mH
Filter resistance	R_f	0.5	Ω

Input frequency	f	50	Hz
Switching frequency	f_s	20	kHz
Reference voltage	V_{ref}	220	V
Input voltage	V_{in}	220±10%	V
Load current	I_{out}	0-10	A

3.3 Simulation Results

3.3.1 Model Validation

The mathematical model with close loop feedback control is established in MATLAB/Simulink and validated with the exact same circuit model in MATLAB/Simpowersystem. The values of components are listed in Table 3-1.

Step-down Mode

The instantaneous output voltage waveform with step change of input voltage in step down mode in open circuit condition is shown in Figure 3.11 and the RMS value in same scenario is shown in Figure 3.12.

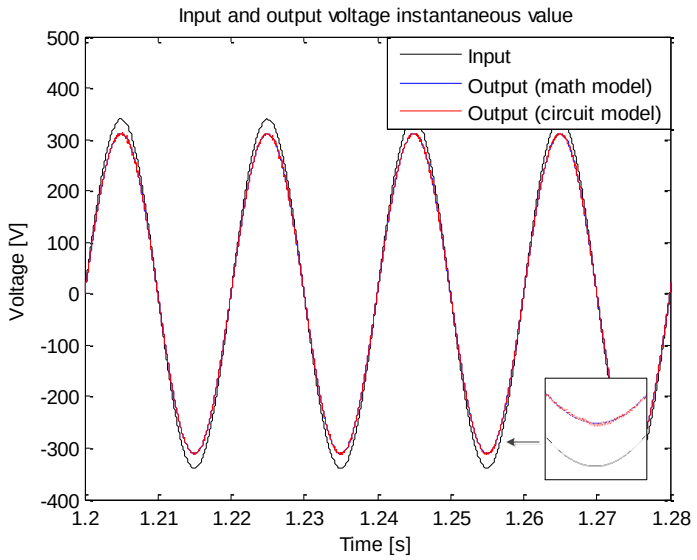

Figure 3.11 Instantaneous output voltage in step down mode

The input voltage in this scenario starts at 230V and increases 10V after 1s passes. In step down mode, the output voltage waveform is a sinusoidal waveform as Figure 3.11 shows. The mathematical model (shown as 'math model' in Figure 3.11- Figure 3. 16) gives the same results as the circuit model in terms of voltage magnitude. In circuit model simulation, some high frequency harmonics are not fully filtered out as it displayed in the zoom-in view of Figure 3.11. The total harmonic distortion of the output voltage is as tiny as 0.18%. In Figure 3.12, it can be noticed that the output voltage of both mathematical model and circuit model reach steady states after 0.2s initially. After a step change of input at 1s, the controller responses to the step change rapidly and the output drops back to its reference voltage again with several variations. The mathematical model has extremely close behaviour as the circuit model and the difference between these two models is negligible as shown in Figure 3.12.

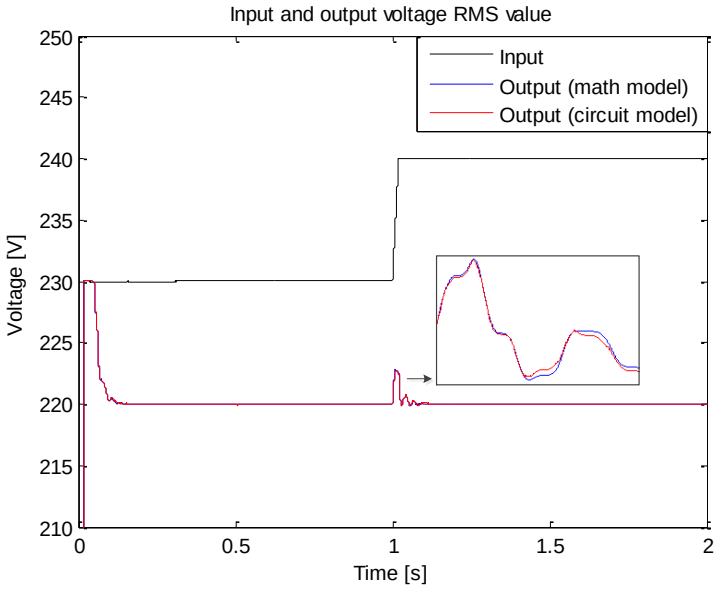

Figure 3.12 Output voltage RMS value in step down mode

Figure 3.13 illustrates the duty ratio of two models against time under the step change input.

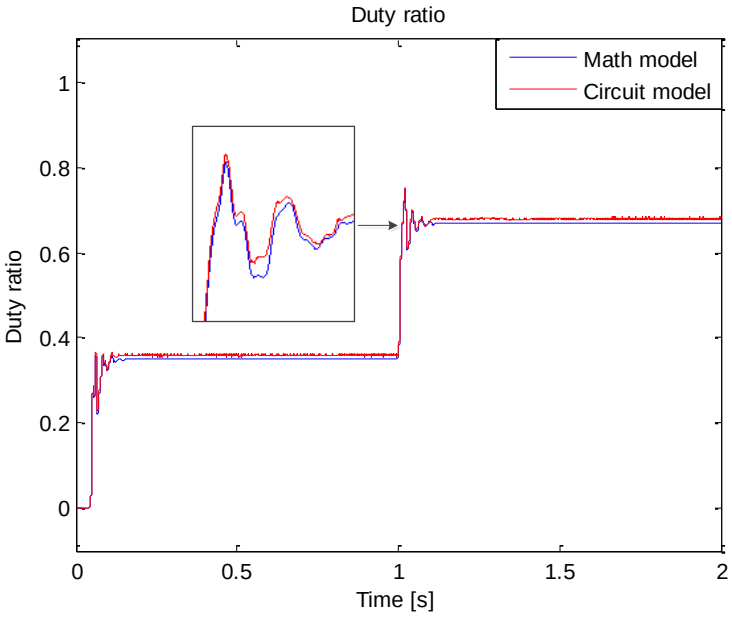

Figure 3.13 Duty ratio in step down mode

To start with, the duty ratio climbs up to reduce the voltage level after RMS value calculation initialised and achieves the reference value. Then it continues to rise up to compensate the step change in 1s and finally sets down within 5 voltage cycles. It can be noticed that the mathematical model requires less duty ratio to reach the reference value compared with circuit model since the voltage drop on the power electronic switches are not considered in mathematical model. Although the voltage drop slightly affects the output voltage, the overall error of duty ratio between two models to obtain the same reference voltage is about 1.12%.

The results show that the system has a fast response with good steady state error and the mathematical model represents the dynamic behaviour of the system properly in step down mode perfectly.

Step-up Mode

With the exact same circuit parameters, the input voltage starts at 200V and a 10V step up change afterwards. The output and input instantaneous voltages of both mathematical model and circuit model are shown as Figure 3.14

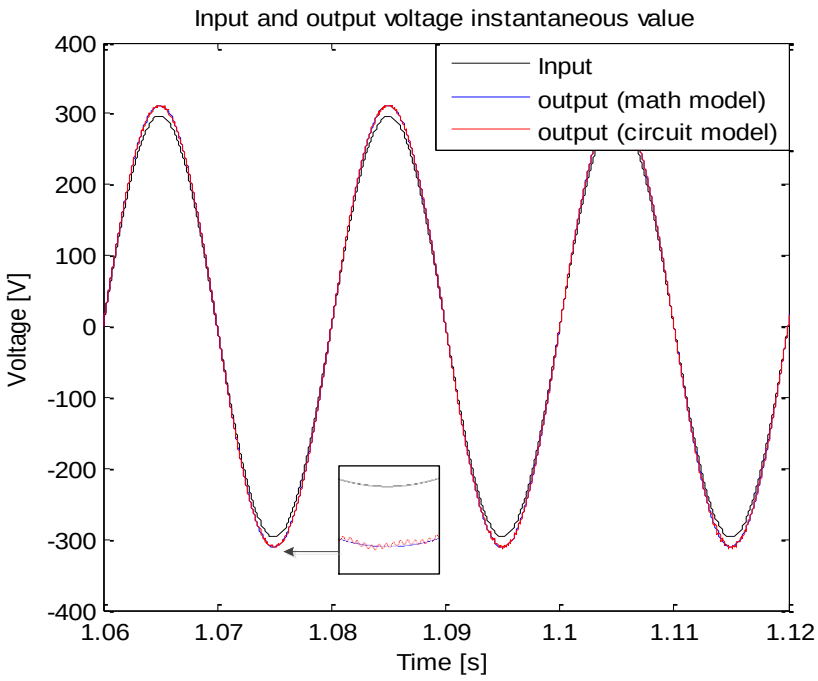

Figure 3.14 Instantaneous output voltage in step up mode

Since the input is smaller than the reference voltage, the system works in step up mode. As is shown in Figure 3.14, the output voltage of the mathematical model has an excellent sinusoidal shape and a slightly larger magnitude compared with the input voltage. It is in good agreement with the output voltage of the circuit model despite of tiny oscillation observed in the circuit model. The outputs of both models are initialised as 200V in the first voltage cycle, which is 0.02s in this case, as Figure 3.15 illustrates.

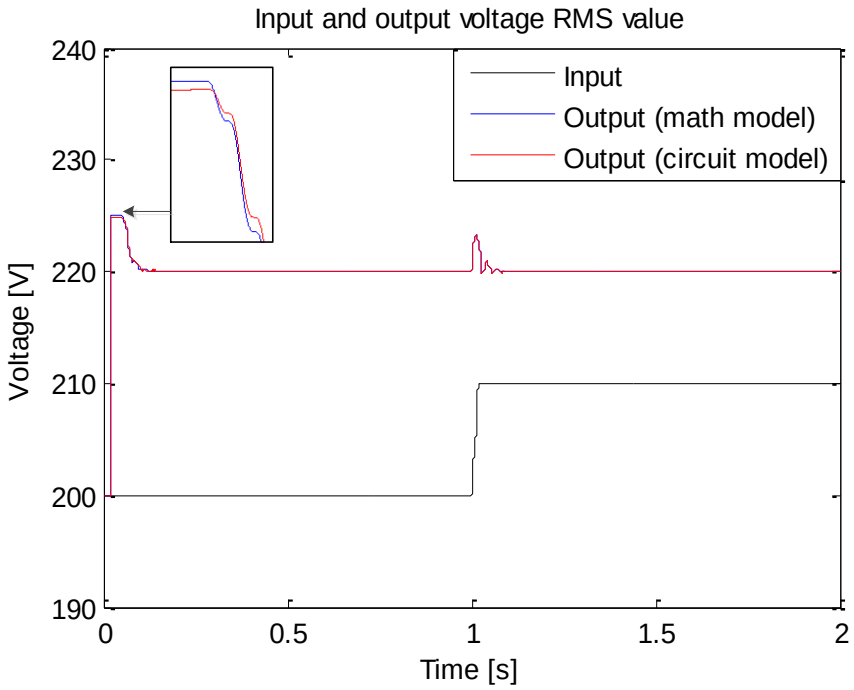

Figure 3.15 Output voltage RMS value in step up mode

Then the controller is engaged and starts to minimise the error between the reference and the output. The system reaches steady state with an error less than 0.05V in 0.15s. The output of the mathematical model has exact same tendency with the output of the circuit model and an error within 0.1V between each other is observed in transient process. After the system sets down, the error is negligible and outputs of the two models overlap as input remains 210V.

The duty ratio in Figure 3.16 demonstrates that it begins at 1 and drops gradually to meet the voltage reference, finally reach its steady error at the same time as the voltage does. When a 10V voltage step up change is applied in 1s, the gap between reference voltage and input is reduced by the same amount. Therefore, less voltage level is required to compensate the gap. Figure 3.16 illustrates the controller begins to reduce the duty ratio in order to eliminate this gap. After having several oscillations, duty ratio stabilises at 0.38 as the new steady state. As the zoomed-in view in Fig. 14 shows, the error of duty ratio between mathematical model and circuit model is within 0.01. Likewise, the error eliminates when the system reaches steady

state. The output voltage has some variations as the duty ratio oscillates when the input voltage increases and then drops back to the reference voltage 220V.

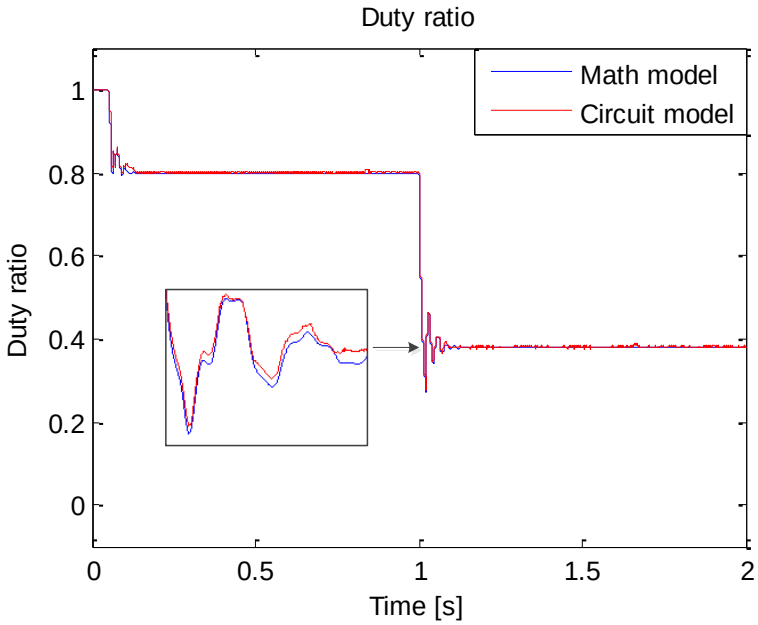

Figure 3.16 Duty ratio in step up mode

Above all, it can be concluded that the mathematical model describes the behaviour of the proposed step up/down voltage stabiliser accurately. In addition, it also demonstrates that the applied controller is able to maintain the voltage level with fast response without steady state error under step change input condition in both step up and step down mode, while limiting the transient within an acceptable range.

3.3.2 Simulation with Different Loads

The mathematical model is also verified with different types of loads, namely resistive load, inductive load and non-linear load in step down mode. With real input voltage profile, a step change applies to each load during the operation process to investigate the behaviour of the proposed voltage stabiliser.

Operation with Resistive Load

Figure 3.17 illustrates the input and the output instantaneous voltage values with a step changed resistive load as follows:

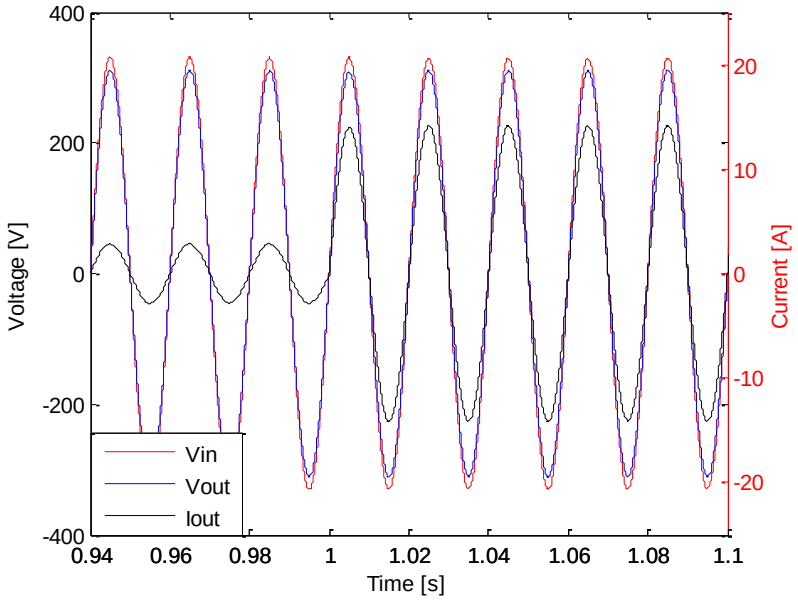

Figure 3.17 Voltage and current instantaneous values of the system with PI controller under resistive load

Since the input voltage is higher than the voltage reference, the output voltage keeps the perfect sinusoidal shape with a reduced magnitude. Although a step change of the load occurs at 1s, the controller is still able to restore the output voltage within a short period of time. As it shown in Figure 3.18, the input voltage RMS value has small variation over time while the out voltage is regulated around the reference voltage value 220V. A sudden drop of output voltage can be observed when the load current raises up at 1 seconds and it reduces to the reference value rapidly with the engagement of controller.

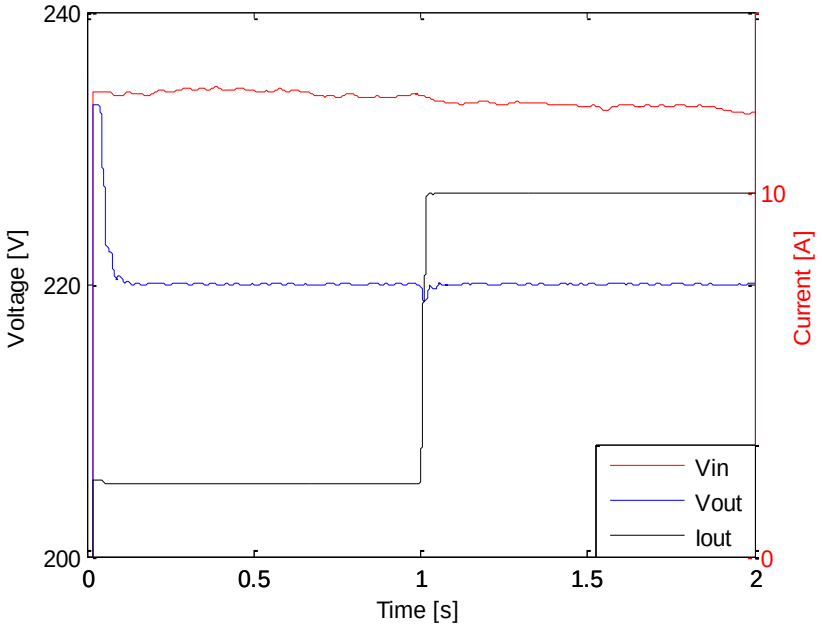

Figure 3.18 Voltage and current RMS values of the system with PI controller under resistive load

Operation with Inductive Load

Figure 3.19 shows the voltage and current instantaneous value when a step changed inductive load is connected. A phase difference between the output voltage and current can be noticed while the output voltage is an excellent sinusoidal shape and in phase with the input voltage.

When the inductive load increases from 2.7A to 9.4A at 1s, the voltage starts to drop slightly and then rises up to the reference value again with settling time as short as 0.1s, which is illustrated in Figure 3.20. It also demonstrates that the proposed voltage stabiliser is capable of providing good waveform quality with fast response and short settling time for inductive load.

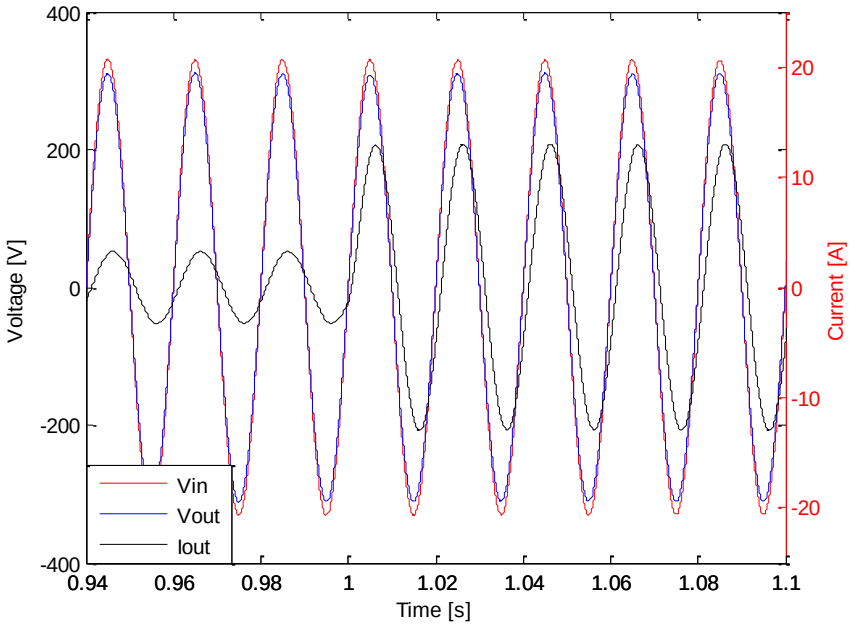

Figure 3.19 Voltage and current instantaneous values of the system with PI controller under inductive load

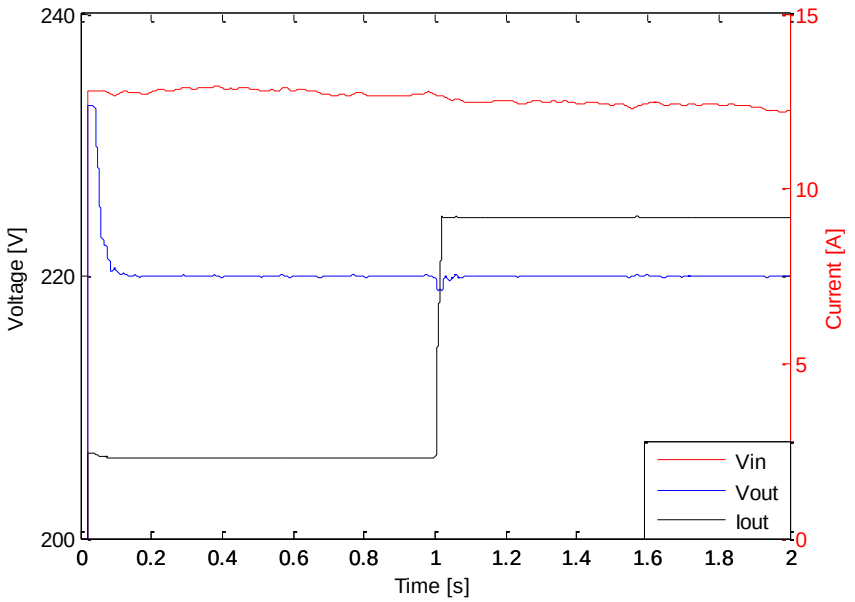

Figure 3.20 Voltage and current RMS values of the system with PI controller under inductive load

Operation with Non-linear Load

Figure 3.21 illustrates the input voltage, output voltage and current instantaneous values for operation with non-linear load. Although the load current is highly distorted, the output voltage displays a sinusoid shape with an extremely low harmonic distortion (0.27%) before the step change at 1s. After the current rises up, the distortion increases to 1.64% and is still with the 5% limit of the standard IEEE 519/92. In terms of the output voltage level, the system experiences a tiny variation when the load goes up at 1s and finally stabilises at the reference value as it can be observed in Figure 3.22.

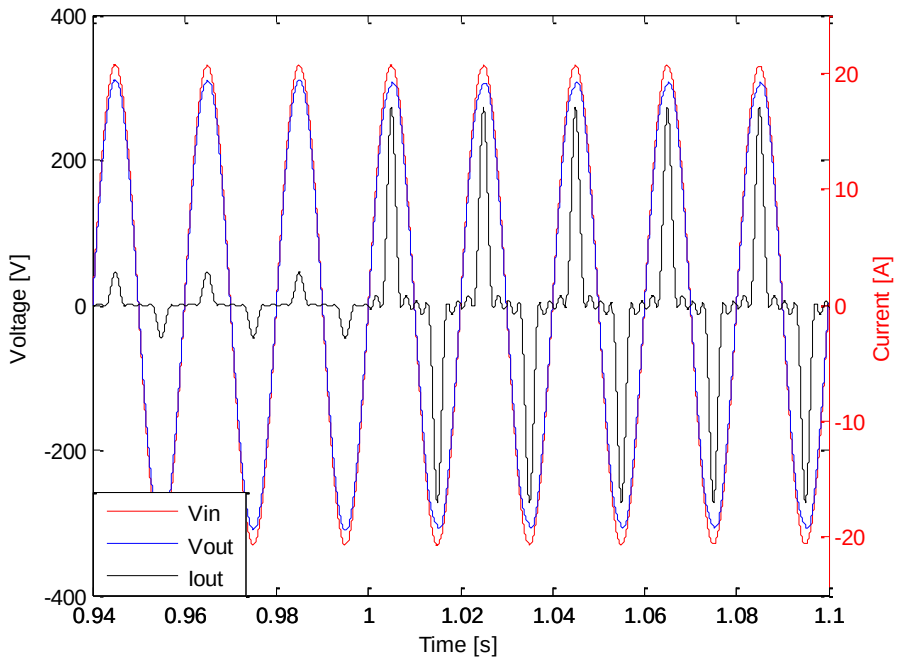

Figure 3.21 Voltage and current instantaneous values of the system with PI controller under non-linear load

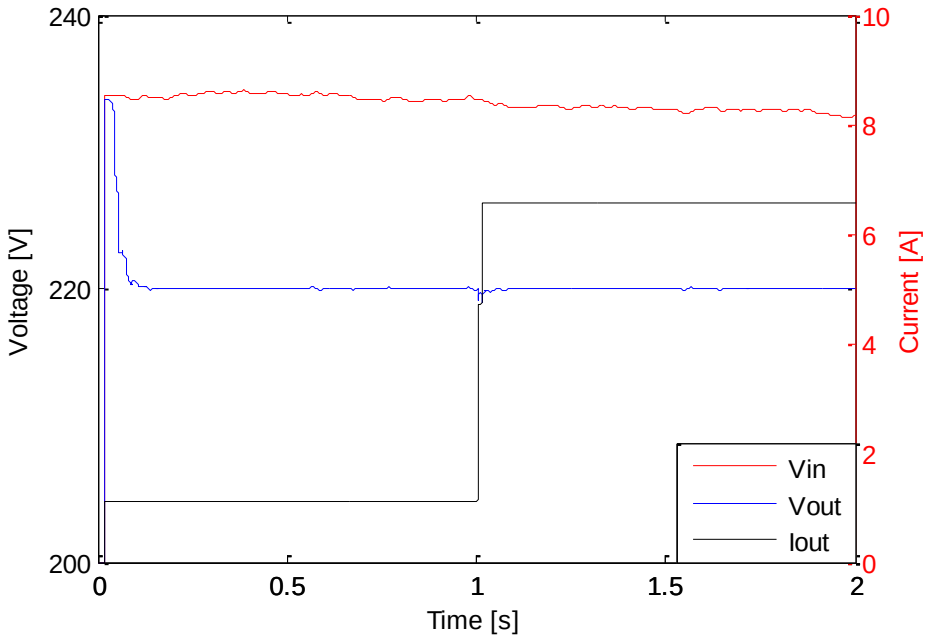

Figure 3.22 Voltage and current RMS values of the system with PI controller under non-linear load

3.4 Implementation & Experiments Results

A prototype based on the proposed topology has been implemented and tested with closed loop control. The parameter of main components is shown as Table 3-1. The cut-off frequency of the applied LC filter is about 1/10 of the switching frequency to ensure the unwanted high frequency harmonics being filtered out properly. The bidirectional switches are made up of two HGTG5N120BND insulated gate bipolar transistors (IGBTs) from Fairchild. Each pair of two IGBTs (21A, 1200V) is connected in emitter to emitter configuration. The dead time of commutation is set as 1μs.

The input voltage, output voltage and output current are measured and logged at 100 kHz for a resistive load step change scenario experiments in step down mode by using National Instruments (NI) data acquisition system. Meanwhile, the chopped voltage on the primary winding of the transformer and switching sequence are observed by using oscilloscope at 100

MHz in order to investigate the switching process of the proposed voltage stabiliser. The implemented hardware along with the measurement connection is shown as Figure 3.23:

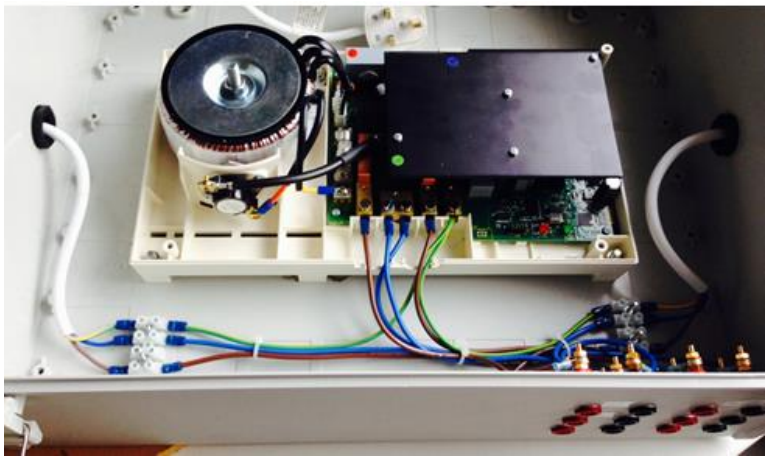

Figure 3.23 Picture of implemented hardware with measurement connection.

Figure 3.24 illustrates the chopped voltage on the primary winding. It can be observed that this voltage is equal to either the input voltage in active state or tiny voltage level in freewheeling state, which is in exact agreements with working principle.

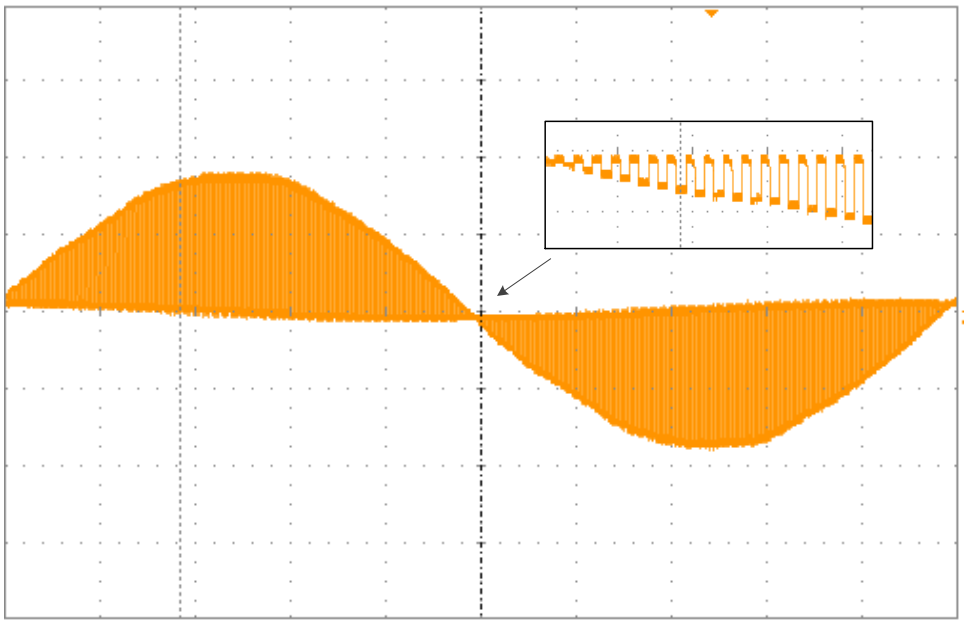

Figure 3.24 Chopped voltage on the primary winding of transformer

In addition, the turn-on resistance of IGBTs leads to some voltage drop on the switches therefore the voltage on primary winding is not exactly zero in freewheeling state as it can be also noticed in Figure 3.24.

The instantaneous input voltage, output voltage and output current are illustrated in Figure 3.25. The output voltage demonstrates a good sinusoidal shape and it is in phase with the input voltage with slight reduced amplitude. As a resistive load is connected in this scenario, no phase delay can be observed between the current waveform and voltage waveform in Figure 3.25. When the load increases from 2.5A to 6A, the output voltage also keeps an excellent sinusoidal shape and in phase with the input voltage.

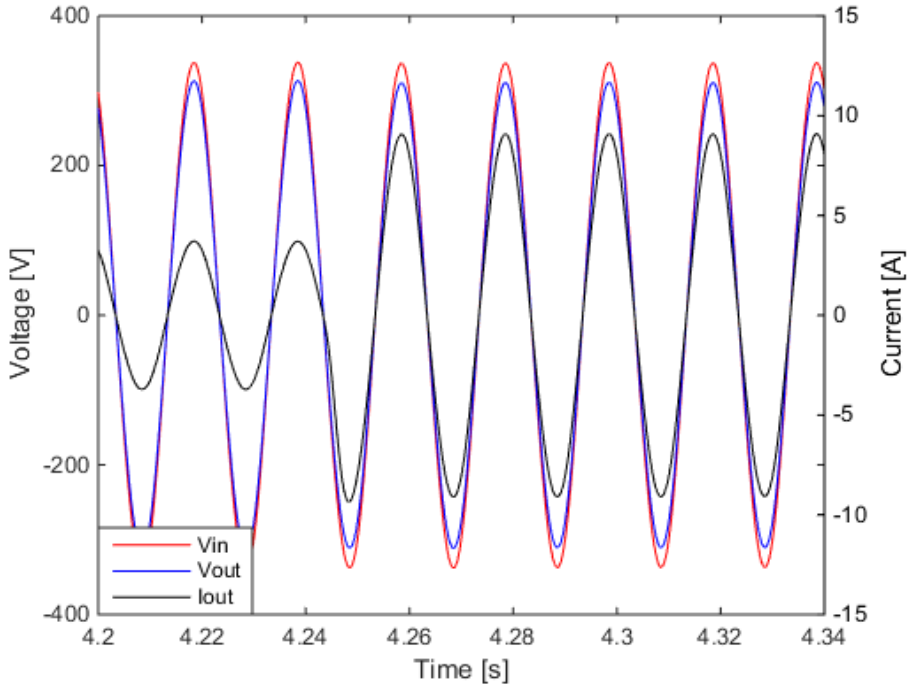

Figure 3.25 Experiments results of input voltage, output voltage and current RMS values.

Figure 3.26 shows the RMS values of input voltage, output voltage and current in long time period. It can be observed that the input voltage fluctuates slightly over time while the output voltage is always controlled to reach the reference voltage during the entire experiment. In

the beginning, the output voltage is equal to the input voltage before the controller engaged. When the controller starts to operate, the output voltage keep reducing for a while and then reach 220V with a duty ratio 0.52 as shown in zoomed area of Figure 3.25. After the step change of the load occurs, the output drops instantly and then the controller plays its role again to raise the voltage up to 220V. As it shown in Figure 3.25, the duty ratio reduces to 0.47 to maintain the output voltage as the reference after the load increases.

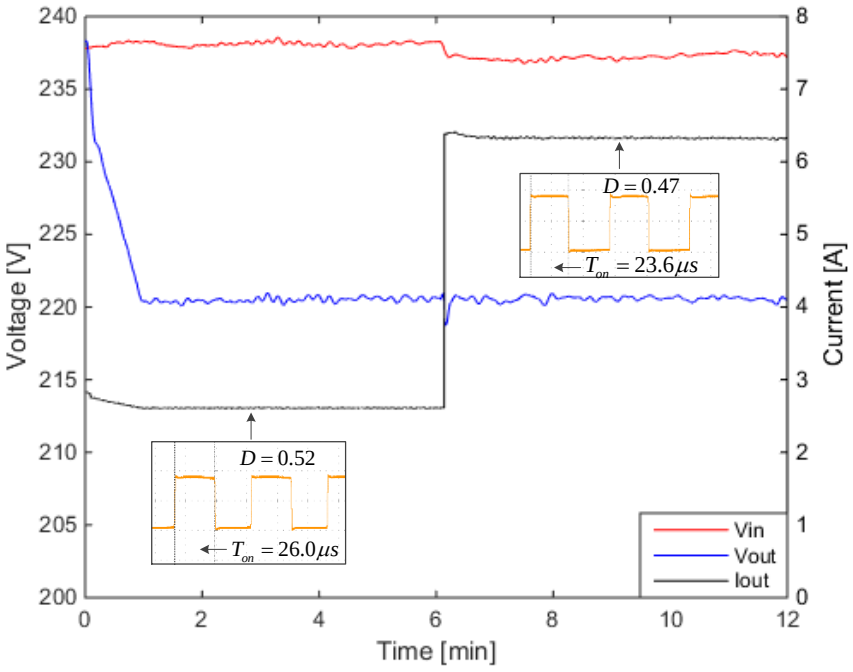

Figure 3.26 Experiments results of input voltage, output voltage and current RMS values.

3.5 Summary

This chapter describes a topology of step up/down voltage stabiliser which combines a conventional PWM AC converter with a multi-windings transformer to optimise voltage. Compared with the conventional topology, this topology is capable of not only reducing the output voltage level but also increasing the output whenever required. A switch S0 is dedicated to control the proposed voltage stabiliser to operate either in step-down or step-up

mode. Furthermore, the connection of the transformer splits the total current into two branches, namely main current loop with the load and the inner current loop with primary winding of the transformer. Hence, only a fraction of total current flows through the IGBTs. To achieve the same power rating as the conventional topology, the proposed voltage stabiliser requires IGBTs with less current rating, which results in large reduction on manufacturing cost and the size.

Meanwhile, the open loop mathematical model of the proposed voltage stabiliser is established and then a control strategy based on PI-controller is designed for regulating the output voltage level. The first step of controlling the proposed voltage stabiliser is to decide the operating mode of it. Therefore, a sign determiner is applied into the control strategy. With the operating mode decision mechanism, a PI controller is then introduced to eliminate the error between the output voltage and the reference voltage. This close loop mathematical model with the designed controller is validated with the circuit model through simulation in MATLAB. The results demonstrate that the mathematical model is in excellent agreement with the circuit model. At last, the close loop system is also simulated with different typed of loads, which includes resistive, inductive and non-linear loads. The simulation results show that the proposed voltage stabiliser along with the controller works properly with all types of loads from 0A to around 10A

Finally, a prototype with 20A current rating and 220V voltage rating is implemented and then tested with a step changed resistive load in step-down mode. Although the controller is tuned slower than the simulation work in this real implementation, the results are still very promising and it can be concluded that the proposed step up/down voltage stabiliser works perfect both theoretically and experimentally and is an excellent variant for voltage regulation in household level in terms of cost reduction and flexibility.

Chapter 4 Modelling and Control of Voltage Stabiliser by DQ Transformation

This chapter introduces the modelling work and control design of the proposed voltage stabiliser in dq rotating reference frame. A fictive axis is assumed running alongside with the original system to create a stationary ab reference frame. Then, the model is transformed from ab reference frame to dq rotating reference frame and linearized under dq reference frame. Finally, an LQR control strategy is designed for the linearized system and the performance of the closed loop system is verified through simulation.

4.1 Introduction

Although the mathematical model established in last chapter is able to present the behaviour of the proposed voltage stabiliser, it is difficult to be used for designing controller analytically due to the following reasons:

- The output voltage is sinusoidal both in steady states and transients.
- The input voltage can be considered as an input variable with disturbance of variable magnitudes and it is sinusoidal both in steady states and transients.
- The load current depends on the load type and is unpredictable.
- The duty ratio, as control input, is varying based on the variations of the input voltage and the load current, which brings the nonlinearity into the system.
- The duty ratio is bounded between 0 and 1.

Since all the variables in the system are sinusoidal waves with fixed frequency and the control purpose is to regulate the magnitude of output voltage, the dq transformation can be

utilized to transform the model and make it easier for theoretical analysis and controller design.

One of the challenges is that the system is single phase while dq transformation requires at least 2 phases. Therefore, fictive axis emulation method is introduced to solve this problem in (Rufer et al. 2009). Basically, it assumes a fictive circuit runs in parallel along the actual circuit. All the variables in this fictive circuit (marked with index 'b') are shifted 90 degree compared to the variables in actual circuits (marked with index 'a'). Therefore, a two-phase system is established and then transformed into dq rotating reference frame. The block diagram of the dq transformation is shown as Figure 4.1

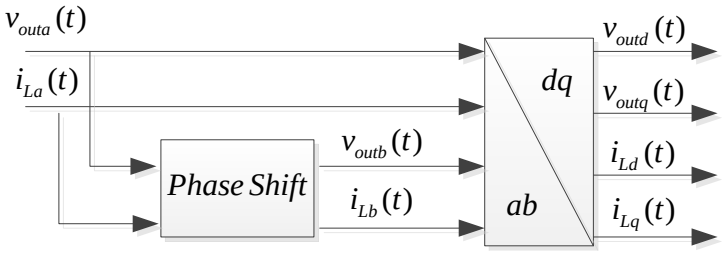

Figure 4.1 Block diagram of dq transformation with fictive axis (Rufer et al. 2009)

4.2 Model Transformation

In order to describe the relationship of the output current in 'a' axis, the equation (3.5) can be rewritten as:

$$i_{La}(t) = C_f \frac{dv_{outa}(t)}{dt} + i_{outa}(t) \qquad (4.1)$$

where

i_{La} is inductor current in 'a' axis.

v_{outa} is output voltage in ‘a’ axis.

i_{outa} is the load current in ‘a’ axis.

Likewise, the corresponding equation of (3.5) in ‘b’ axis is obtained as:

$$i_{Lb}(t) = C_f \frac{dv_{outb}(t)}{dt} + i_{outb}(t) \qquad (4.2)$$

where

i_{Lb} is inductor current in ‘b’ axis.

v_{outb} is output voltage in ‘b’ axis.

i_{outb} is the load current in ‘b’ axis.

Then the equation (3.5) for two-phase system can be put into a complex form as:

$$i_{Lab}(t) = C_f \frac{dv_{outab}(t)}{dt} + i_{outab}(t) \qquad (4.3)$$

where

$i_{Lab}(t) = i_{La}(t) + ji_{Lb}(t)$, $v_{outab}(t) = v_{outa}(t) + jv_{outb}(t)$ and $i_{outab}(t) = i_{outa}(t) + ji_{oub}(t)$

Introduce dq orthogonal reference frame rotating with the velocity equal to the angular frequency ω of input voltage v_{in}. Therefore, any vector in the ab stationary reference frame can be transformer to the dq rotating reference frame through rotating it by angle $-\theta$, where θ is the angle between the dq and ab frames and $d\theta/dt = \omega$. Inductor current i_{Lab} can be transformed into dq rotating reference frame as:

$$i_{Ldq}(t) = i_{Lab}(t) * e^{-j\theta} \quad (4.4)$$

where

$$i_{Ldq}(t) = i_{Ld}(t) + j i_{Lq}(t)$$

i_{Ld} and i_{Lq} are the output voltage in 'd' axis and 'q' axis respectively

The relationship of ab frame and dq frame is shown as

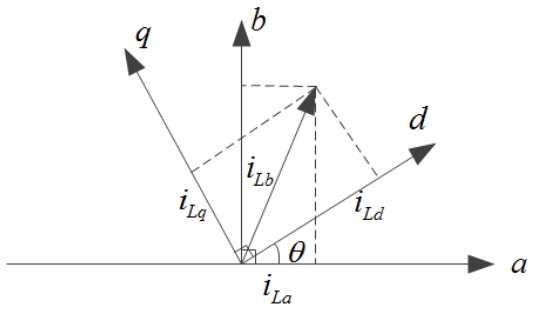

Figure 4.2 Diagram of ab frame and dq frame

Considering that $e^{-j\theta} = \cos\theta - j\sin\theta$, the equation (4.4) can be rewritten and put into vector form as:

$$\begin{bmatrix} i_{Ld}(t) \\ i_{Lq}(t) \end{bmatrix} = \begin{bmatrix} \cos\theta & \sin\theta \\ -\sin\theta & \cos\theta \end{bmatrix} \begin{bmatrix} i_{La}(t) \\ i_{Lb}(t) \end{bmatrix} \quad (4.5)$$

Note that the transformation between ab reference frame and dq reference frame can be applied to all the variables in this two-phase system. Therefore, the following can be obtained:

$$v_{outdq}(t) = v_{outab}(t) * e^{-j\theta} \quad (4.6)$$

$$i_{outdq}(t) = i_{outab}(t) * e^{-j\theta} \quad (4.7)$$

where

$v_{outdq}(t) = v_{outd}(t) + jv_{outq}(t)$ and $i_{outdq}(t) = i_{outd}(t) + ji_{outq}(t)$

v_{outd} and v_{outq} are the output voltage in 'd' axis and 'q' axis respectively

i_{outd} and i_{outq} are the input voltage in 'd' axis and 'q' axis respectively

Based on equation (4.7), the derivative of v_{outab} can be derived as:

$$\begin{aligned}\frac{dv_{outab}(t)}{dt} &= \frac{d(v_{outdq}(t)e^{j\theta})}{dt} = \frac{dv_{outdq}(t)}{dt}e^{j\theta} + v_{outdq}(t)\frac{d(e^{j\theta})}{dt} \\ &= \frac{dv_{outdq}(t)}{dt}e^{j\theta} + v_{outdq}(t)e^{j\theta} j\frac{d\theta}{dt} \\ &= e^{j\theta}(\frac{dv_{outdq}(t)}{dt} + v_{outdq}(t) j\frac{d\theta}{dt})\end{aligned} \qquad (4.8)$$

Note that $d\theta / dt = \omega$ and substitute equation (4.6), (4.7) and (4.8) into equation (4.3), it can be transformed in dq reference frame as:

$$i_{Ldq}(t) = C_f(\frac{dv_{outdq}(t)}{dt} + v_{outdq}(t) j\omega) + i_{outdq}(t) \qquad (4.9)$$

Rearrange the real and imaginary parts in equation (4.9) and convert them into matrix form as:

$$\begin{bmatrix} i_{Ld}(t) \\ i_{Lq}(t) \end{bmatrix} = C_f \frac{d}{dt}\begin{bmatrix} v_{outd}(t) \\ v_{outq}(t) \end{bmatrix} + C_f\omega\begin{bmatrix} 0 & -1 \\ 1 & 0 \end{bmatrix}\begin{bmatrix} v_{outd}(t) \\ v_{outq}(t) \end{bmatrix} + \begin{bmatrix} i_{outd} \\ i_{outq} \end{bmatrix} \qquad (4.10)$$

Based on the derivation in Chapter 3, the relationship of output voltage, input voltage and duty ratio in 'a' axis can be rewritten as:

$$v_{outa}(t) = v_{ina}(t)(1 \pm \frac{D(t)}{k}) - L_f\frac{di_{La}(t)}{dt} + i_{La}(t)R_f \qquad (4.11)$$

where

v_{ina} is the input voltage in ‘a’ axis

Since $D(t)$ is a scalar rather than a vector, it is same in both ‘a’ axis and ‘b’ axis. Therefore, the relationship of equation (4.11) in ‘b’ axis can be obtained as:

$$v_{outb}(t) = v_{inb}(t)(1 \pm \frac{D(t)}{k}) - L_f \frac{di_{Lb}(t)}{dt} + i_{Lb}(t)R_f \qquad (4.12)$$

where

v_{inb} is the input voltage in ‘b’ axis.

Based on the equation (4.11) and (4.12), the relationship of output voltage and input voltage can in ab reference frame is obtained as:

$$v_{outab}(t) = v_{inab}(t)(1 \pm \frac{D(t)}{k}) - L_f \frac{di_{Lab}(t)}{dt} + i_{Lab}(t)R_f \qquad (4.13)$$

where

$v_{inab}(t) = v_{ina}(t) + jv_{inb}(t)$

Since the dq transformation can be also applied to input voltage $v_{in}(t)$, the input voltage in dq reference frame is obtained as:

$$v_{inab}(t) = v_{indq}(t) * e^{-j\theta} \qquad (4.14)$$

where

$v_{indq}(t) = v_{ind}(t) + jv_{inq}(t)$

v_{ind} and v_{ind} is the input voltage in 'd' axis and 'q' axis respectively

Based on equation (4.14), the derivation of inductor current i_L can be derived as:

$$\begin{aligned}\frac{di_{Lab}(t)}{dt} &= \frac{d(i_{Ldq}(t)e^{j\theta})}{dt} = \frac{di_{Ldq}(t)}{dt}e^{j\theta} + i_{Ldq}(t)\frac{d(e^{j\theta})}{dt} \\ &= \frac{di_{Ldq}(t)}{dt}e^{j\theta} + i_{Ldq}(t)e^{j\theta}\, j\frac{d\theta}{dt} \\ &= e^{j\theta}(\frac{di_{Ldq}(t)}{dt} + i_{Ldq}(t)\, j\frac{d\theta}{dt})\end{aligned} \qquad (4.15)$$

Substituting equation (4.3), (4.6), (4.14) and (4.15) into equation (4.13) and rearrange, it can be transformed into dq reference frame as:

$$v_{outdq}(t) = v_{indq}(t)(1-\frac{D(t)}{k}) - L_f(\frac{di_{Ldq}(t)}{dt} + j\omega i_{Ldq}(t)) + i_{Ldq}(t)R_f \qquad (4.16)$$

Separate the real part and imaginary part of equation (4.16) and it can be obtained:

$$\begin{bmatrix} v_{out,d}(t) \\ v_{out,q}(t) \end{bmatrix} = \begin{bmatrix} v_{in,d}(t) \\ v_{in,q}(t) \end{bmatrix}(1\pm\frac{D(t)}{k}) - L_f\frac{d}{dt}\begin{bmatrix} i_{L.d}(t) \\ i_{L,q}(t) \end{bmatrix} - L_f\omega\begin{bmatrix} 0 & -1 \\ 1 & 0 \end{bmatrix}\begin{bmatrix} i_{L.d}(t) \\ i_{L_q}(t) \end{bmatrix} + \begin{bmatrix} i_{L.d}(t) \\ i_{L,q}(t) \end{bmatrix}R_f \qquad (4.17)$$

As it is shown in equation (4.10) and (4.17), all the variables are transformed into 'dq' reference frame and an additional term ω is introduced into the equations. In steady state, the components in 'dq' reference frame are all constant rather than sinusoidal value as in 'ab' reference frame.

Combine equation (4.10) and (4.17) together, the mathematical model in 'dq' reference frame is expressed in state space form as:

$$\dot{\mathbf{X}} = \mathbf{A}\mathbf{X} + \mathbf{B}u + \mathbf{W} \qquad (4.18)$$

where

$$\mathbf{X} = \left[v_{outd}(t)\, v_{outq}(t)\, i_{Ld}(t)\, i_{Lq}(t) \right]^T \text{ and } u = D(t)$$

$$\mathbf{A} = \begin{bmatrix} 0 & \omega & \frac{1}{C_f} & 0 \\ -\omega & 0 & 0 & \frac{1}{C_f} \\ \frac{-1}{L_f} & 0 & \frac{-R_f}{L_f} & \omega \\ 0 & \frac{-1}{L_f} & -\omega & \frac{-R_f}{L_f} \end{bmatrix} \text{ and } \mathbf{B} = \begin{bmatrix} 0 \\ 0 \\ \frac{\pm v_{ind}}{kL_f} \\ \frac{\pm v_{inq}}{kL_f} \end{bmatrix}$$

$$\mathbf{W} = \begin{bmatrix} -\frac{1}{C_f} & 0 \\ 0 & -\frac{1}{C_f} \\ 0 & 0 \\ 0 & 0 \end{bmatrix} \begin{bmatrix} i_{outd} \\ i_{outq} \end{bmatrix} + \begin{bmatrix} 0 & 0 \\ 0 & 0 \\ \frac{1}{L_f} & 0 \\ 0 & \frac{1}{L_f} \end{bmatrix} \begin{bmatrix} v_{ind} \\ v_{inq} \end{bmatrix}$$

Note that taking $\omega = 0$ in equation (4.18) gives the model in ‘ab’ reference frame.

The approach from (Rufer et al. 2009) introduces a decoupling control to make the d and q axes equations independent. Inspired by the methodology reported in (Rufer et al. 2009), a new solution with simplified dq model and new control input is introduced in this work.

Align the d-q reference frame with the output voltage vector, and then it can be obtained that:

$$v_{outd} = |v_{out}|, v_{outq} = 0, \dot{v}_{outq} = 0 \qquad (4.19)$$

where

$|v_{out}|$ is the magnitude of the actual single phase output voltage.

Note that the magnitudes of any vector in dq and ab reference frame is the same and it is equal to the multiplication between its RMS value and $\sqrt{2}$. Since $v_{outq} = 0$, this variable v_{outq} and the second equation can be ignored. The order of the state space model is reduced by 1. The first equation can be also simplified as:

$$\frac{dv_{outd}}{dt} = \frac{1}{C_f} i_{Ld} - \frac{1}{C_f} i_{outd} \qquad (4.20)$$

The second equation of (4.18) in the accepted reference frame also gives the following algebraic equation for relating i_{Lq} to the output voltage and current.

$$i_{Lq} = C_f \omega v_{outd} + i_{outq} \qquad (4.21)$$

It can be noticed that the fourth differential equation in (4.18) also describes the relationship of i_{Lq} with the output voltage and current. This equation and equation (4.21) contradict each other, therefore only one of them should be included in the model. Considering algebraic equation (4.21) can reduce the order of (4.18) by 1 again. Therefore, substitute equation (4.21) into the third equation and it can be obtained as:

$$\frac{di_{Ld}}{dt} = -\frac{1}{L_f} v_{outd} - \frac{R_f}{L_f} i_{Ld} + \left(C_f \omega v_{outd} + i_{outq} \right) \omega \pm \frac{v_{ind}}{kL_f} u + \frac{1}{L_f} v_{ind} \qquad (4.22)$$

Finally, the original fourth order state space model can be simplified by combing equation (4.20) and (4.22) and rewritten as:

$$\dot{\mathbf{X}}_1 = \mathbf{A}_1 \mathbf{X}_1 + \mathbf{B}_1 u + \mathbf{W}_1 \qquad (4.23)$$

Where

$\mathbf{X}_1 = \begin{bmatrix} v_{outd} & i_{Ld} \end{bmatrix}^T$

$$\mathbf{A_1} = \begin{bmatrix} 0 & \frac{1}{C_f} \\ C_f\omega^2 - \frac{1}{L_f} & \frac{-R_f}{L_f} \end{bmatrix},\ \mathbf{B_1} = \begin{bmatrix} 0 \\ \frac{\pm v_{ind}}{kL_f} \end{bmatrix}, \text{ and } \mathbf{W_1} = \begin{bmatrix} \frac{-1}{C_f} & 0 \\ 0 & \omega \end{bmatrix} \begin{bmatrix} i_{outd} \\ i_{outq} \end{bmatrix} + \begin{bmatrix} 0 \\ \frac{1}{L_f} \end{bmatrix} v_{ind}$$

In the real implementation, the parameters of the filter are chosen in such way to provide a negligible phase shift between the input and output vector. Therefore, for control purpose it can be assumed that $v_{ind} = |v_{in}|$.

4.3 Control Design

The goal of the control is to adjust automatically the duty ratio to stabilise the output voltage magnitude (or RMS value v_{ref}) at rated value in presence of disturbances due to changes of the magnitude of the grid voltage and the voltage drop on the filter as the result of the load change.

Model (4.23) allows straightforward application of theoretical control methodologies to design the voltage controller in the d-q reference frame with improved performance and robustness. In this work, a linear-quadratic regulator (LQR) is applied based on the second order state space model as in (4.23).

Although $|v_{in}|$ varies within a small range, the input voltage variation from grid side is slow compared with the control action and the change of magnitude is fairly small. Therefore, the following new control input u' is introduced to linearize the system.

$$u = \frac{u'}{|v_{in}|} \qquad (4.24)$$

Define v_{outd} and i_{Ld} as state variables x_1 and x_2. Taking the operation of step down mode as an example, the sign in matrix $\mathbf{B_1}$ can be determined as negative. The equation (4.23) with new control input can be rewritten as:

$$\begin{bmatrix} \dot{x}_1 \\ \dot{x}_2 \end{bmatrix} = \begin{bmatrix} 0 & \frac{1}{C_f} \\ C_f\omega^2 - \frac{1}{L_f} & \frac{-R_f}{L_f} \end{bmatrix} \begin{bmatrix} x_1 \\ x_2 \end{bmatrix} + \begin{bmatrix} 0 \\ \frac{-1}{kL_f} \end{bmatrix} u' + \begin{bmatrix} \frac{-1}{C_f} & 0 \\ 0 & \omega \end{bmatrix} \begin{bmatrix} i_{outd}(t) \\ i_{outq}(t) \end{bmatrix} + \begin{bmatrix} 0 \\ \frac{|v_{in}|}{L_f} \end{bmatrix} \qquad (4.25)$$

To obtain a zero steady state control error, an additional state coordinate and a corresponding equation are introduced into the model as an integral of the voltage magnitude control error as follows:

$$x_3 = \int_0^t (x_1 - x_{ref})dt \qquad (4.26)$$

where

$$x_{ref} = v_{ref} * \sqrt{2}$$

Combine equation (4.25) and (4.26), the augmented state space model is expressed as:

$$\dot{\mathbf{X}}_\mathbf{2} = \mathbf{A}_2\mathbf{X}_2 + \mathbf{B}_2 u' + \mathbf{W}_3 \qquad (4.27)$$

where

$$\mathbf{X_2} = [x_1 \quad x_2 \quad x_3]^T \cdot \mathbf{A}_2 = \begin{bmatrix} 0 & \frac{1}{C_f} & 0 \\ C_f\omega^2 - \frac{1}{L_f} & \frac{-R_f}{L_f} & 0 \\ 1 & 0 & 0 \end{bmatrix}, \mathbf{B}_2 = \begin{bmatrix} 0 \\ \frac{-1}{kL_f} \\ 0 \end{bmatrix} \text{ and } \mathbf{W}_2 = \begin{bmatrix} \frac{-i_{outd}}{C_f} \\ \omega i_{outq} + \frac{|v_{in}|}{L_f} \\ 0 \end{bmatrix}$$

Based on equation (4.27), the quadratic performance index can be defined as:

$$J = \frac{1}{2}\int (\mathbf{X}^{\mathbf{T}}\mathbf{Q}\mathbf{X} + \mathbf{u}^{\mathbf{T}}\mathbf{R}\mathbf{u})\,\mathrm{dt} \qquad (4.28)$$

where

$\mathbf{Q}$ and $\mathbf{R}$ are the matrices of positive symmetric weighting, expressed as diagonal matrices.

The optimal control law with integral feedback is expressed as:

$$u' = -\mathbf{K} * \begin{bmatrix} x_1 & x_2 & x_3 \end{bmatrix}^T \qquad (4.29)$$

where

$\mathbf{K}$ is the gain matrix of LQR controller.

The gain matrix $\mathbf{K} = \mathbf{B}^{\mathbf{T}}\mathbf{P}$ is obtained by solving the *Riccati* equation in Matlab using instruction *lqr(A, B, Q, R)*:

$$\mathbf{PA} + \mathbf{A}^{\mathbf{T}}\mathbf{P} - \mathbf{PBR}^{-1}\mathbf{B}^{\mathbf{T}}\mathbf{P} + \mathbf{Q} = \mathbf{0} \qquad (4.30)$$

Considering the control input u' is defined as the multiplication of duty ratio and input voltage magnitude based on (4.24), duty ratio can be computed as:

$$D(t) = \frac{u'}{|v_{in}|} \qquad (4.31)$$

Once the duty ratio is obtained, the switching sequences for the switches can be obtained by pulse width modulation (PWM) and then drive the circuit.

Above all, the control strategy of the proposed voltage stabiliser with dq transformation and LQR control in step down mode is shown as Figure 4.3. Likewise, the control strategy can be also extended to step up mode by changing the sign of a parameter in matrix parameter $\mathbf{B_1}$.

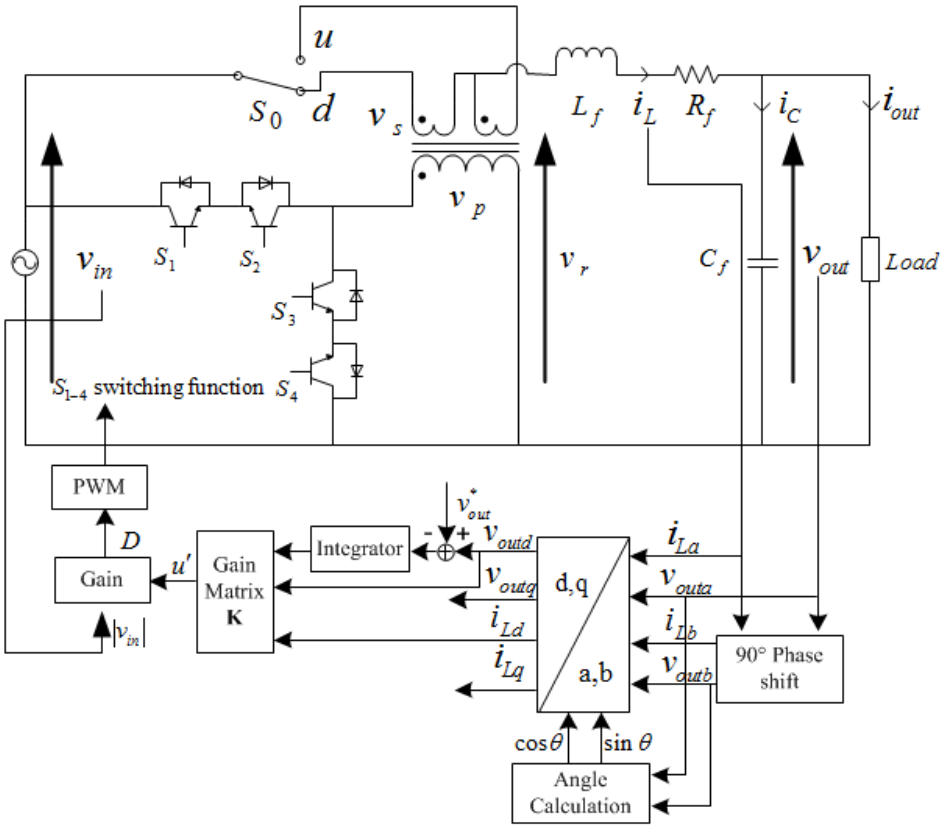

Figure 4.3 Control strategy of proposed voltage stabiliser with dq transformation and LQR control

Note that the angle difference θ between ab and dq reference frame is required to be known in the control process and the sine and cosine of θ can be obtained as:

$$\sin\theta = \frac{v_{outb}}{\sqrt{v^2_{outa} + v^2_{outb}}} \text{ and } \cos\theta = \frac{v_{outa}}{\sqrt{v^2_{outa} + v^2_{outb}}} \qquad (4.32)$$

After several attempts of simulation work in Matlab, the best estimated weighting symmetric $\mathbf{Q}$ and $\mathbf{R}$ are found as follows:

$$\mathbf{Q} = \begin{bmatrix} 0.25 & 0 & 0 \\ 0 & 0.25 & 0 \\ 0 & 0 & 25 \end{bmatrix} \text{ and } \mathbf{R} = [1]$$

The gain matrix $\mathbf{K}$ can be then calculated by using MATLAB instruction $\mathbf{K} = lqr(\mathbf{A},\mathbf{B},\mathbf{Q},\mathbf{R})$ as follows:

$$\mathbf{K} = [-3.289*10^{-6} \quad -0.0026 \quad -5.000]$$

4.4 Simulation Results

The simulation model is established in Matlab/Simulink and the parameters of the circuits are the same as the simulation work in Chapter 3. This part demonstrates dq transformation of output voltage v_{out} and inductor current i_L firstly and then provides the results of close loop control with LQR control designed in last part.

4.4.1 Vectors in dq Reference Frame

The dq transformation of output voltage v_{out} is shown as Figure 4.4. It can be noticed that the input voltage and output voltage are all sinusoidal functions while output voltage has a slightly smaller magnitude due to step down model selected. After the dq transformation, the components v_{outd} and v_{outq} are not sinusoidal values any more. The d component v_{outd} is equals to the magnitude of output voltage in steady state. When 20V input voltage step change is applied at 1s, a slight change on v_{outd} can be observed. This is because change of output voltage magnitude leads to change of output voltage d component v_{outd}. Since the

reference frame is aligned with ‘d’ axis, the q component v_{outq} is equal to 0 constantly no matter if the d component v_{outd} changes.

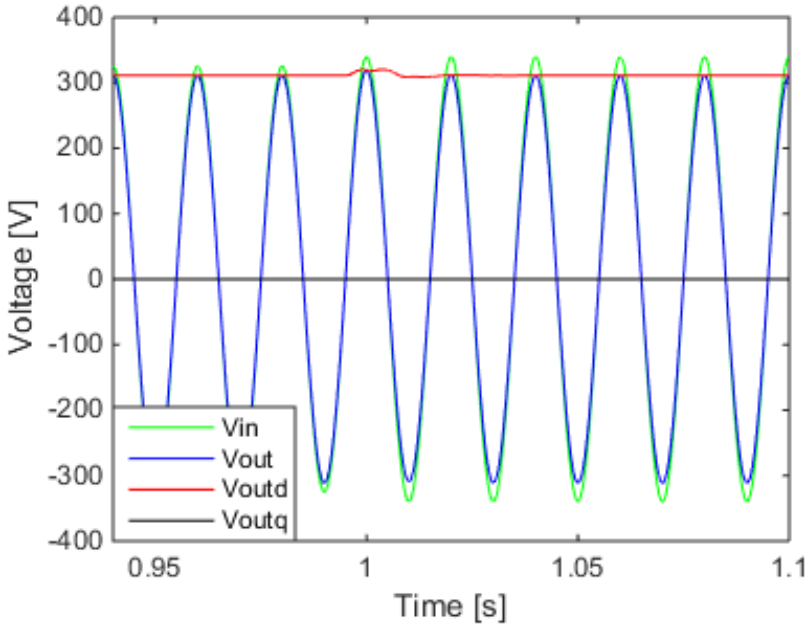

Figure 4.4 dq transformation of output voltage v_{out}

The dq transformation of inductor current is shown as Figure 4.5. In this case, an 84 Ohm resistive load is connected with the circuit. It is reduced to 22Ohm at 1s, which results in a roughly 7A current step change.

As it is shown in Figure 4.5, the d component i_{Ld} is almost equal to the magnitude of inductor current in steady state. When the current increases at 1s, the d component i_{Ld} also goes up after transient state. As for q component i_{Lq}, it is a very small constant but not exactly zero since the inductor current vector is not exactly in phase with the output voltage due to the effect of the filter. Furthermore, it also has a transient change when current increases and falls down to its original values again in steady state.

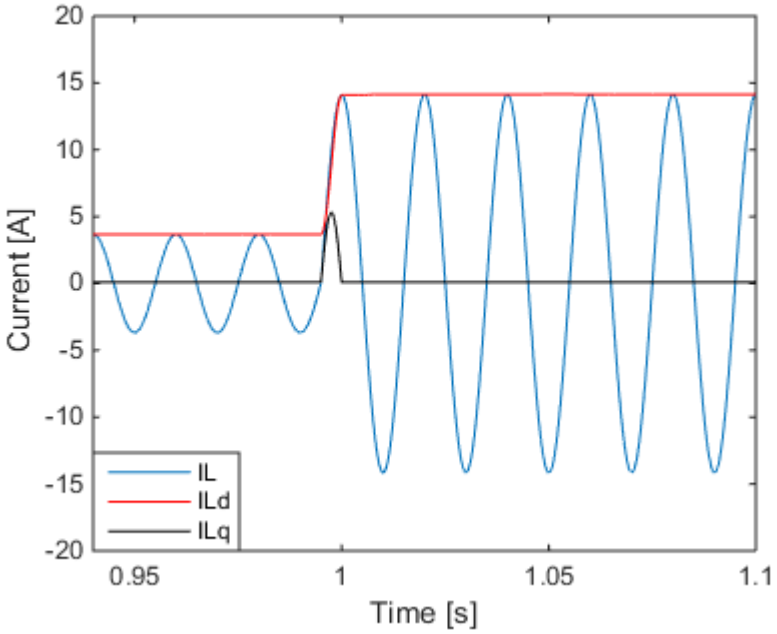

Figure 4.5 dq transformation of inductor current i_L

4.4.2 Simulation with Different Loads

The model in dq reference frame with LQR controller is verified with different types of loads, namely resistive load, inductive load and non-linear load in step down mode. With real input voltage profile, a step change applies to each load during the operation process to investigate the behaviour of proposed control strategy. The results are also compared with the results from last chapter with a PI controller.

Operation with Resistive Load

Figure 4.6 shows the input voltage, output voltage and current instantaneous values under a step changed resistive load. The output voltage is in a good sinusoidal waveform as expected. Compared with input voltage, the magnitude of output voltage is slightly smaller as expected, the phase difference in between can be hardly noticed and ignored. After a step change is applied on the output current at 1s, the output voltage remains its sinusoidal shape and is still

in phase with the input voltage. The current rises up immediately according to the step up change on load.

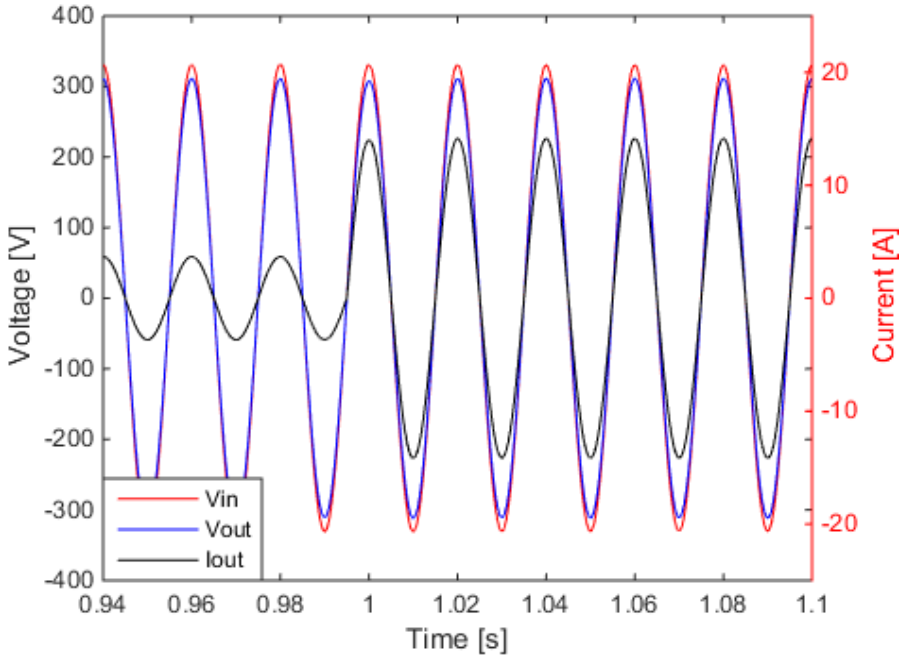

Figure 4.6 Voltage and current instantaneous value of the system with LQR controller and PI controller under resistive load

Figure 4.7 illustrates RMS value of input voltage, output voltage and current. Meanwhile, the output voltage of PI control with exact same input and load is also presented for comparison purpose. It is shown that the designed LQR control bring down the output voltage from 237V to 220V after it engaged in the beginning. The setting time of LQR controller is 0.02s quicker than PI controller designed in Chapter 3. The output voltage is then kept at 220V by LQR controller even though the input voltage slightly varies during the whole operation.

Operation with Inductive Load

Figure 4.8 illustrates the input voltage, output voltage and current instantaneous values when an inductive load is connected. A phase difference between output voltage and current can be observed while the output voltage still has the same phase with input voltage.

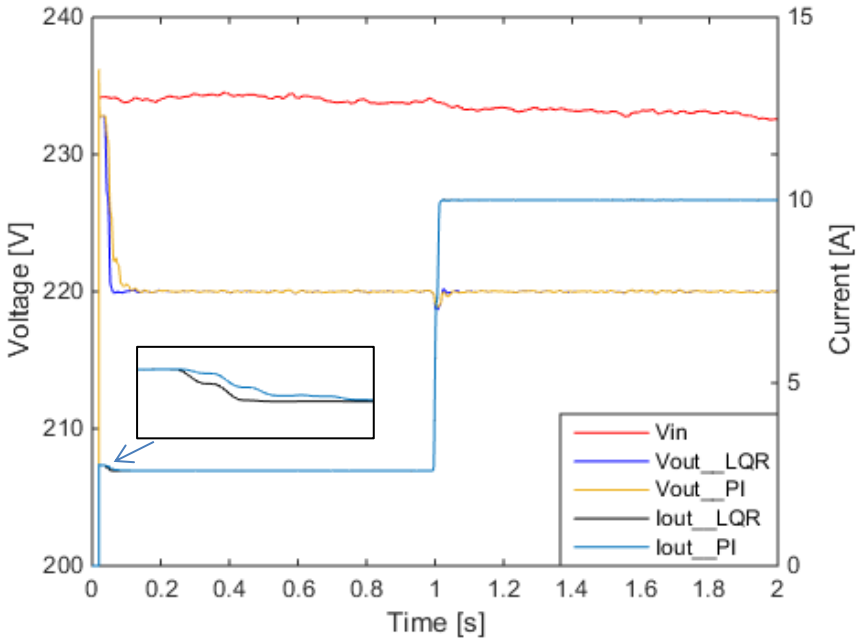

Figure 4.7 Voltage and current RMS value of the system with LQR control and PI control under resistive load

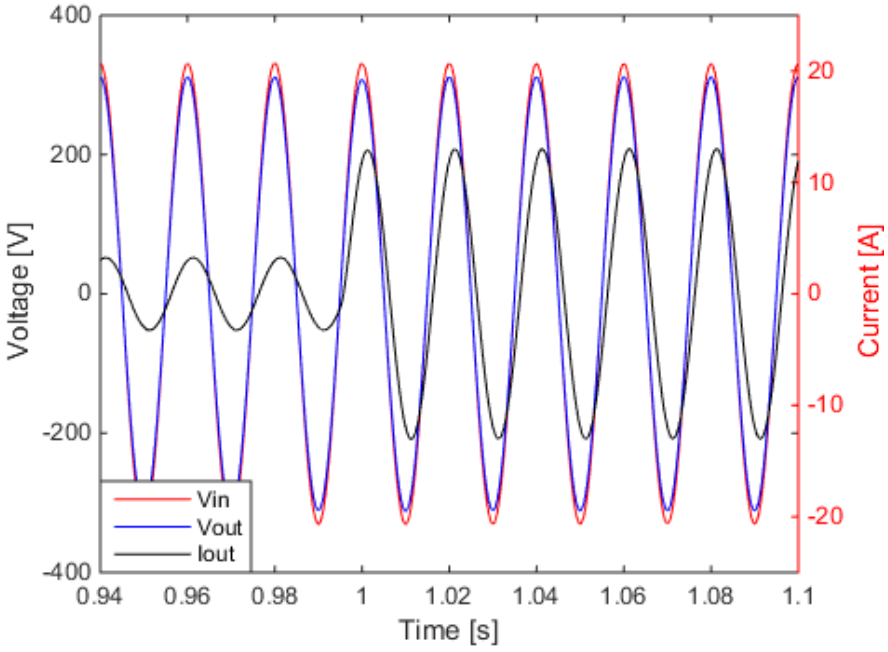

Figure 4.8 Voltage and current instantaneous value of the system with LQR control under inductive load

When a step change of load is applied at 1s, the output voltage decreases slightly and then rises up to the reference value rapidly as shown in Figure 4.9. Compared with PI control, the proposed LQR stabilises the output voltage with less setting time.

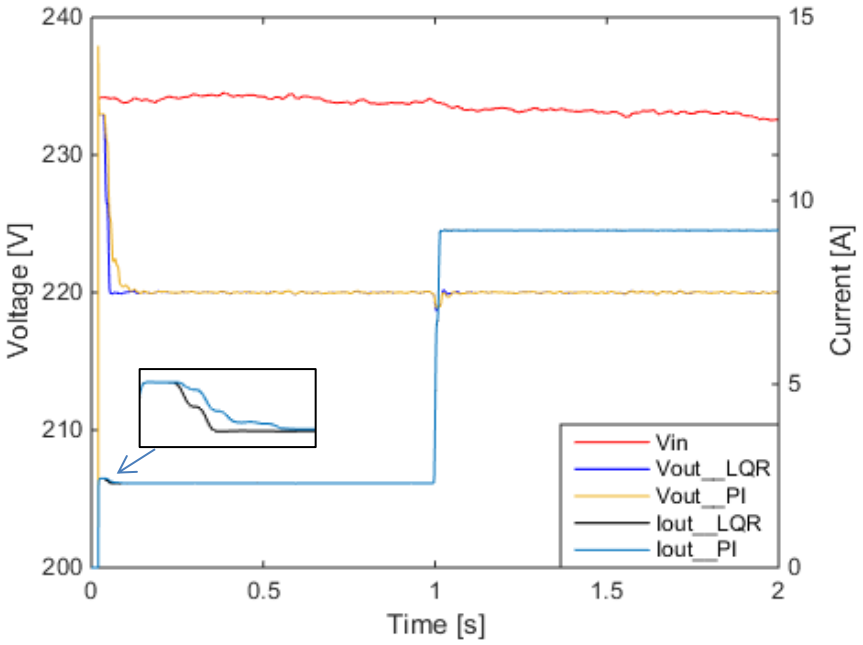

Figure 4.9 Voltage and current RMS value of the system with LQR control and PI control under inductive load

Operation with Non-Linear Load

Figure 4.10 illustrates the input voltage, output voltage and current instantaneous values for operation with non-linear load. Although the current waveform is highly distorted, the output voltage still keeps a good sinusoidal waveform and in phase with input voltage. As displayed in Figure 4.11, the output voltage is regulated at reference voltage in the presence of varying input voltage and step changed. It can be also noticed that the output voltage reaches steady state faster under LQR control as expected. After the non-linear load increases, a small drop on output voltage is seen and then the controller brings it back to reference value shortly. The current doesn't varies as voltage since the load is non-linear as shown in Figure 4.11.

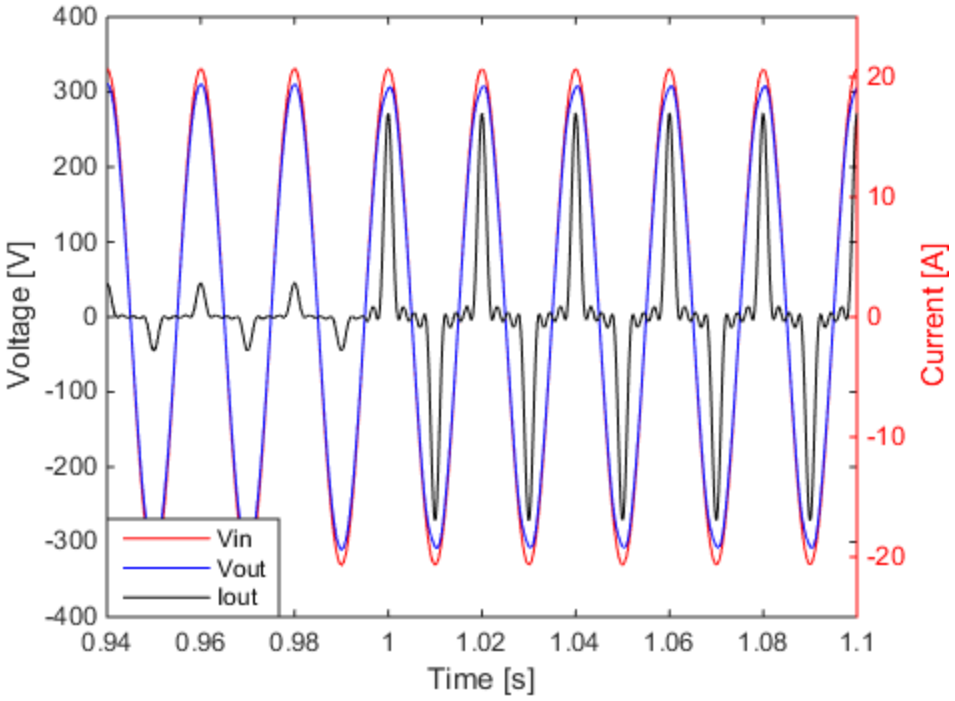

Figure 4.10 Voltage and current instantaneous value of the system with LQR control under non-linear load

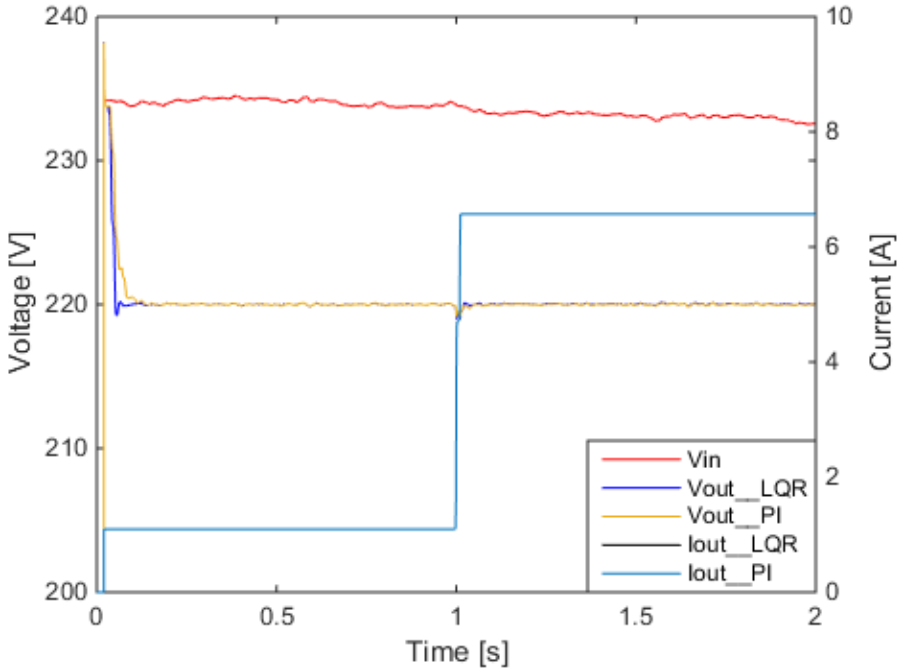

Figure 4.11 Voltage and current RMS value of the system with LQR control and PI control under non-linear load

4.5 Simulation Study of Energy Saving

The power consumption of operation with and without voltage stabiliser is analysed and the energy saving achieved by installation of a voltage stabiliser is also discussed in this part. The results of both LQR controller and PI controller are compared to investigate the performance of two controllers in terms of the energy saving.

With the same voltage profile and step-change load condition, the power consumption of operation under resistive load with and without voltage stabiliser is shown in Figure 4.12.

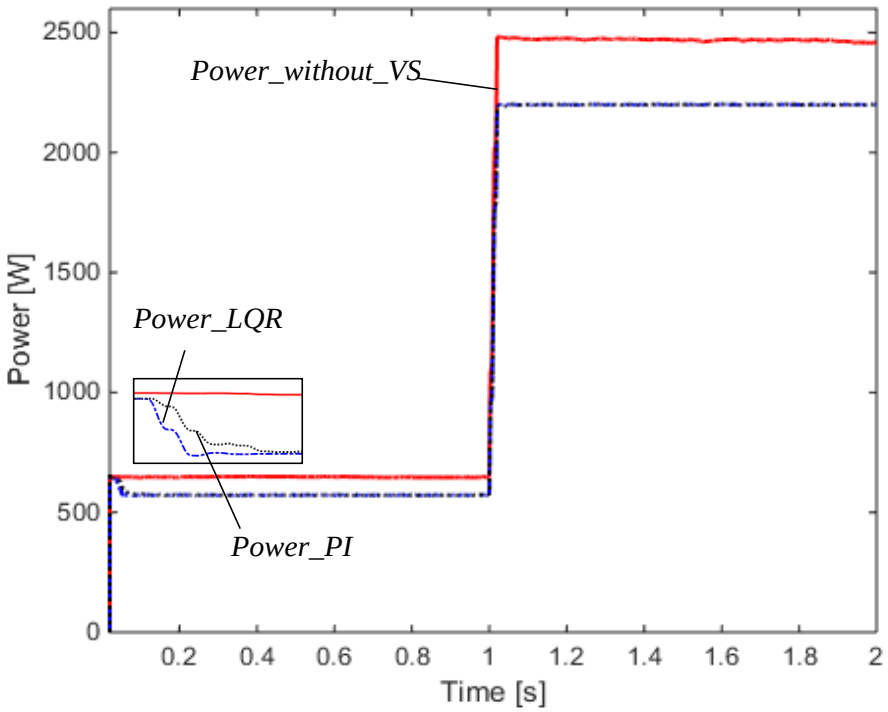

Figure 4.12 Power consumption of operation under resistive load with and without voltage stabiliser.

The power consumption without voltage stabiliser (Power_without_VS in Figure 4.12) is constantly higher than the power consumption with voltage stabiliser since the voltage regulation engaged. After a step-up change of load happens at 1 seconds, the power difference between with and without voltage stabiliser is increased as well. The power

consumption of the voltage stabiliser with LQR controller and PI controller keep the exact same at steady state. As for the transient response, the power consumption of voltage stabiliser with LQR has quicker response compared with the voltage stabiliser with PI control since it has fast voltage transient response as demonstrated in last part. In real life, the voltage stabiliser works at steady state mostly and the transient period is extremely short. Considering that the energy consumption is the integration of power consumption, the difference of energy saving between two control approaches is negligible. The energy consumption of operation under this case with and without voltage stabiliser is shown as Figure 4.13.

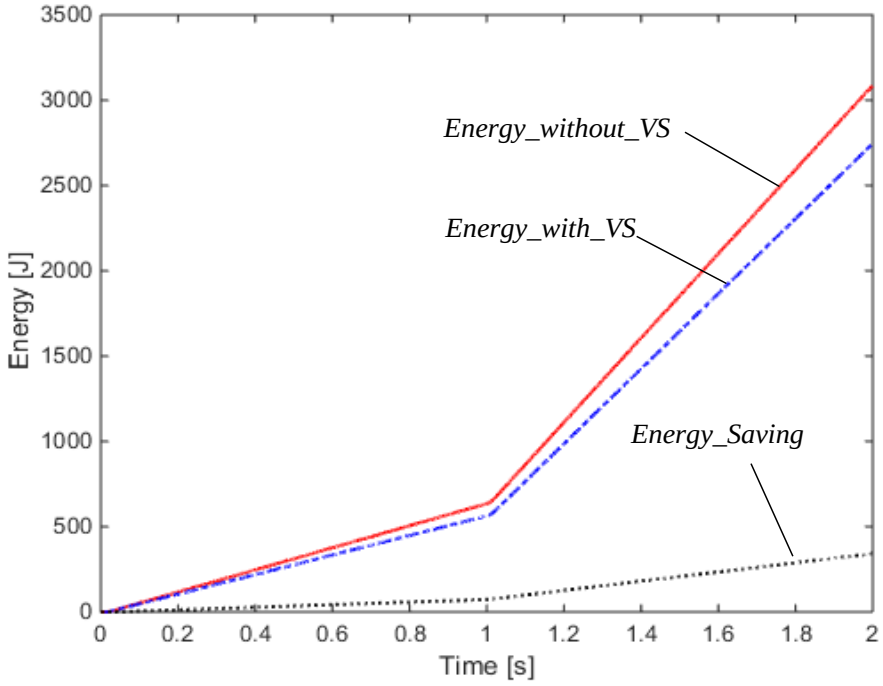

Figure 4.13 Energy consumption of operation under resistive load with and without voltage stabiliser

As shown in Figure 4.13, the energy saving of installing a voltage stabiliser increases as the load is consumption power. The slope of energy saving also rise up after the load increases to 10A at 1s. The total percentage energy saving in this case is 11.05%.

The simulations of operation under inductive load and non-linear load are also conducted. The differences between responses of power consumption under inductive load and non-linear load are quite similar as it under resistive load. The response of LQR controller is slightly faster that PI controller, however it can be ignored in real life considering the total energy saving. The percentage energy saving under inductive load and non-linear load are 11.08% and 5.90% respectively. It can be noticed that linear loads, which includes resistive load and inductive load, has better savings over non-linear loads.

4.6 Summary

The chapter introduces the dq transformation for modelling the proposed single phase voltage stabiliser to linearize the model in dq reference frame. A fictive axis with 90 degree shift is assumed to work in parallel with the original converter. Therefore, a two phase system is created and regarded as ab stationary reference frame. Then all the variables in ab reference frame are transformed into a dq rotating reference frame, which is rotating with an angular velocity which is the same as the input sinusoidal waveform. After proper alignment and linearization, the system model is simplified as a second order linear system.

Based on the second order system, a LQR controller with integral feedback is designed to regulate the output voltage at reference value with the disturbance from input voltage and output current. The model with close loop control is then established in Matlab/Simulink. The simulation results demonstrate the performance in terms of response speed and robustness. It is shown that the LQR controller requires less setting time to stabilise the output voltage compare with the PI controller designed in Chapter 3.

Chapter 5 Power Saving Estimation through Voltage Optimisation

One main benefit of installing a voltage regulation unit in household is to make power saving of the total power consumption. There is still no well recognised approach to estimate the power saving achieved by voltage optimisation technology. This chapter introduced a power saving algorithm which estimates the power saving of voltage regulator in real time. A test rig is also discussed and established to verify the proposed algorithm. Meanwhile, the algorithm is implemented in LabVIEW and works alongside with the test rig.

5.1 Power Saving Algorithm

5.1.1 Introduction

The main objective of the power saving algorithm is to estimate the power saving between the total power consumption with and without voltage optimisation technology. Basically, there are two scenarios considered in the comparison, which are a power supplying system with voltage optimisation and another one without voltage optimisation.

The key challenge is that it is not possible to have two exact same systems with same loads and external conditions for evaluation in real world. Therefore, it is required that the power consumption without voltage optimisation can be estimated based on the information acquired during the operation of the system with voltage optimisation unit installed. A general method for power saving estimation of transformer based voltage optimisation is patented in (Jihong Wang, Pub.No.: Wo/2014/027198). It is pointed out that the power saving made by applying the voltage optimisation technology is in linear relationship with the power consumption on the primary winding of the transformer used in voltage optimisation unit and the ratio between them is determined by the voltage reduction made by the unit. This relationship has been analysed and proved theoretically in next part.

5.1.2 Theoretical analysis

The circuit diagram of the system is shown as Figure 5.1. There are two set of system operating in parallel, in which one involves voltage optimisation connected with Load1 and another is directly connected with Load2.

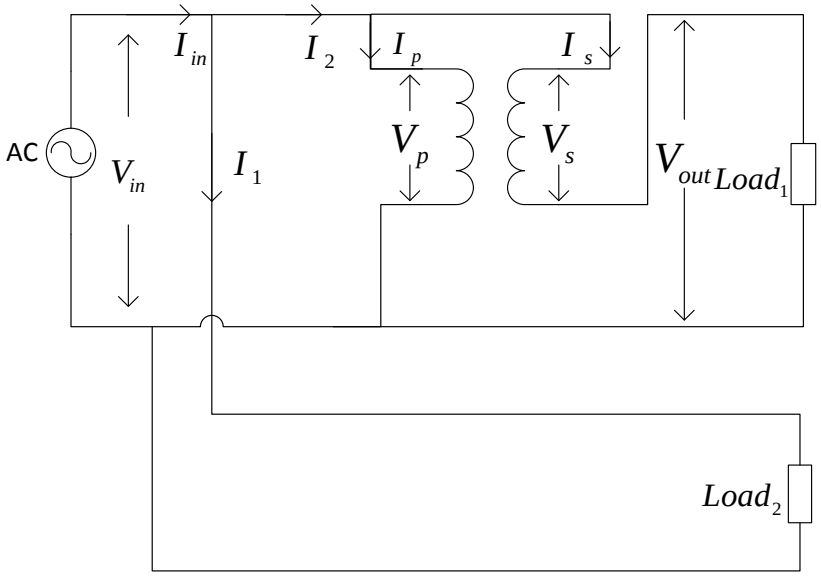

Figure 5.1 Circuit diagram of a power supply system with voltage optimisation unit

The following assumptions are made during the proof process for simplification reasons.

- The transformer used in the voltage optimisation unit is considered as idea transformer.
- The Load1 and Load2 are all linear loads with exact same characteristic.

Since the transformer is assumed as ideal with turn ratio k , the following relationship can be obtained:

$$\frac{V_p}{V_s} = \frac{I_s}{I_p} = k \qquad (5.1)$$

where

V_p is the RMS value of primary winding current.

V_s is the RMS value of secondary winding current.

I_p is the RMS value of primary winding current

I_s is the RMS value of secondary winding current

According to Kirchhoff voltage laws, the relationship of input, output voltage and voltage on the transformer windings are obtained as follows:

$$\begin{aligned} V_s &= V_{in} - V_{out} \\ V_p &= V_{in} \end{aligned} \qquad (5.2)$$

where

V_{in} and V_{out} are the RMS value of input voltage and output voltage respectively.

Considering the load1 and load 2 are assumed to be linear with same characteristic, the voltage and current relationship of them can be expressed as follows:

$$\frac{V_p}{I_1} = \frac{V_{in}}{I_1} = \frac{V_{out}}{I_s} \qquad (5.3)$$

Rearrange equation (5.4), the following relationship is obtained:

$$I_1 = \frac{V_{in}}{V_{out}} I_s \qquad (5.5)$$

Since the loads are considered as the same, the phase angle difference of the voltage and current are assumed as μ. Therefore, the active power consumptions of load1 and load2 are expressed as follows:

$$\begin{aligned} P_1 &= V_{in} * I_1 * \cos\mu \\ P_2 &= V_{out} * I_s * \cos\mu \end{aligned} \qquad (5.6)$$

where

P_1 is the active power of the load1

P_2 is the active power of the load2

The power saving is defined as the difference between the active power without voltage optimisation P_1 and the active power with voltage optimisation P_2. Hence, it is stated as follows:

$$P_{saving} = P_1 - P_2 = V_{in} * I_1 * \cos\mu - V_{out} * I_s * \cos\mu \qquad (5.7)$$

where

P_{saving} is the power saving by applying voltage optimisation

Substituting equation (5.8) into (5.9) to replace I_1 , it is rearranged as follows:

$$\begin{aligned} P_{saving} &= V_{in} * \frac{V_{in}}{V_{out}} * I_s * \cos\mu - V_{out} * I_s * \cos\mu \\ &= (\frac{V_{in}^2}{V_{out}} - V_{out}) * I_s * \cos\mu \\ &= \frac{(V_{in} + V_{out})(V_{in} - V_{out})}{V_{out}} * I_s * \cos\mu \end{aligned} \qquad (5.10)$$

Substituting equation (5.11) and (5.12) into equation (5.13) and rearranging, the following equation is obtained:

$$\begin{aligned} P_{saving} &= \frac{V_{in}+V_{out}}{V_{out}} * V_s * I_s * \cos\mu \\ &= \frac{V_{in}+V_{out}}{V_{out}} * V_p * I_p * \cos\mu \\ &= \left(1+\frac{V_{in}}{V_{out}}\right) * V_p * I_p * \cos\mu \end{aligned} \qquad (5.14)$$

As it demonstrated in equation (5.15) , the power saving is in linear relationship with the active power on primary winding, which is expressed as $V_p * I_p * \cos\mu$. The ratio is determined by input voltage V_{in} and output voltage V_{out} . The conclusion accords with the power saving algorithm mentioned previously.

5.1.3 Discussion

Some limitations should be noticed in practical implementation and verification. Firstly, the transformer is assumed as ideal in the previous mathematical proof. In reality, the transformer includes winding resistances and winding inductances for both primary and secondary windings. The winding resistance leads to voltage drops on them, hence the voltage relationship shown as equation (5.16) is not exact accurate, it will result in some tiny error of the power saving estimation.

Secondly, the winding inductances affect the phase angle difference between voltage and current across the windings and the loads as well. Likewise, the change of phase angle will also cause some error on the algorithm. What's more, the error tends to increase heavily as the phase angle increasing towards 90 degree because of the nonlinearity of cosine function. The error in cosine value caused by 4 degree error is only 0.002 if the original phase angle

difference is 0 degree (error computed as: $\cos 0 - \cos(0+4) = 0.002$), while the error in cosine value caused by same amount is 0.046 if the original phase angle difference is 40 degree (error computed as: $\cos 40 - \cos(40+4) = 0.046$). Therefore, it can be concluded that the power saving algorithm is very accurate when unity power factor achieved and the accuracy will decline as the phase angle difference increases.

Thirdly, the saturation of the transformer is not considered during the mathematical proof. The relationship between primary winding and secondary winding may be not exactly same as the equation (5.17) when the transformer is in saturation. Thus, the accuracy of the power saving algorithm is affected if the current drawn by the load exceeds the limit of the rated operating value.

Finally, the power saving of non-linear loads cannot be estimated by using the proposed algorithm. In fact, the transformer-based voltage optimisation technology rarely made power saving for non-linear loads. Most of nonlinear loads have AC-DC conversion internally. The converter could be switching mode, regulated or unregulated power supplies. The output DC voltage is very stable as long as the input voltage stays within the specified range. Although the efficiency of AC-DC converter may vary due to different input AC voltage level, the influence is hardly noticeable. Hence, the power consumption of the non-linear is not affected by voltage optimisation unit and the power saving algorithm is not applicable in this case.

In conclusion, the proposed power saving algorithm is proved mathematically with the assumption of ideal transformer and linear loads applied in the circuit. In practice, the non-ideal transformer and non-linear loads may results in some errors of the power saving estimation. As long as the loads is within the current rating and close to unity power factor, the estimated power saving can still achieve excellent accuracy.

5.2 Implementation and Verification

5.2.1 Verification System

The verification system is illustrated in Figure 5.2 as follows. In the system, two sets of loads with the same component combinations are prepared, one of which is connected to or powered by the voltage optimiser and the other is directly connected to the main power supply.

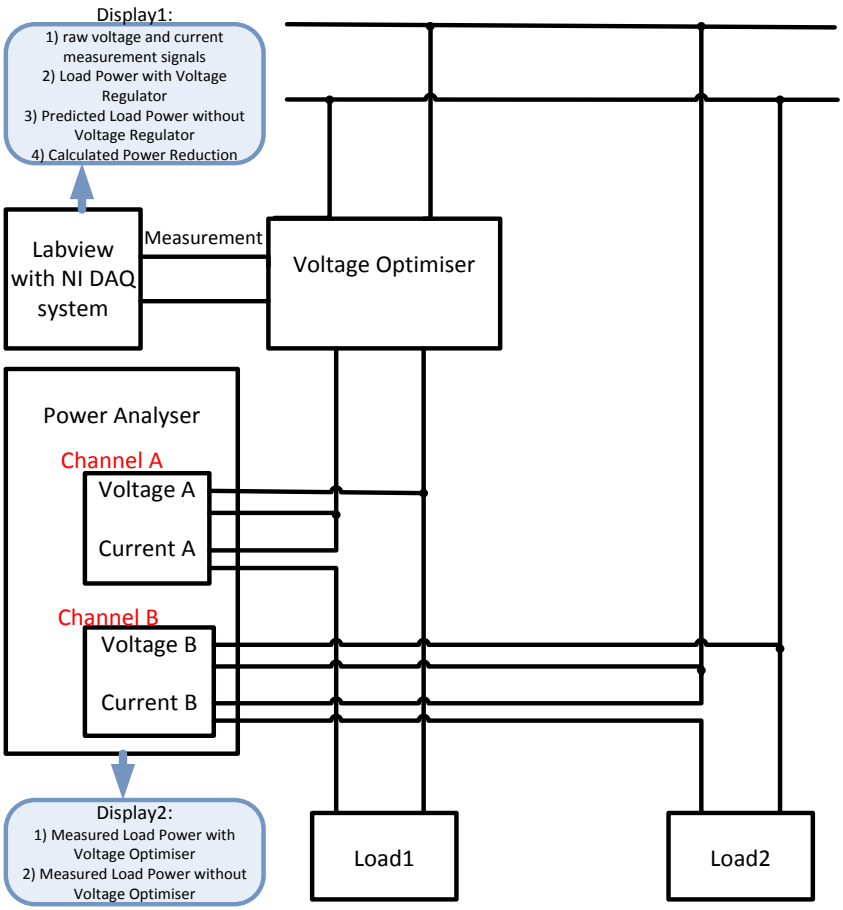

Figure 5.2 Overview of the verification system

On one hand, the power consumptions of two sets of the loads will be measured through the calibrated Yokogawa WT3000 Power Analyser as reference for comparison purpose. On the other hand, the voltages and the currents of loads are also measured by a series of voltage and

current sensors for the power saving algorithm. The measurement data are collected by the NI DAQ data acquisition system and transferred to an industrial PC through LabVIEW. The algorithm is implemented in LabVIEW as well, based on the acquired data and it manipulates the data in real-time to calculate the real power consumption of the load and to estimate the power consumption for the same load without connecting to the voltage optimiser. A series of tests have been conducted to verify and validate the power saving algorithm.

5.2.2 Equipment and Sensors

Power Analyser (PA)

As shown in Figure 5.2, the power analyser is used in the verification system to measure the power values for both load1 and load2. The Yokogawa WT3000 Power Analyser is selected I this test and it is calibrated at the time of purchased. The front and back views of the power analyser are shown in Figure 5.3.

Figure 5.3 Power analyser front view and back view

This power analyser, which includes four channels, has a basic power accuracy of ± 0.02 percentage of reading and bandwidth from DC up to 1 MHz. For each channel, it measures the voltage as well as the current and then computes the active power, reactive power, power factor, and harmonics and so on. The measurement can be either shown on the screen or transferred to a separate PC for future analysis. In this particular verification work, the power

analyser is applied to measure the voltage and current of two exact same loads and the measurement is used as reference and comparison to verify the power saving algorithm. In addition, the power analyser is also utilised for sensor calibration and minimise the error introduced by measurement system before the experiments conducted.

Data acquisition system

The data acquisition system (DAQ) used in this test rig is the PXIe-1082 chassis with PXIe-6358 multifunction DAQ board from National Instruments (NI). Two analogue inputs are configured to acquired voltage and current signals with 16bits resolution and 10 kHz sampling rate. The device is shown as follows:

Figure 5.4 NI PXIe-1082 chassis with PXIe 6358 DAQ device

The DAQ device is designed to work with the software LabVIEW from National Instruments (NI) which is a tool of having multi useful/powerful software functions. The power saving algorithm are implemented using LabVIEW which perform data analysis, calculation, and comparison. The results displayed include: voltages, currents, active power, reactive power, apparent power, power factor, power saving and accumulated energy saving.

Sensors

In this verification work, the voltage is to have the range of 210-250V and the current is up to 32A. The analogue input of the NI DAQ device has the voltage range of ±10 V. Thus, the outputs from the sensors need to match the input voltage level of the DAQ which can be achieved through the selection of a matched resistance and the isolated voltage converting interface circuits. The sensors must provide isolation between the measuring high voltage circuits and the NI DAQ low voltage analogue inputs. Requirement for all sensors would be a wide range of measurement, excellent accuracy, linearity and reliability. Calibration of the sensors is conducted priory to the entire test of measurement and calculations.

The selected voltage sensor is voltage transducer LV 25-p manufactured by LEM Company. The selected current sensor is through-hole current transducer LA 25-P from LEM Company as well. 3 voltage transducers LV 25-P, 3 current transducers LA 25-P, along with the power circuit and other necessary components are all soldered on a circuit board, which is shown as follows:

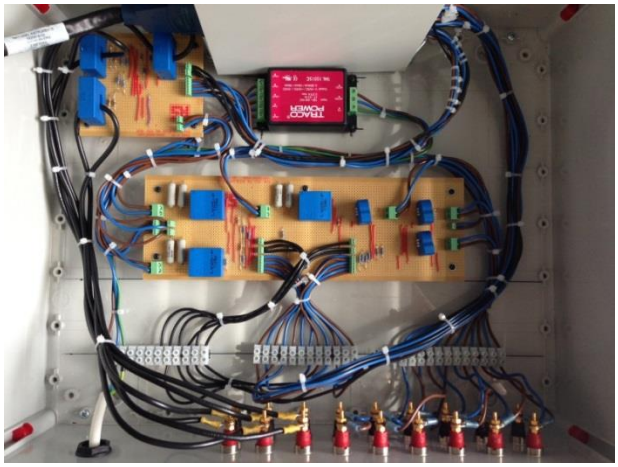

Figure 5.5 Sensor board which contains three voltage transducers and three current transducers

All the sensors are calibrated through comparing the sensor measurement reading displayed in software with power analyser prior to real experiments. The parameters corresponding to

the measurement readings in software are then adjusted to achieve best accuracy. After calibrating the sensors individually, the outputs of the sensors are connected to the differential analogue inputs of the DAQ device and through 22k Ohm resistors to the ground within the terminal box.

5.2.3 Load Bank

One challenge of this verification work is to provide two exact same sets of loads with wide current range and different types. In this verification work, a high current (up to 32A) load bank, including resistors, capacitors and inductors is set up for test. Two fans are also mounted insides the frame of the load bank for heat dissipation. The font view and side view of the load bank are shown in Figure 5.6

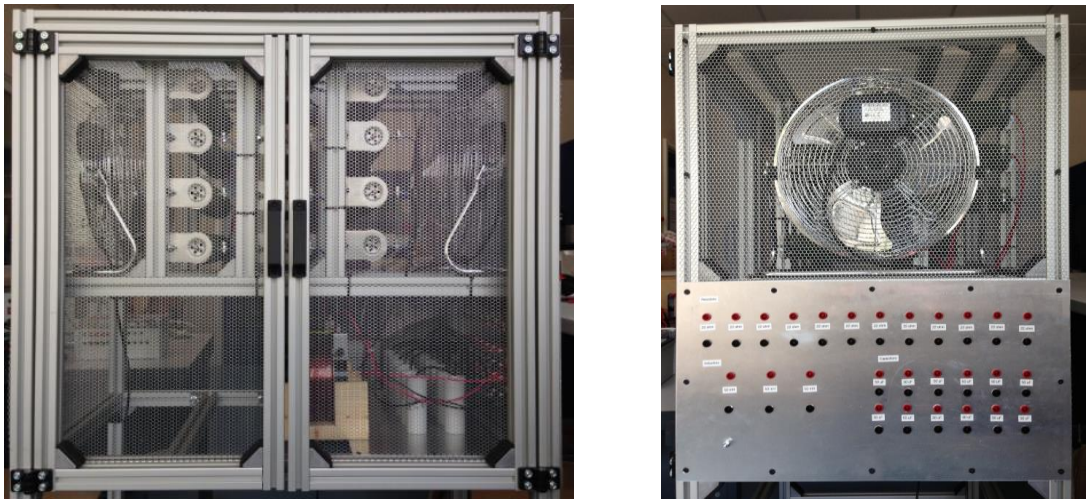

Figure 5.6 Font view and side view of the load bank

As it shown above, the resistors are mounted in the upper layer while the capacitors and inductors are fitted in the lower layer. The sockets are located on the side panel for connection purpose. The details of components inside the load are present in Table 5-1.

Table 5-1 List of internal components in load bank

Name	Numbers	Specification
Resistors	12	22 Ohm, 1500 W
Capacitors	12	50 μF, 450 V, AC
Inductors	3	50-70 mH, 10A, adjustable
Fans	2	14 inches, for cooling

Additional type of load used in the verification work is the centrifugal fan driven by Simens three phase squirrel cage induction motor. Two identical fans REM 48-0200-2D-07 produced by Nicotra-Gebhardt Ltd are deployed for experiments.

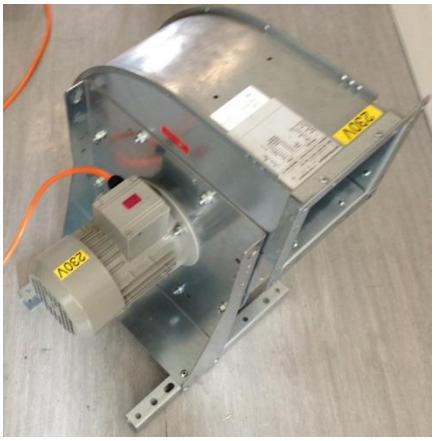

Figure 5.7 Centrifugal fan REM 48-0200-2D-07

The parameters of the fans are as follows: rated velocity 2840 rpm, efficiency 0.59, rated pressure 700 Pa, rated flow rate 1200 m^3/hour, maximum pressure 1200 Pa. The rated parameters of the motors: power 0.37 KW, frequency 50 Hz, velocity 2840 rpm, voltage 230 V (Δ)/ 400 V (Y), stator current 1.63 A/ 0.94 A, power factor 0.77.

For single phase application, the stator windings of the motors are Δ connected. One of the phases is connected to the Live, another one is connected to the Neutral. The third phase is connected through 30 μF capacitor to the Neutral. The load of the motor is controlled through changing the cross-section of the fan's discharge.

5.3 Experiments Results and Analysis

With the test system described previously, a series of tests have been conducted to verify the power saving algorithm. The procedures adopted for all the tests and the test results are reported in this section.

5.3.1 Procedures of the Test

The circuit diagram of test system is illustrated in Figure 5.8, in which two sets of identical loads are used.

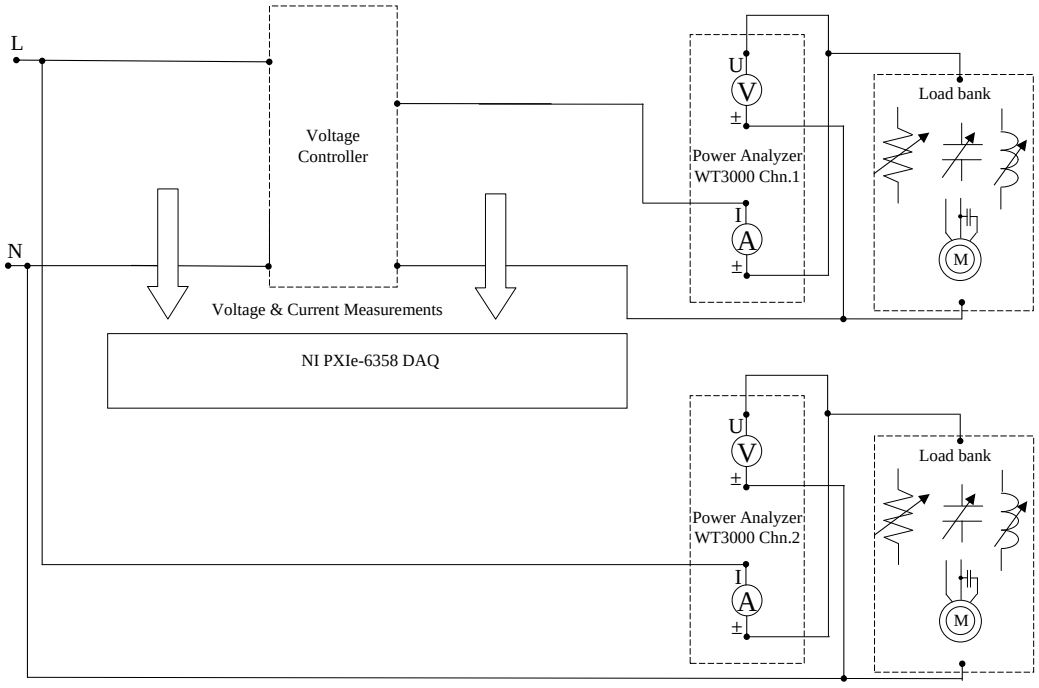

Figure 5.8 Circuit diagram of the test system

One set is connected with the voltage optimisation unit output while another set is directly connected to the mains. Meanwhile, the sensors are connected with the voltage optimisation unit to measure the voltages and currents and the DAQ system samples the raw measurement signals from the sensors and transmits the measurement to the PC for displaying and processing. The algorithm implemented in the software not only computes the power saving but also output the predicted active power of the load without voltage optimisation unit. The power analyser is also connected with the two loads and measures the voltage and current along with power values including active power, reactive power and power factor of them. The predicted active power from implemented algorithm is then compared with the real measured value from power analyser. The data from both DAQ device and the Power analyser are displayed in real time and are also recorded and stored for further analysis in MATLAB. The actual test system and environment are shown as Figure 5.9

Figure 5.9 Actual test system and environment

In general, four types of loads including resistive, capacitive, inductive and motoring loads are used in the test and verify the power saving algorithm. The current for each type of load varies 3 A to 30A. The two display panels from the NI system and the Power Analyser are placed with the information shown in Figure 5.10. Based on the measurements from the NI system, the active power is predicted for the case while the load is connected to the mains directly without using the voltage optimisation unit. The predicted active power is displayed

and compared to the active power measurement from the power analyser for the same load connected directly to the mains. The results are presented in the following sections.

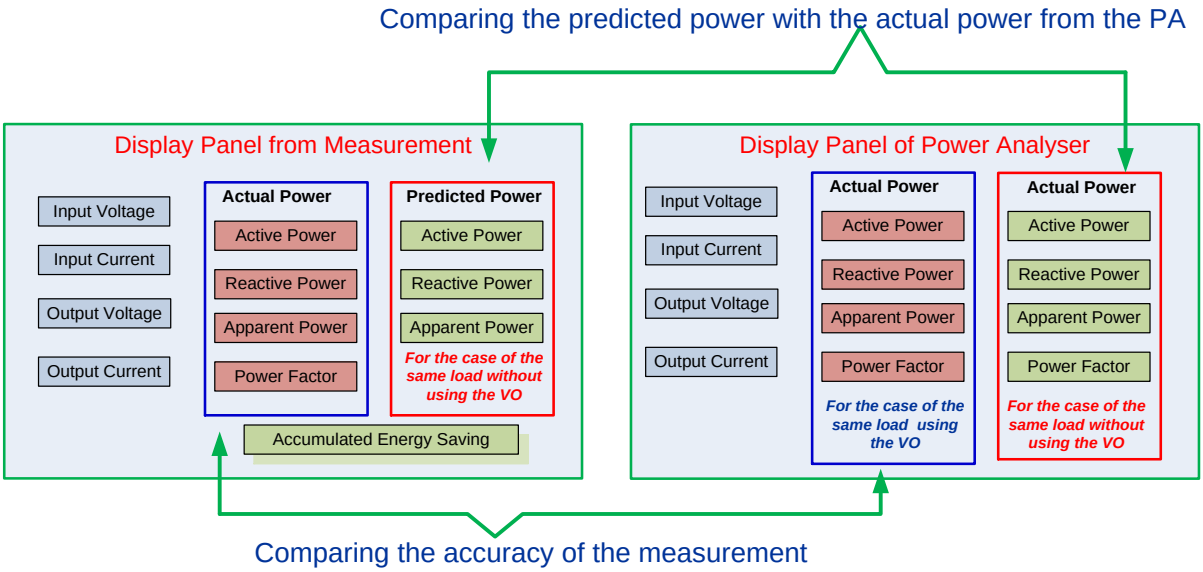

Figure 5.10 Display panels of the software in LabVIEW (left) and the power analyser (right)

5.3.2 Test with resistive loads

The resistive load is formed by combining series and parallel connections of twelve 22 Ohm resistors in the load bank. The range of resistance values obtained is from around 8 Ohm to 66 Ohm. Nine cases of resistive load test are conducted within the current range of 3-30 A. Figure 5.11 illustrates a voltage, currents, and power measurements for a particular case with 22 Ohm resistance load and the data collected are from both the NI DAQ device (NI) and the power analyser (PA). It includes the voltages at the input and output of the voltage optimisation unit, the current through the load connected to the voltage optimisation unit, the power consumed at the output of the voltage optimisation unit, the actual active power of the load that is directly connected to the mains without connecting to a voltage optimisation unit (actual active power), the predicted active power for the load directly connected to the mains (predicted active power). The predicted power is plotted on the same graph with the PA measured actual active power.

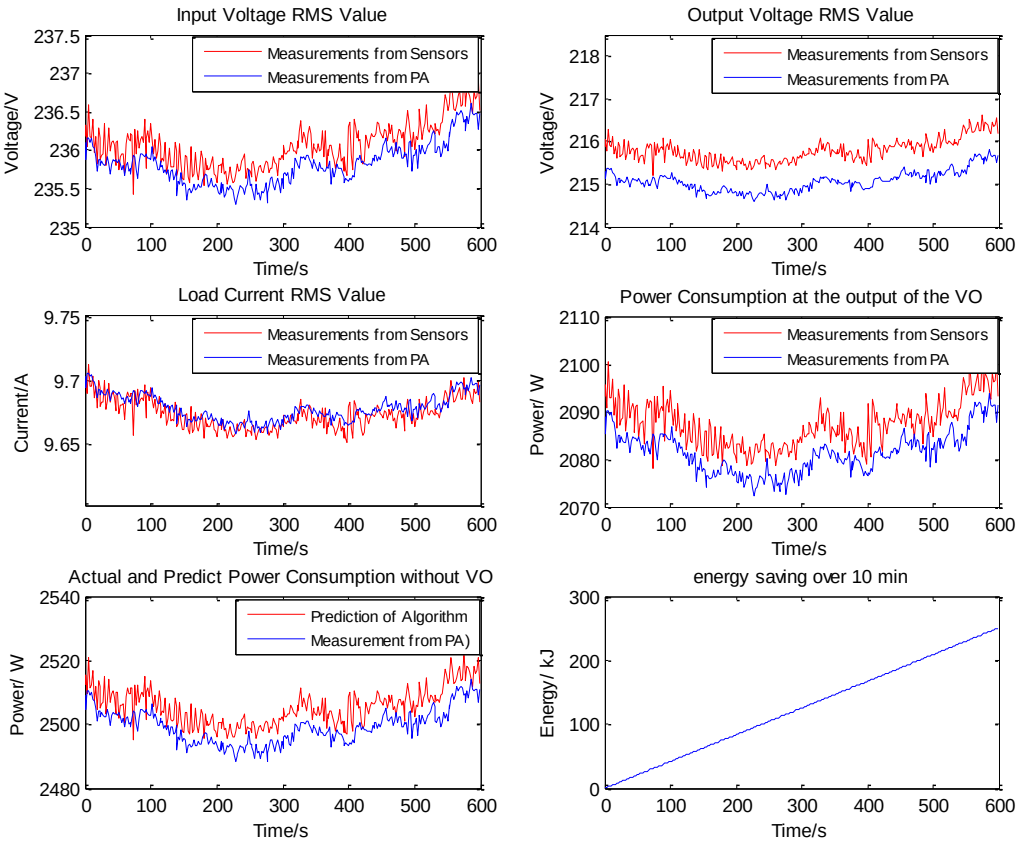

Figure 5.11Test results for a resistive load (1KWh = 3600 J)

From Figure 5.11, it can be observed that the voltage and current measured through the NI DAQ system and the power analyser are in excellent agreement. The average power consumptions over the tested period and prediction errors for 9 cases with different resistive loads are summarized in Table 5-2. The error for power predicted using the algorithm is less than 1% as it shows.

Table 5-2 Summary of resistive load tests results

Load	Predicted active power computed by Software (W)	Actual active power measured by PA (W)	Absolute error (W) $e_{abs} = \lvert P_{predict} - P_{actual} \rvert$	Relative error $error = e_{abs} / P_{actual}$
66 Ohm	858.42	853.81	4.61	0.54%
44 Ohm	1280.50	1269.30	11.20	0.88%
33 Ohm	1685.66	1673.98	11.68	0.70%
22 Ohm	2505.68	2499.22	6.46	0.26%
19 Ohm	2955.33	2955.10	0.23	0.01%
15 Ohm	3764.56	3778.03	13.47	0.36%
11 Ohm	4941.35	4937.38	3.97	0.08%

8.8 Ohm	6125.11	6165.81	40.70	0.66%
7.3 Ohm	6445.57	6426.60	18.97	0.30%

5.3.3 Test with capacitive loads

Different resistive/capacitive loads can be obtained based on different connections of twelve 22 Ohm resistors and twelve 50 µF capacitors. The range of capacitance is from around 50µF to 600 µF. 9 cases of resistive/capacitive connection load test are conducted within the allowed current range. Figure 5.12 shows the data collected for a specific load case with a 22 Ohm resistor in series connection with a 300µF capacitor.

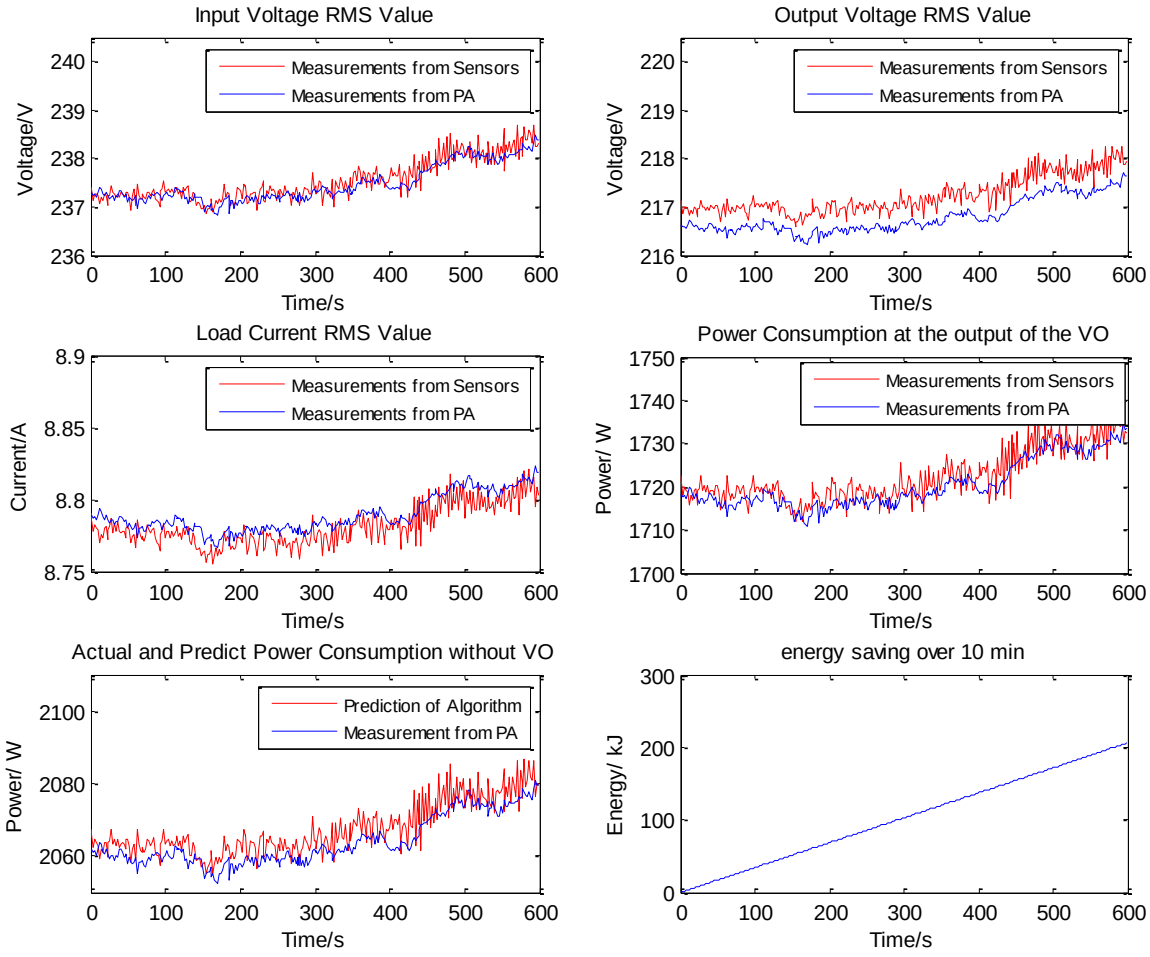

Figure 5.12 Test results for a capacitive load (1 KWh = 3600 KJ)

The average power consumptions and the prediction errors of all the tested resistive/capacitive cases are listed in Table 5-3.

Table 5-3 Summary of capacitive load test results

Load	Predicted active power computed by NI (W)	Actual active power measured by PA (W)	Absolute error (W) $e_{abs} = \left\lvert P_{predict} - P_{actual} \right\rvert$	Relative error $error = e_{abs} / P_{actual}$
44 Ohm, 150μF	1045.64	1035.90	9.74	0.94%
33 Ohm, 200μF	1405.00	1395.21	9.79	0.70%
22 Ohm, 200μF	1670.78	1663.92	6.86	0.41%
22 Ohm, 300μF	2067.25	2063.96	3.29	0.16%
19 Ohm, 300μF	2284.42	2288.55	4.13	0.18%
15 Ohm, 300μF	2557.95	2564.70	6.75	0.26%
11 Ohm, 400μF	3333.71	3355.73	22.02	0.66%
8.8Ohm, 600μF	4568.08	4550.32	17.76	0.39%
7.3Ohm, 600μF	4906.58	4916.93	10.35	0.21%

From the results listed above, it can be concluded that the errors of the power prediction are within 1% for all capacitive loads in the test.

5.3.4 Test with inductive loads

The inductive load can be combined from twelve 22 Ohm resistors in series with three 50-70 mH adjustable inductors based on various combinations. Eight cases of resistive/inductive in series connection loads are tested. Figure 5.13 shows the plot of the test results of the case with a 22 Ohm resistor and a 50mH inductor.

The average power consumptions and the prediction errors of all inductive cases are summarized in Table 5-4. The error of predicted power compared with the actual power is from 0.1%-1.5%. Considering that the inductor is tuned manually, it is likely that the value of two inductors have an error around 1%, therefore the error of the test is relatively higher than previous case, especially for the 44 ohm & 60mh case and 33 ohm & 60mh case.

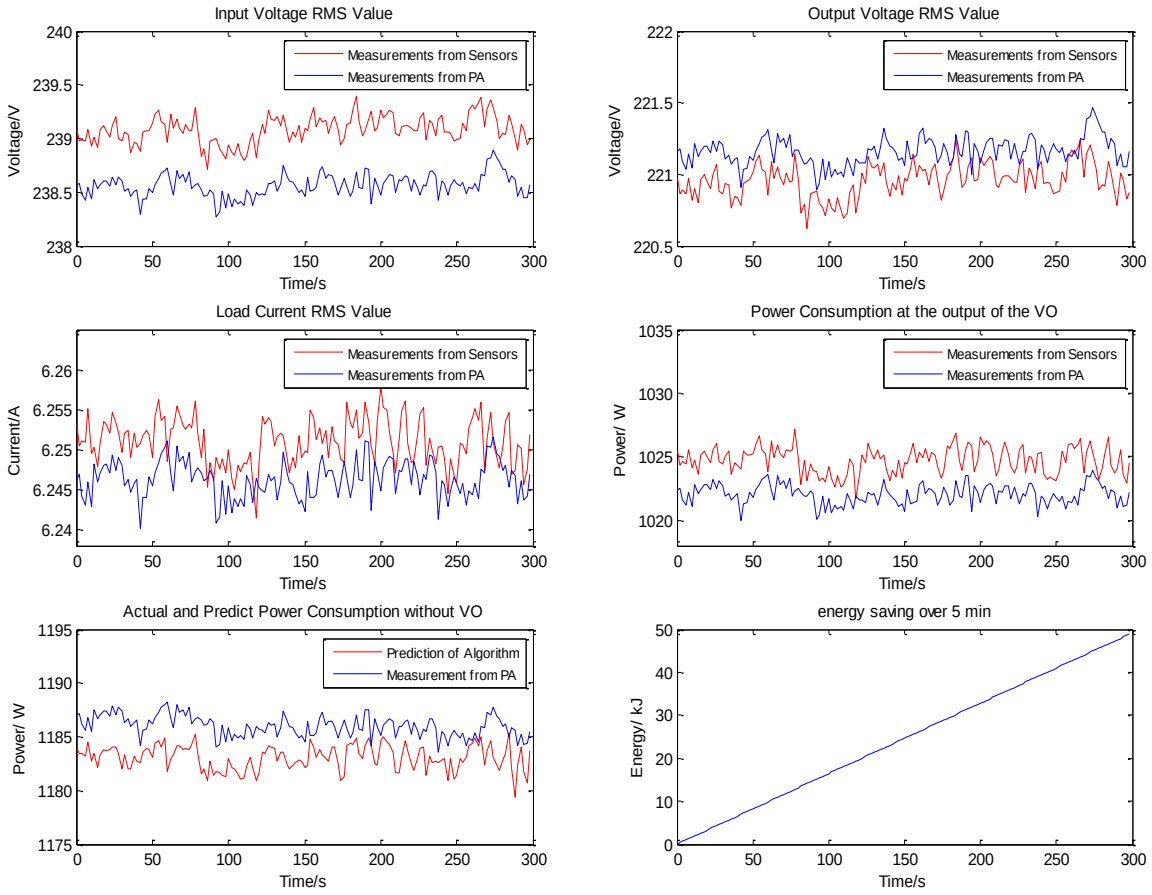

Figure 5.13 Test results of a inductive load (1 KWh = 3600KJ)

Table 5-4 Summary of inductive load tests results

Load	Predicted active power computed by NI (W)	Actual active power measured by PA (W)	Absolute error (W) $e_{abs} = \left\|P_{predict} - P_{actual}\right\|$	Relative error $error = e_{abs} / P_{actual}$
44 Ohm, 60mH	739.63	750.10	10.47	1.4144%
33 Ohm, 60mH	787.74	799.39	11.65	1.4795%
22 Ohm, 50mH	1183.07	1185.99	2.92	0.2474%
19 Ohm, 50mH	1196.85	1196.45	0.40	0.0331%
15 Ohm, 50mH	1173.65	1172.39	1.26	0.1077%
11 Ohm, 30mH	2359.37	2353.06	6.31	0.2676%
8.8 Ohm, 25mH	2355.57	2364.97	9.40	0.3990%
7.3 Ohm, 25mH	2307.38	2297.31	10.07	0.4366%

5.3.5 Test with motor loads

The tests of the motoring load are very limited subject to the availability in the lab. Two identical motor-driven fans with capacitor connected are used in the test. The variation of the motoring load is achieved by part-choking the discharge air flow of the fans. In order to

increase the load current rating, some resistors are connected in parallel with the motor. Figure 5.14 shows the plots of one motoring load case. The average power consumptions and the prediction errors for all the cases are summarised in Table 5-5.

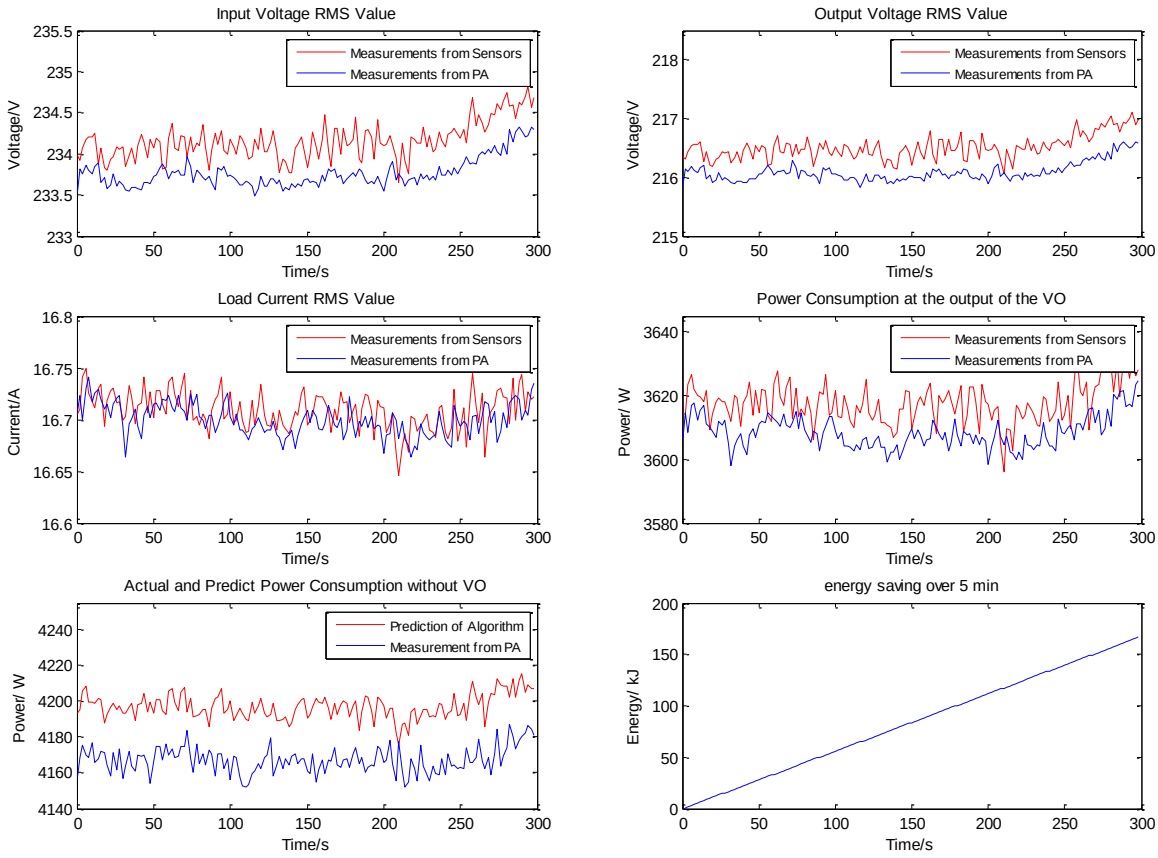

Figure 5.14 Test results of motor load (1 kWh = 3600KJ)

Table 5-5 Summary of motor loads tests results

Load	Predicted active power computed by NI (W)	Actual active power measured by PA (W)	Absolute error (W) $e_{abs} = \lvert P_{predict} - P_{actual} \rvert$	Relative error $error = e_{abs} / P_{actual}$
22 Ohm, motor load	3017.93	2969.62	48.31	1.60%
19 Ohm, motor load	3437.98	3387.40	50.58	1.47%
15 Ohm, motor load	4197.05	4167.24	29.81	0.71%

The error of power prediction for motor load is within the range from 0.7% to 1.6%. As the power rating of the load increases, the relative error decreases significantly from 1.6% to 0.7%. Due to the size/power limitation for the motoring load, the test should be extended for

bigger load tests although there are no restrictions for the algorithms to be used for higher load range.

5.3.6 Robust test of 1 hour duration time

In order to investigate the relationship between the accuracy of the power prediction and the running time length, one hour test of a 15 ohm resistive load is conducted as an example and the results is illustrated in Figure 5.15.

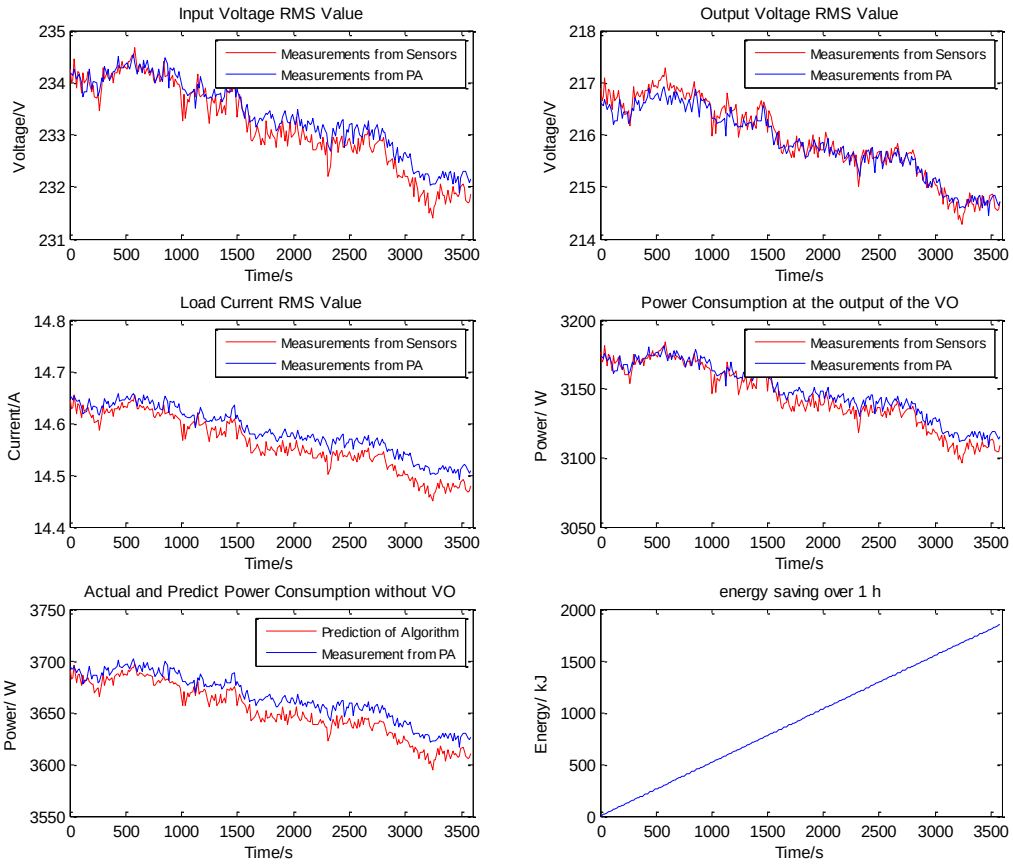

Figure 5.15 One hour test for 15 ohm resistive load (1kWh = 3600kJ)

As it is shown in Figure 5.15, the predict power consumption shows excellent agreement with the actual power consumption measured by power analyser and the overall error is computed as 0.36%. The overall error is similar to the previous test for same load as 0.25%. Therefore,

it can be concluded that the algorithm is not time-dependent and absolutely applicable for long running time.

5.4 Summary

This chapter introduces a power saving algorithm used to estimate the power saving made by installing a transformer-based voltage optimisation unit. The theoretical analysis of the proposed algorithm is discussed into detail in the beginning of this chapter. The algorithm is then implemented in LabVIEW and a test system is established to verify it. Four types of the load, which are resistive, capacitive, inductive and motor, are adopted in the test. The measurement from the precision power analyser WT3000 from Yokogawa is utilised as a benchmark for analysing the accuracy of the test results.

From all the tests carried out, it can be concluded that the accuracy of the calculated and predicted power saving due to the installation of voltage optimisation unit can be maintained for most types of electrical loads including resistive load, capacitive load, inductive load and motor load. Taking account of the errors from the sensors, the overall errors of the power saving algorithm are within 1% for the entire test range.

The power saving algorithm requires the current and voltage measurement from the voltage optimisation unit which can be easily acquired by applying nowadays measuring approaches. It is also simple enough to be implemented in a low cost microprocessor. Therefore, it is possible to integrate the measurement circuit and algorithm into a single circuit board fitted in the voltage optimisation unit.

Chapter 6 Load Signature and Classification

This chapter proposes load signatures and classification of appliance in household level. To start with, it introduces several features of a load signature. Then, a novel load signature is proposed and its definition as well as deviation is provided. Next, this chapter demonstrates how the proposed load signature can be used to represent the features. In addition, load classification is established based on computation of the proposed load signature. Two new parameter derived from load signature are used for classifying appliance into different categories.

6.1 Features of Load Signature

6.1.1 Introduction

A load signature describes the electrical behaviour and some features of an individual appliance when it is in operation including both start-up and steady state (Liang et al. 2010). It not only presents the uniqueness of an appliance but also can be applied in load monitoring algorithm for recognising appliance patterns. Therefore, it is essential that the load signature involved in the disaggregation algorithm is typical, unique and consistent. In order to describe a load signature specifically and explicitly, some features, including current waveform, active & reactive power, current waveform, switch transient waveform, instantaneous power waveform and so on, are introduced into load signature study (Liang et al. 2010).

Millions of electrical appliances, with different types, functionalities and manufactures, are installed and in operation in residential buildings nowadays. It is unrealistic and impractical to obtain a complete data for all those appliances (Wang et al. 2013). Therefore, 13 typical

appliances in household including some with multiple operation modes are investigated in this work, which are shown in Table 6-1.

Table 6-1 List of appliances

No	Appliances	Modes	No	Appliances	Modes
1	Heater	1	**6**	Microwave	1
		2	**7**	Kettle	1
		3	**8**	Light bulb1	1
2	Electrical fan	1	**9**	Light bulb2	1
		2	**10**	Hair drier	1
		3	**11**	Fan heater	1
3	Energy saving bulb	1	**12**	Laptop1	1
4	Monitor	1	**13**	Laptop2	1
5	Fridge	1			

Have introduced the load signatures and some of its features, the detail of several features are investigated based on the measurements of the appliances in Table 6-1

6.1.2 Current Waveform

The current waveform in the time domain contains vast of information to describe the characteristic of a load. The amplitude of it represents the amount of power drawn from the power supply and the shape of it describes the type and characteristic of the load itself. It can be noticed that some appliances have unique features in their current waveform. Figure 6.1-6.3 show the current waveform of three appliances namely light bulb1, laptop1, monitor.

As shown in Figure 6.1, the waveform of light bulb1 is a sinusoidal waveform with RMS value as 0.17A. Since it is conventional incandescent lamp, the light bulb generates light with a metal filament heated by a current going through it. Therefore, it can be regarded as pure

resistive load and consumes sinusoidal current and it contains little harmonics, which can be also observed in Figure 6.1.

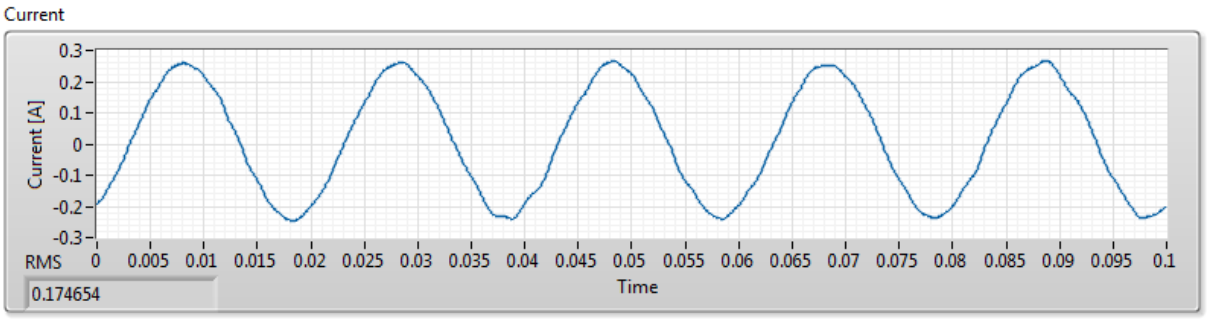

Figure 6.1 Current waveform of the light bulb 1

Figure 6.2 illustrates that the current of laptop 1 is distorted with RMS value 0.63A. In general, laptop consumes DC power hence an AC/DC converter is required in power adapter for every laptop. Since a rectifier is used to convert AC into DC, there are spikes observed in the current waveform. The spikes in the waveform may vary in width, amplitude and tooth shape. The current waveform of laptop 1 tends to have a wide, symmetrical tooth with peak value 1A as shown in Figure 6.2.

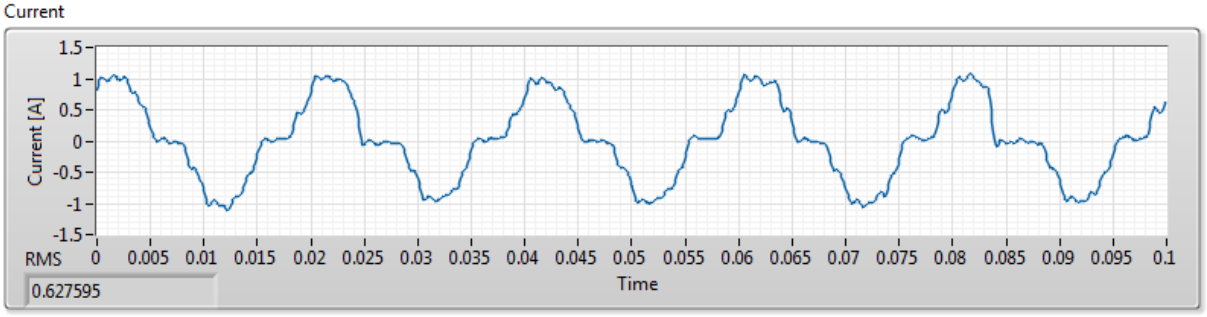

Figure 6.2 Current waveform of the laptop1

The waveform of monitor is similar with laptop1 and has two spikes in each cycle. The spike of it is thin and long with peak value 1A along with RMS value 0.23A as it illustrated in Figure 6.3.

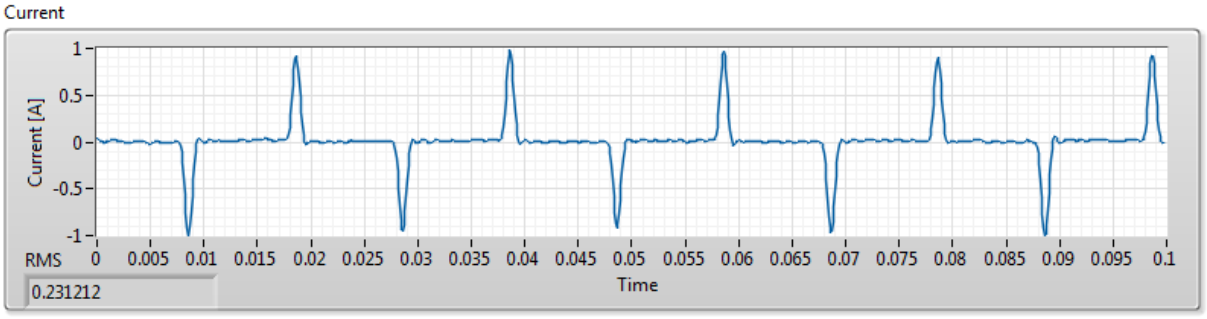

Figure 6.3 Current waveform of the monitor

Considering the presented three cases of current waveform, current waveform reflects the important information of appliance and it may contains very unique characteristic. However, it is difficult to use current waveform directly as a load signature to identify load. Precise current waveform requires high sampling frequency (higher than 1 kHz) to acquire and large space to store completely. Describing the similarity of two current waveforms is normally done by cross correlation, which takes long computation time and massive resources. Finally, it doesn't include the relationship between voltage and current. In another word, the angle difference in between is not specified. Therefore, two appliances with same current waveform may have different behaviours and power consumptions as long as the angle differences of them are different.

6.1.3 Active & Reactive Power

Another measurement of an appliance is active and reactive power and it is directly linked with the electricity bill of the customers. Generally, the formula of calculating active and reactive power is shown as follows(Arrillaga et al. 2000):

$$P = \sum_{k=0}^{\infty} P_k = \sum_{k=0}^{\infty} V_k I_k \cos(\phi_k) \quad (6.1)$$

$$Q = \sum_{k=0}^{\infty} Q_k = \sum_{k=0}^{\infty} V_k I_k \sin(\phi_k) \quad (6.2)$$

where

V_k and I_k are the amplitude of voltage and current kth order harmonic respectively.

ϕ_k is the phase angle difference between voltage and current kth order harmonic.

These formulas account for all harmonic components in voltage and current and return the accurate active power P and reactive power Q. Compared with the basic power calculation with fundamental frequency only, this method takes more steps and times to get the fine power values. The active power and reactive power can be shown in Table 6-2.

Table 6-2 List of active and reactive power values

No	Appliances	Modes	P [W]	Q [Var]
1	heater	1	657.1	6.2
		2	971.1	7.9
		3	1285.1	9.6
2	fan	1	30.1	11.7
		2	32.7	9.4
		3	42.7	4.7
3	energy saving bulb	1	17.9	19.3
4	monitor	1	25.7	48.54
5	fridge	1	74.8	36.3
6	microwave	1	421.1	120.1
7	kettle	1	2602.8	16.9
8	light bulb1	1	41.3	0.5
9	light bulb2	1	14.1	0.2
10	hair drier	1	1105.3	30.7
11	fan heater	1	687.1	11.7
12	laptop1	1	129.6	64.6
13	laptop2	1	15.1	39.3

It can be noted that the active power consumption of some appliances can be very close while the reactive power of them are quite distinct. As shown in Table 6-2, the light bulb2 and laptop2 both has power consumption around 15W while the difference between reactive powers of them is as large as 39 Var. The similar situation also applies to fan mode 3 and

light bulb1, fan mode 1 and mode 2. The PQ scatter diagram of 13 appliances is plotted in Figure 6.4. The closer two appliances are located in this figure, the more difficult they can be distinguished. A number of appliance lie near the origin of PQ scatter diagram therefore it makes the load identification among those appliances much more difficult. Furthermore, the PQ values also vary as the voltage of power supply changes, which means the noise in power value calculation is likely to affect the accuracy of load identification by applying signatures with PQ features only.

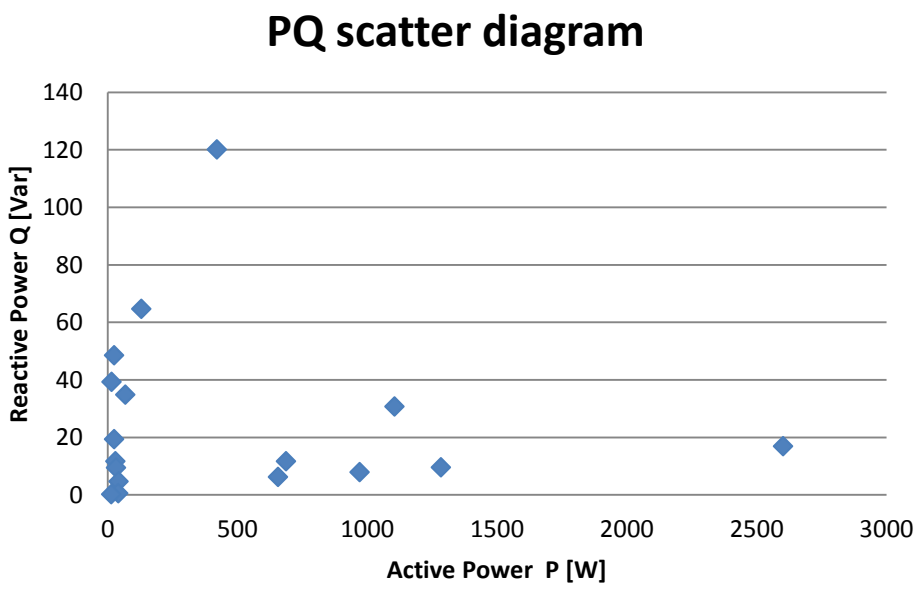

Figure 6.4 PQ scatter diagram of appliances

6.1.4 Current Spectrum

The harmonic spectrum can be obtained by applying Fast Fourier Transformation (FFT) to the voltage and current measurements. It unveils the features of different appliance in frequency domain. With known sequence of N complex number x_0, $x_1 \ldots, x_{n-1}$, an N-periodic sequence of complex numbers can be computed as:

$$X_k = \sum_{n=0}^{N-1} x_n e^{-i 2\pi k n / N}, \quad k = 0,1,2\ldots, N-1 \qquad (6.3)$$

where

x is the voltage or current measurement sequence .

X is complex number that encodes both amplitude and phase of a harmonic component of x. N is the number of samples

In terms of current waveform, linear load including resistive and motor load appears to contain little high order harmonics and nonlinear load, for instance, energy saving light bulb (ES light bulb), monitors and laptops has considerable 3rd and 5th harmonics. The spectrums of light bulb1 and monitor are shown in Figure 6.5 and Fig 6.6 respectively.

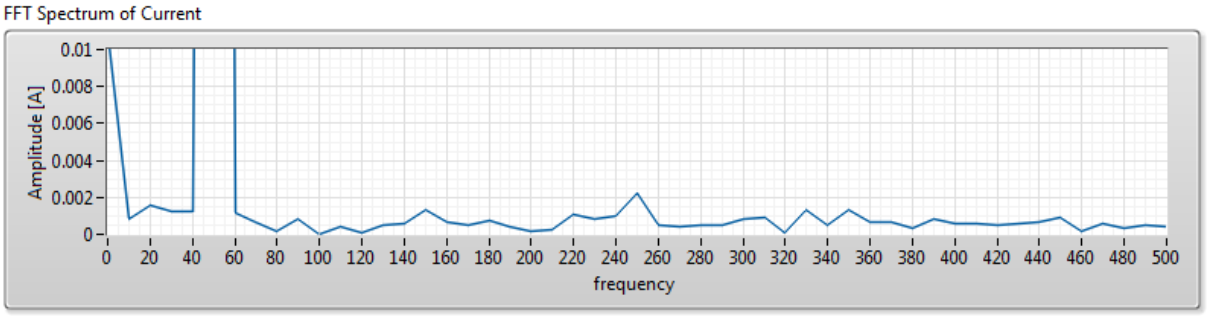

Figure 6.5 Current spectrum of the light bulb1

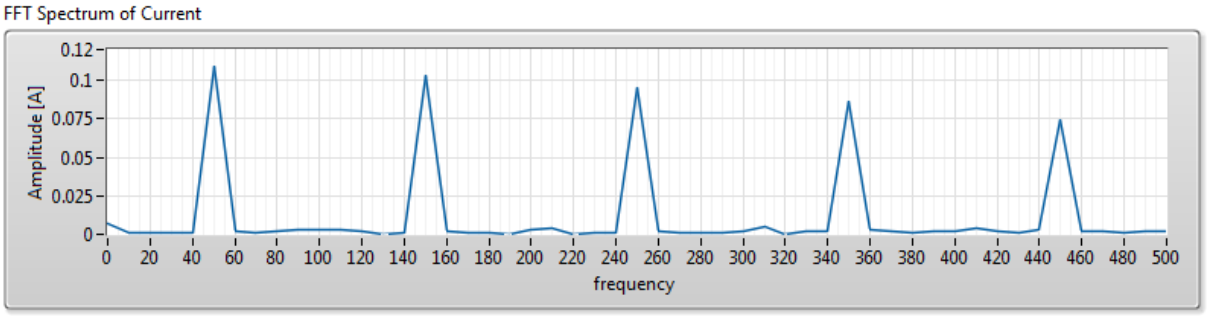

Figure 6.6 Current spectrum of the monitor

As it illustrates in Figure 6.1, the current of the light bulb1 is a pure sinusoidal waveform; therefore, the high order harmonics are negligible which coincide with Figure 6.5. However,

the current waveform of the monitor is highly distorted and it can be noted that the 3rd, 5th, 7th harmonic are as significant as the fundamental one. Thus, the current spectrum can be used to tell the difference between linear load and nonlinear load easily and efficiently. However, the current spectrum only contains the magnitudes but not phase angles of all the harmonics. It is difficult to decompose or disaggregate a current spectrum of composite load into individual load without the information of phase angles. .

6.1.5 Switch Transient Waveform

The features aforementioned are obtained in near steady-state or steady-state conditions. In reality, some appliance has different transient behaviour compared with its steady-state behaviour. The active power values within 15 seconds after an appliance being switched on is defined as the switching transient waveform in this study. The switching transient waveform of Laptop 1, lightbulb1 and fan mode 3 are shown in Figure 6.7.

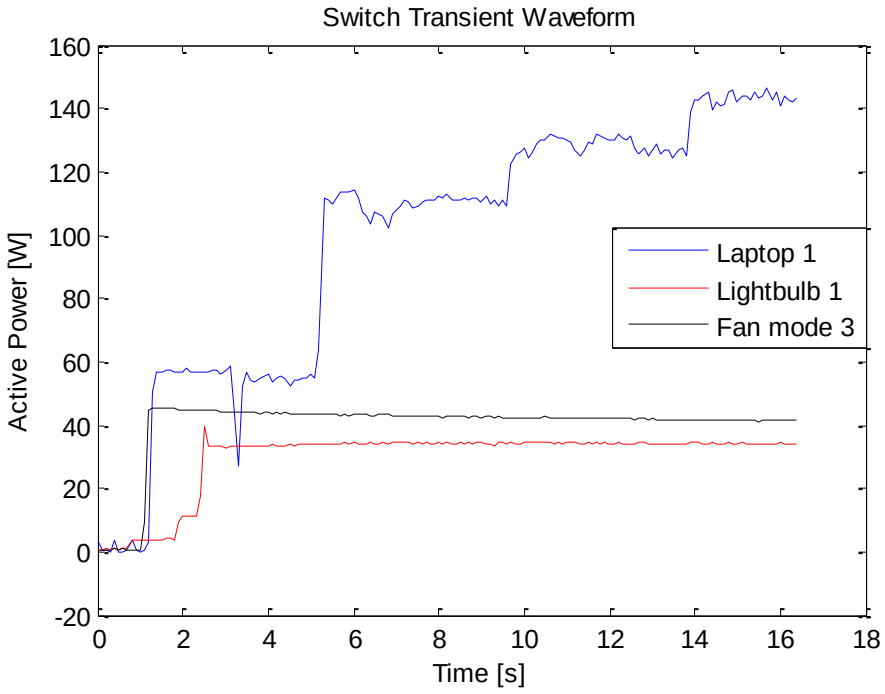

Figure 6.7 Switch transient waveforms of laptop1, light bulb1 and fan mode 3

The Laptop 1 has 4 step power changes in sequence before it reaches its steady state in 15s. The power of light bulb1 encounters a slight overshoot and then stabilises immediately. As for the fan, its power consumption climbs up sharply and keeps constant afterwards. It is interestingly noted that the switch transient waveforms can be quite different and potentially applied to identify appliances. Unfortunately, this feature is not very consistent and can be random for same appliances in some cases. Furthermore, the transients of some appliance are still difficult to be captured without failure despite of high sampling frequency used.

6.2 Proposed Load Signature

Each feature mentioned above somehow reflects the characteristic of appliances, but none of them is really unique and specific enough to be used as signature for identification and disaggregation. Some features occupy much resource, require long computation time or have difficulty being obtained. All of those disadvantages make them unsuitable to be utilized as a signature solely. In this work, a signature based on FFT is proposed and used for appliances monitoring. It is able to represent the most of aforementioned features with less resource. Apart from this, the mathematical operation between multiple signatures, including summation and subtraction, can be also defined and conducted with individual signatures.

6.2.1 Definition and Derivation

The load signature proposed in this work is a matrix with two rows, in which the first row includes the amplitude of current harmonics from 1^{st} to 9^{th} odd order and the second row includes the angle difference between voltage and current harmonics of the corresponding orders. One example of is shown as follows:

$$A = \begin{bmatrix} I_1 & I_3 & I_5 & I_7 & I_9 \\ \phi_1 & \phi_3 & \phi_5 & \phi_7 & \phi_9 \end{bmatrix}$$

where

A is the proposed signature of an appliance.

I_k is the amplitude of current harmonic kth order.

ϕ_k is the phase angle difference between voltage and current kth order.

In order to derive this signature, it starts with applying FFT to both acquired voltage and current. Based on the definition of FFT, the complex form of voltage and current FFT can be obtained as:

$$\mathrm{V}_k = \sum_{n=0}^{N-1} v_n e^{-i2\pi kn/N} \quad (6.4)$$

$$\mathrm{I}_k = \sum_{n=0}^{N-1} i_n e^{-i2\pi kn/N} \quad (6.5)$$

where

V_k and I_k are the complex form of voltage and current FFT.

v_n and i_n are the acquired voltage and current measurement.

Secondly, the amplitude (RMS value) and phase angle of both voltage and current can be derived based on the complex number V_k and I_k as follows:

$$V_k = \frac{1}{N}|\mathrm{V}_k| = \frac{1}{N}\sqrt{\mathrm{Re}(\mathrm{V}_k)^2 + \mathrm{Im}(\mathrm{V}_k)^2}, \alpha_k = \arctan(\mathrm{Im}(\mathrm{V}_k), \mathrm{Re}(\mathrm{V}_k)) \quad (6.6)$$

$$I_k = \frac{1}{N}|\mathrm{I}_k| = \frac{1}{N}\sqrt{\mathrm{Re}(\mathrm{I}_k)^2 + \mathrm{Im}(\mathrm{I}_k)^2}, \beta_k = \arctan(\mathrm{Im}(\mathrm{I}_k), \mathrm{Re}(\mathrm{I}_k)) \quad (6.7)$$

where

V_k and I_k are the kth order amplitude of voltage and current respectively.

α_k and β_k are the kth order phase angle of voltage and current respectively.

I_k can be directly put into the first row as one part of signature, and the phase angle difference is computed as follows:

$$\phi_k = \beta_k - \alpha_k \tag{6.8}$$

Taking the ES light bulb as an example, the signature of it is shown as follows:

$$\begin{aligned} A &= \begin{bmatrix} I_1 & I_3 & I_5 & I_7 & I_9 \\ \phi_1 & \phi_3 & \phi_5 & \phi_7 & \phi_9 \end{bmatrix} \\ &= \begin{bmatrix} 0.08 & 0.06 & 0.04 & 0.02 & 0.02 \\ 25.17 & 115.13 & -170.33 & 39.93 & 50.15 \end{bmatrix} \end{aligned} \tag{6.9}$$

Unlike some graphical signature such as current waveform, the proposed signature is purely numerical. Hence it is much easier for analysis and load disaggregation in later stage. What's more, the signature involves the information of 9^{th} harmonic components, which makes it quite unique and distinguishable. It is more likely to tell two different appliances by using this signature rather than power values. Compared with the features including either voltage or current characteristic, the relationship between voltage and current is also described in this signature.

6.2.2 Representation of Features

Most of features can be derived or reconstructed with this signature given. In another word, it somehow represents most of the features of an appliance especially steady-state

characteristics. Since the voltage is main voltage and regarded as constant, the voltage signature can be obtained as follows and used as a reference.

$$\begin{aligned}\bar{V} &= \begin{bmatrix} V_1 & V_3 & V_5 & V_7 & V_9 \\ \alpha_1 & \alpha_3 & \alpha_5 & \alpha_7 & \alpha_9 \end{bmatrix} \\ &= \begin{bmatrix} 236.39 & 2.01 & 1.29 & 1.95 & 0.79 \\ 2.05 & -36.30 & -42.98 & -174.69 & -83.36 \end{bmatrix}\end{aligned} \qquad (6.10)$$

6.2.2.1 Current Waveform

As one of the most essential features, current waveform includes massive information and characteristics of an appliance. Normally, it is recorded by storing the consecutive current values for at least one period with frequency higher than 10k. This approach requires high sampling time and large space to acquire and then log the data. However, the proposed signature which only has 10 numbers is able to represent the waveform, which can be expressed as follows:

$$I = \sum_{k=1}^{9} \sqrt{2} I_k \cos(100k\pi t + (\alpha_k + \phi_k) * \pi / 180) \quad k = 1,3,5,7,9 \qquad (6.11)$$

where

I_k and ϕ_k are known as the signature and α_k is the phase angle of the voltage.

Taking the energy saving bulb as an example, the reconstructed current waveform can be obtained by substituting equation (6.9) and (6.10) into (6.11) and is shown as follows:

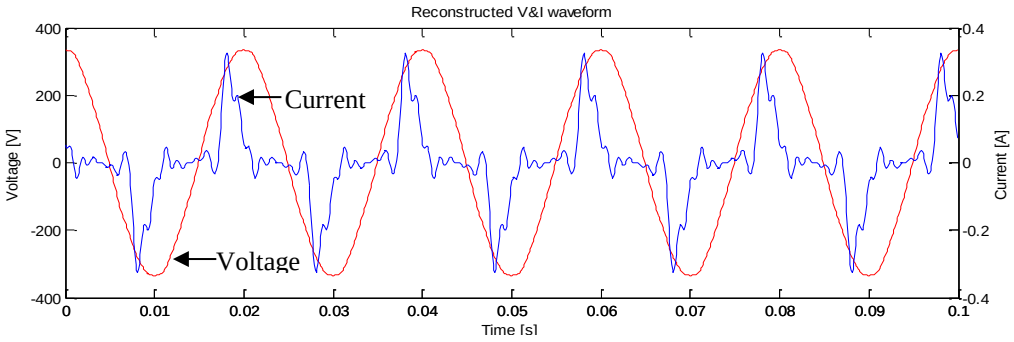

Figure 6.8 reconstructed current waveform of ES light bulb (blue) & voltage waveform (red)

Figure 6.9 illustrates the measured current waveform of energy saving light bulb at 10 kHz and it is shown as follows:

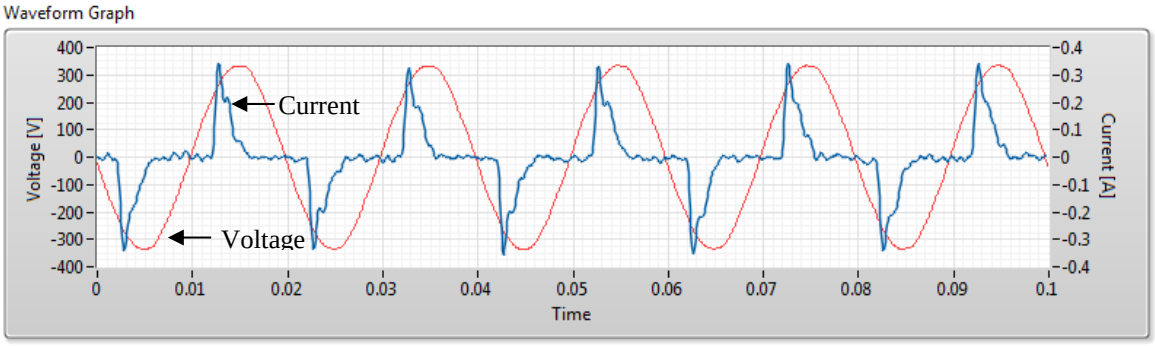

Figure 6.9 measured current waveform of ES light bulb (blue) and voltage waveform (red)

Although the phase in Figure 6.8 is shifted compare with Figure 6.9, the reconstructed current waveform has not only the same spike shape but also the same amplitude as measured one. Apart from this, it can be also observed that the angle differences between voltage and current waveform are also identical in Figure 6.8 and Figure 6.9.

Compared with the traditional consecutive value logging, the proposed signature is able to represent the current waveform with only 10 numerical numbers regardless of some tiny errors, which can be minimised further by involving more harmonic components if necessary.

6.2.2.2 Active & Reactive Power

Considering that the voltage is extremely small at high frequency, both the active and reactive power contributed by the frequency higher than 500Hz can be negligible. Therefore, the active and reactive power can be obtained by using proposed signature as:

$$P = \sum_{k=1}^{9} P_k = \sum_{k=1}^{9} V_k I_k \cos(\phi_k) \qquad k = 1,3,5,7,9 \qquad (6.12)$$

$$Q = \sum_{k=1}^{9} Q_k = \sum_{k=1}^{9} V_k I_k \sin(\phi_k) \qquad k = 1,3,5,7,9 \qquad (6.13)$$

The equation (6.12) and (6.13)is a five term approximation of active and reactive power definition as equation (6.1) and (6.2). With the known signatures of several appliances, the active and reactive power can be computed as Table 6-3 shows.

As it demonstrated in Table 6-3, the computed active power values are extremely close to the measurement with error ranging from 0.28% to 6.55%. Although the relatively errors of reactive power values are relatively large for some appliances, the differences between measured and reconstructed reactive power of most appliances are less than 5 Var. The measuring system applies different equations to calculate reactive power and it is accurate for sinusoidal waveforms only. Energy saving light bulb has quite different reconstruct reactive power compared with measurement since it has massive harmonic components.

Table 6-3 Comparison between measured and reconstructed PQ values

	Active power [P]			Reactive power [Var]		
	measured	represented	error	measured	represented	error
fan mode 1	27.1	28.2	3.90%	10.7	11.5	6.96%
fan mode 2	31.6	31.7	0.32%	9.5	9.3	2.11%
fan mode 3	36.1	35.2	2.49%	4.8	3.8	20.83%

heater mode 1	657.1	659.5	0.36%	6.2	7.2	13.89%
heater mode 2	953.3	945.5	0.82%	7.9	4.9	37.97%
heater mode 3	1590.8	1586.3	0.28%	14.1	8.3	41.13%
fridge	71.8	67.1	6.55%	36.3	32.7	9.92%
ES light bulb	16.9	17.2	1.74%	20.7	7.2	65.22%
light bulb	41.7	40.1	3.84%	0.5	0.7	28.57%

6.2.2.3 Current Spectrum

Based on the definition, the proposed signature has the amplitudes of 1st-9th order current harmonics in the first row; therefore the current spectrum can be plotted by simply using those figures. Figure 6.10 and Figure 6.11 illustrate the reconstructed and measured current spectrums of ES light bulb respectively.

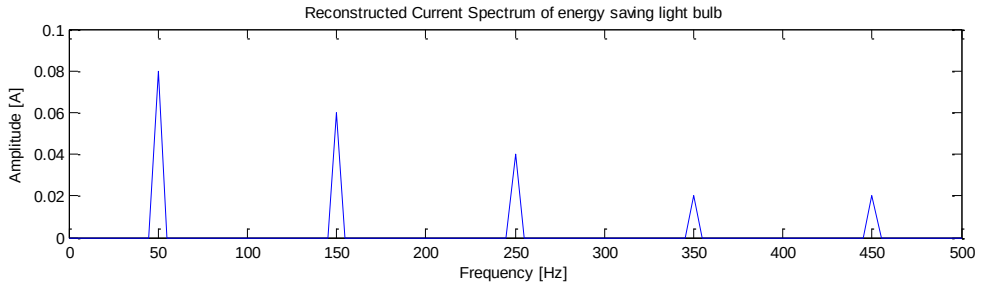

Figure 6.10 Reconstructed current spectrum of ES light bulb

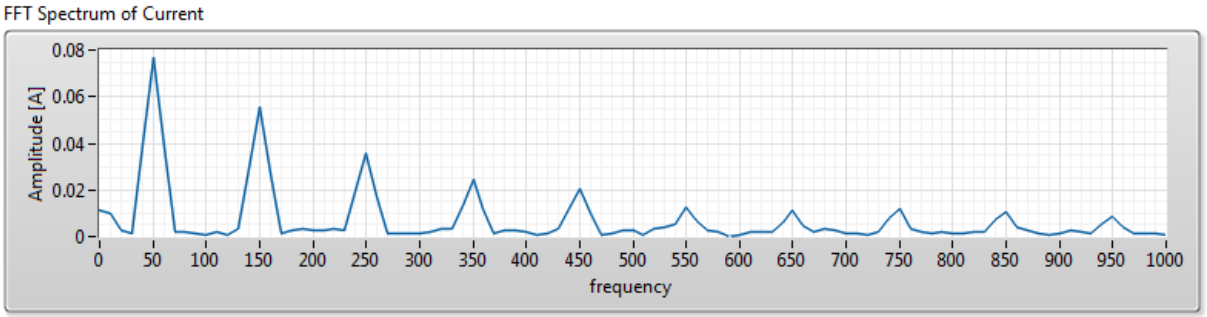

Figure 6.11 Measured current spectrum of ES light bulb

Non-linear loads may involve harmonics with frequency higher than 500Hz. As for linear loads, the harmonic higher than 5^{th} order is extremely small and can be ignored. Although the high harmonics are not presented by Figure 6.10, the most significant harmonics are all displayed and identical as the measurement in Figure 6.11. It can be concluded that the current spectrum is also well presented by utilising the proposed signature.

6.2.3 Mathematical Operation of Signatures

So far, the proposed signature is defined and utilised to represent the features of an appliance. It demonstrates that the proposed signature is unique and competent of representing most features of an appliance. In this part, the mathematical operation between signatures is derived and analysed since it is essential for computing the composite signature of multiple load or decomposing one signature from composite signature.

6.2.3.1 Addition of Signatures

Generally, multiple appliances working together generate a composite signature which can be derived from the individual appliance signatures. To start with, the addition of two individual signatures is analysed. The operation of two given signatures, A and B, are expressed as follows:

$$\begin{aligned} C = A \oplus B &= \begin{bmatrix} I_1^A & I_3^A & I_5^A & I_7^A & I_9^A \\ \phi_1^A & \phi_3^A & \phi_5^A & \phi_7^A & \phi_9^A \end{bmatrix} \oplus \begin{bmatrix} I_1^B & I_3^B & I_5^B & I_7^B & I_9^B \\ \phi_1^B & \phi_3^B & \phi_5^B & \phi_7^B & \phi_9^B \end{bmatrix} \\ &= \begin{bmatrix} I_1^C & I_3^C & I_5^C & I_7^C & I_9^C \\ \phi_1^C & \phi_3^C & \phi_5^C & \phi_7^C & \phi_9^C \end{bmatrix} \end{aligned} \qquad (6.14)$$

where

I_k^X is the amplitude of kth order harmonic of signature X.

ϕ_k^X is the phase angle difference between kth order harmonic of signature X and voltage.

Both two signatures are composed of 1st-9th harmonic components, therefore the approach to obtain the combined signature is to add the components with same order together individually and then put the results into the new signature. Taking the first order harmonic component as an example, the addition can be illustrates as follows:

$$\begin{aligned}
&I_1^A\cos(100\pi t+\phi_1^A)+I_1^B\cos(100\pi t+\phi_1^B)\\
&=I_1^A(\cos 100\pi t*\cos\phi_1^A-\sin 100\pi t*\sin\phi_1^A)+I_1^B(\cos 100\pi t*\cos\phi_1^B-\sin 100\pi t*\sin\phi_1^B)\\
&=\cos 100\pi t(I_1^A\cos\phi_1^A+I_1^B\cos\phi_1^B)-\sin 100\pi t(I_1^A\sin\phi_1^A+I_1^B\sin\phi_1^B) \qquad (6.15)\\
&=I_1^C(\cos 100\pi t*\frac{I_1^A\cos\phi_1^A+I_1^B\cos\phi_1^B}{I_1^C}-\sin 100\pi t*\frac{I_1^A\sin\phi_1^A+I_1^B\sin\phi_1^B}{I_1^C})\\
&=I_1^C\cos(100\pi t+\phi_1^C)
\end{aligned}$$

where

$$\begin{aligned}
I_1^C&=\sqrt{(I_1^A\cos\phi_1^A+I_1^B\cos\phi_1^B)^2+(I_1^A\sin\phi_1^A+I_1^B\sin\phi_1^B)^2}\\
&=\sqrt{(I_1^A)^2(\cos^2\phi_1^1+\sin^2\phi_1^1)+(I_1^B)^2(\cos^2\phi_1^A+\sin^2\phi_1^B)+2I_1^AI_1^B(\cos\phi_1^A\cos\phi_1^B+\sin\phi_1^A\sin\phi_1^B)}\\
&=\sqrt{(I_1^A)^2+(I_1^B)^2+2I_1^AI_1^B\cos(\phi_1^A-\phi_1^B)}
\end{aligned}$$

$$\phi_1^C=\arctan(\frac{I_1^A\sin\phi_1^A+I_1^B\sin\phi_1^B}{I_1^A\cos\phi_1^A+I_1^B\cos\phi_1^B})$$

Equation (6.15) can be also applied to other orders of harmonics, therefore the general equation of addition can be summarised as follows:

$$\begin{aligned}
I_k^C&=\sqrt{(I_k^A)^2+(I_k^B)^2+2I_k^AI_k^B\cos(\phi_k^A-\phi_k^B)}\\
\phi_k^C&=\arctan(\frac{I_k^A\sin\phi_k^A+I_k^B\sin\phi_k^B}{I_k^A\cos\phi_k^A+I_k^B\cos\phi_k^B}) \qquad ..k=1,3,5,7,9 \qquad (6.16)
\end{aligned}$$

Example1 is shown to derive the signature of composite load by using equation (6.16). The signatures of ES light bulb and fan mode 1 are given as follows, namely A and B:

$$A=\begin{bmatrix} 0.08 & 0.06 & 0.04 & 0.02 & 0.02 \\ 25.17 & 115.13 & -170.33 & 39.93 & 50.15 \end{bmatrix} \text{ and } B=\begin{bmatrix} 0.13 & 0 & 0 & 0 & 0 \\ 23.16 & 0 & 0 & 0 & 0 \end{bmatrix}$$

Applying equation (6.16) to all the elements in the above two signatures, the composite signature can be computed as:

$$C = A \oplus B = \begin{bmatrix} 0.21 & 0.06 & 0.04 & 0.02 & 0.02 \\ 23.93 & 115.13 & -170.33 & 39.93 & 50.15 \end{bmatrix}$$

The current waveform of this composite signature can be also reconstructed by applying equation (6.11)with the signature C as follows:

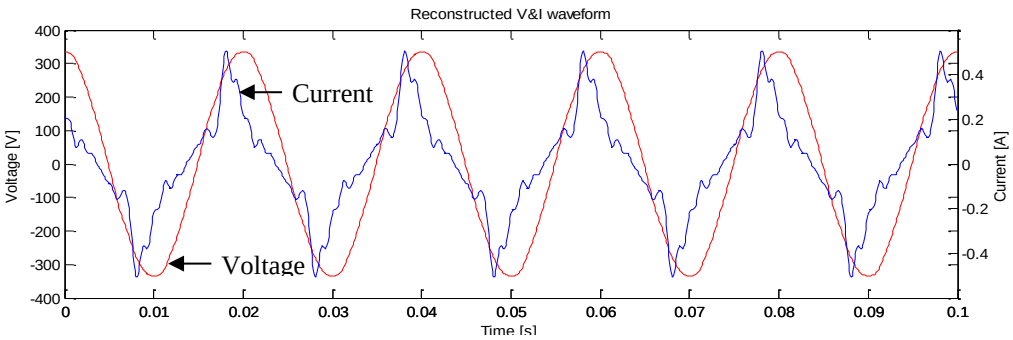

Figure 6.12 Reconstructed current waveform of composite load with signature C

In experiments, the signature of a composite load combing ES light bulb and fan mode 1 is shown as Figure 6.13 for comparisons:

$$C_{measured} = \begin{bmatrix} 0.20 & 0.06 & 0.04 & 0.02 & 0.02 \\ 23.88 & 116.22 & -167.29 & 44.58 & 51.29 \end{bmatrix}$$

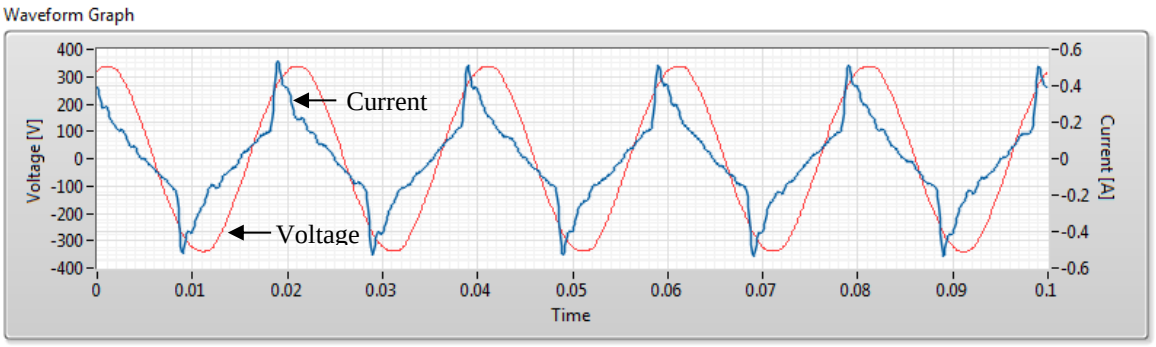

Figure 6.13 Measured current waveform of composite load in Example1

In terms of the signatures, the errors of calculated current amplitudes are all within 0.01 A and the errors of phase angles are less than 5 degree for all orders. As for the current waveform, it can be noticed that the reconstructed one not only has exact amplitude but also is in same phase and shape as the measurement. This example demonstrates that the signature of a composite load can be obtained with known signature of its addends. Under the circumstances of multiple appliances, the composite signature can be obtained by adding them pairwise step by step.

6.2.3.2 Subtraction of Signatures

The subtraction of signatures is defined as taking away a either individual or composite signature from a composite signature and shown as follows:

$$C = A\Theta B = \begin{bmatrix} I_1^A & I_3^A & I_5^A & I_7^A & I_9^A \\ \phi_1^A & \phi_3^A & \phi_5^A & \phi_7^A & \phi_9^A \end{bmatrix} \Theta \begin{bmatrix} I_1^B & I_3^B & I_5^B & I_7^B & I_9^B \\ \phi_1^B & \phi_3^B & \phi_5^B & \phi_7^B & \phi_9^B \end{bmatrix} = \begin{bmatrix} I_1^C & I_3^C & I_5^C & I_7^C & I_9^C \\ \phi_1^C & \phi_3^C & \phi_5^C & \phi_7^C & \phi_9^C \end{bmatrix} \quad (6.17)$$

Similar as addition, the subtraction is also done by different orders individually in the first step and then the results are put together to get the new residual signature. The first order subtraction is shown as follows:

$$
\begin{aligned}
& I_1^A \cos(100\pi t + \phi_1^A) - I_1^B \cos(100\pi t + \phi_1^B) \\
&= I_1^A (\cos 100\pi t * \cos\phi_1^A - \sin 100\pi t * \sin\phi_1^A) - I_1^B (\cos 100\pi t * \cos\phi_1^B - \sin 100\pi t * \sin\phi_1^B) \\
&= \cos 100\pi t (I_1^A \cos\phi_1^A - I_1^B \cos\phi_1^B) - \sin 100\pi t (I_1^A \sin\phi_1^A - I_1^B \sin\phi_1^B) \qquad (6.18) \\
&= I_1^C (\cos 100\pi t * \frac{I_1^A \cos\phi_1^A - I_1^B \cos\phi_1^B}{I_1^C} - \sin 100\pi t * \frac{I_1^A \sin\phi_1^A - I_1^B \sin\phi_1^B}{I_1^C}) \\
&= I_1^C \cos(100\pi t + \phi_1^C)
\end{aligned}
$$

Where

$$
\begin{aligned}
I_1^C &= \sqrt{(I_1^A \cos\phi_1^A - I_1^B \cos\phi_1^B)^2 + (I_1^A \sin\phi_1^A - I_1^B \sin\phi_1^B)^2} \\
&= \sqrt{(I_1^A)^2(\cos^2\phi_1^1 + \sin^2\phi_1^1) + (I_1^B)^2(\cos^2\phi_1^A + \sin^2\phi_1^B) - 2I_1^A I_1^B(\cos\phi_1^A \cos\phi_1^B + \sin\phi_1^A \sin\phi_1^B)} \\
&= \sqrt{(I_1^A)^2 + (I_1^B)^2 - 2I_1^A I_1^B \cos(\phi_1^A - \phi_1^B)}
\end{aligned}
$$

$$
\phi_1^C = \arctan(\frac{I_1^A \sin\phi_1^A - I_1^B \sin\phi_1^B}{I_1^A \cos\phi_1^A - I_1^B \cos\phi_1^B})
$$

Applying the equation (6.18)to all orders, the elements of new residual signature can be computed as follows:

$$
\begin{aligned}
I_k^C &= \sqrt{(I_k^A)^2 + (I_k^B)^2 - 2I_k^A I_k^B \cos(\phi_k^A - \phi_k^B)} \\
\phi_k^C &= \arctan(\frac{I_k^A \sin\phi_k^A - I_k^B \sin\phi_k^B}{I_k^A \cos\phi_k^A - I_k^B \cos\phi_k^B}) \qquad k = 1,3,5,7,9 \qquad (6.19)
\end{aligned}
$$

In terms of signature addition, it is normally used to verify composite load which is made up of different individual appliances. However, signature subtraction can be applied to identify event of current change and also extract signatures from composite signature.

Example2 is shown to derive the signature of an event. The signature and its current waveform of an unknown composite signature are measured as follows:

$$
A = \begin{bmatrix} 0.68 & 0.06 & 0.04 & 0.02 & 0.02 \\ 7.28 & 112.68 & -159.76 & 35.23 & 44.27 \end{bmatrix}
$$

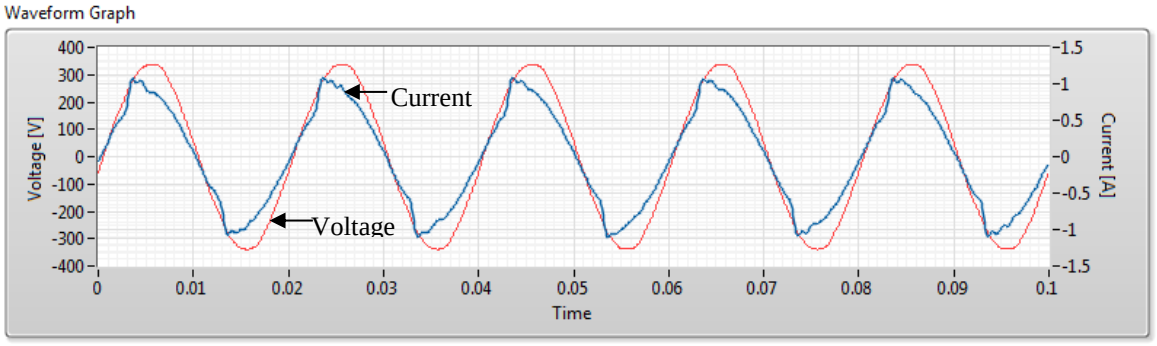

Figure 6.14 Current waveform of an unknown composite load in Example2

After an event occurred, the signature and its current waveform is measured as follows:

$$B = \begin{bmatrix} 0.61 & 0.01 & 0 & 0 & 0 \\ 5.23 & 21.35 & 0 & 0 & 0 \end{bmatrix}$$

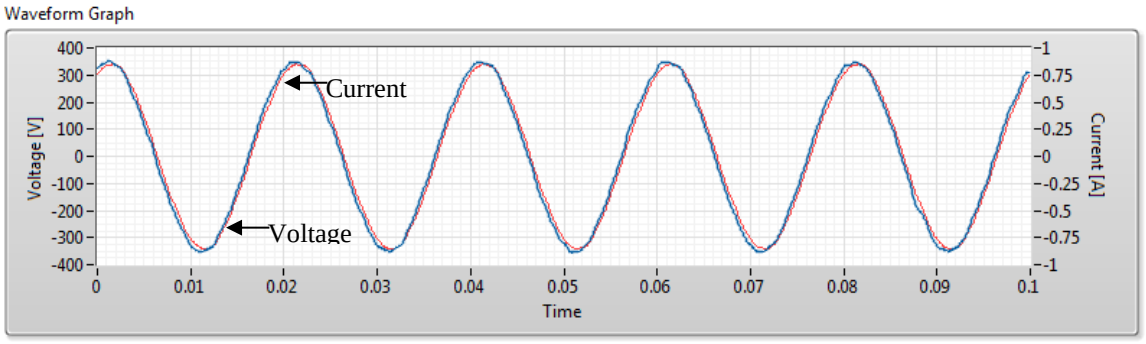

Figure 6.15 Current waveform of the composite load after event in Example2

The residual signature, which is also the signature of the event, can be computed by applying equation (6.19) and the reconstructed current waveform based on residual signature C is shown as follows:

$$C = A\Theta B = \begin{bmatrix} 0.07 & 0.06 & 0.04 & 0.02 & 0.02 \\ 24.50 & 122.11 & -159.76 & 35.23 & 44.27 \end{bmatrix}$$

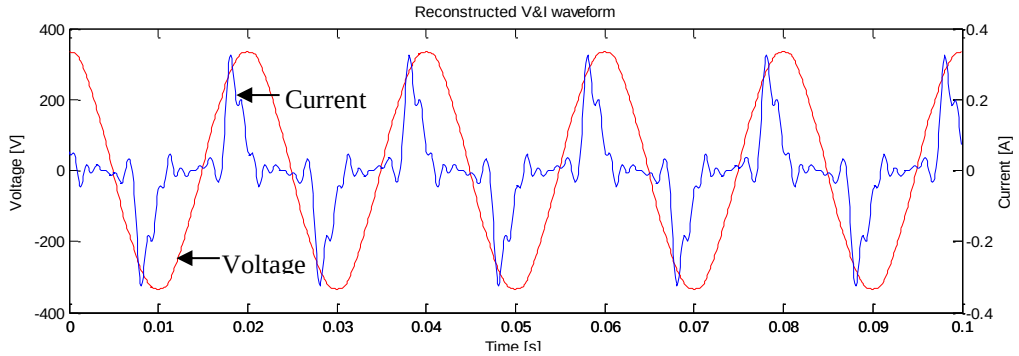

Figure 6.16 Reconstructed current waveform of residual signature C in Example2

It can be interestingly observed that the current waveform of residual signature C have same shape and phase angle as the ES light bulb, which is illustrated in Figure 6.9. Comparing residual signature C with the signature of energy saving light bulb demonstrates that the amplitude of all harmonic components between those two are extremely close within 0.01A error and error of phase angles are less than 7 degree. It then can be concluded that the event is changing on-off state of ES light bulb.

6.3 Load Classification

The characteristics of loads are normally investigated by looking into the different features of appliance, including start-up transient current and its envelope, steady-state current waveform, power values and voltage-current trajectory under start up and steady-state conditions. However, most of those features can be represented with proposed signatures as introduced previously. It is worthwhile exploring an approach to classify different loads with known signatures instead of previous features. This approach is able to make most of the proposed signatures and simplify the classification process once the signatures of loads figured out. On other hand, the signatures play an essential role in the load monitor algorithm in this work; therefore it would be fairly straightforward if a signature-based classification approach is introduced. Two parameters, namely **harmonic to fundamental ratio (HFR)** and

fundamental angle difference (FAD) ,are defined based on appliance signature and then a taxonomy taking advantage of HFR and FAD is introduced.

Based on field tests and working principle, household appliances can be classified into six groups: resistive, pump-operated, motor-driven, electronically-fed, electronic power control and fluorescent lighting(Sultanem 1991). In the point of view of harmonic, they can be also put into 3 groups: resistive, motive (inductive) and nonlinear(Burch et al. 2003). In (Akbar & Khan 2007), appliances are simply divided into linear loads and nonlinear loads depending on if the current is pure sinusoidal. In this work, Motor-driven, pump-operated and fluorescent lighting are all treated as inductive load whereas electronically-fed and electronic power control is classified as nonlinear load. Therefore, the majority of household appliances can be categorised into three group as discussed in (Burch et al. 2003), namely resistive load, inductive load and nonlinear load.

6.3.1 Definitions of HFR & FAD

Harmonic to fundamental ratio (HFR) is defined as the ratio of 3rd harmonic component amplitude over fundamental frequency amplitude and is shown as

$$HFR = \frac{I_3}{I_1} \qquad (6.20)$$

where

I_1 & I_3 are the amplitude of fundamental frequency and 3rd harmonic respectively and can be obtained directly from signature.

Generally, the amplitude of 3rd harmonic I_3 implies whether the current waveform has distortion or not. In some cases, it is not possible to identify the type of an appliance by only

considering the amplitude of 3rd harmonics. For instance, the heater, which is apparently a resistive load, has a 3rd harmonic component with 0.05A amplitude while an energy saving light bulb ,whose current waveform is highly distorted as Figure 6.9 illustrates, has 0.06A of 3rd harmonic as the heater. If fundamental frequency is also taken into account for distinguishing them, HFR of them can be calculated as

$$HFR_{heater} = \frac{0.04}{4.09} = 1.0\% \text{ and } HFR_{ES\,light\,bulb} = \frac{0.06}{0.08} = 75.0\%$$

It can be noticed that the HFR of heater is much small than the HFR of energy saving light bulb although the 3rd harmonic is same. Therefore, the HFR of an appliance, rather than the amplitude of harmonics, describes the nonlinearity and distortion of an appliance. Generally, an appliance is classified as non-linear load if its HFR is greater than 30%.

Fundamental angle difference (FAD) is defined as the phase angle difference of the fundamental frequency between current and voltage and shown as follows:

$$FAD = \beta_1 - \alpha_1 = \phi_1 \qquad (6.21)$$

where

α_1 and β_1 are the phase angles of fundamental frequency of voltage and current.

ϕ_1 is the element at row 2, column 1 of a signature.

FAD describes the basic phase angle relationship of voltage and current, especially for linear loads. Since the current waveforms of linear loads are purely sinusoidal, FAD is the only parameter to distinguish the type of a load. Appliances, such as incandescent light bulb, heater and kettle have no angle difference between voltage and current and are classified as

resistive load. On the contrast, the FAD of appliances including fan and fridge is non-zero. It implies that they consume reactive power and their power factors are less than 1. Considering the current normally lags the voltage of this load type, they are classified as inductive load. In conclusion, appliances can be also classified into three groups, namely resistive, inductive and non-linear, by using HFR and FAD instead of traditional features such as power factor, reactive power and total harmonic distortion (THD).

6.3.2 Resistive load

This category mainly includes the appliances which are normally used for heating and lighting purposes, for instances, incandescent light bulb and electrical heater. Some appliances combine heating with fan (such as fan heater and hair drier) and hence consume a little reactive power. Since the resistive characteristic completely dominates, they are also considered as members of this group. All the appliances in this group regularly operate close to unity power factor and their harmonic content is extremely small and can be ignored. Some examples can be shown as Figure 6.17 and Figure 6.18As shown in the figures, the THDs of those appliances are small than 5% and power factor are almost 1 despite of small reactive power can be noticed. Apart from fundamental frequency, the harmonic components can be hardly observed. All those features are in good agreement with the description of this category.

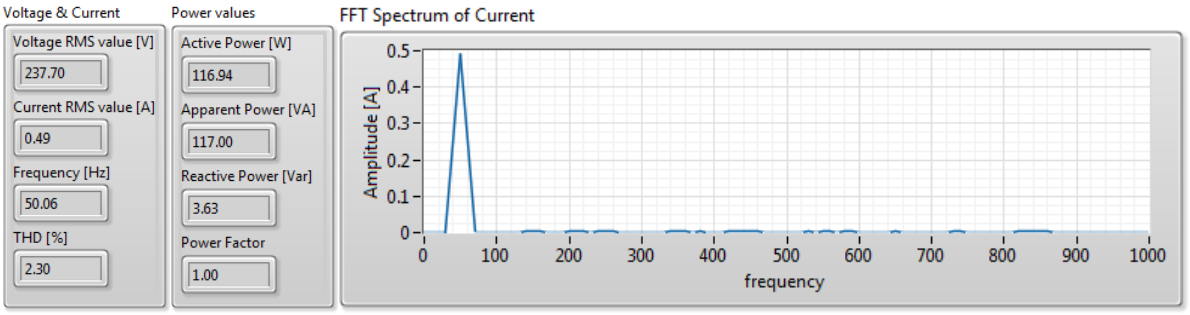

Figure 6.17 Voltage & current, power values and current harmonic content of incandescent light bulb

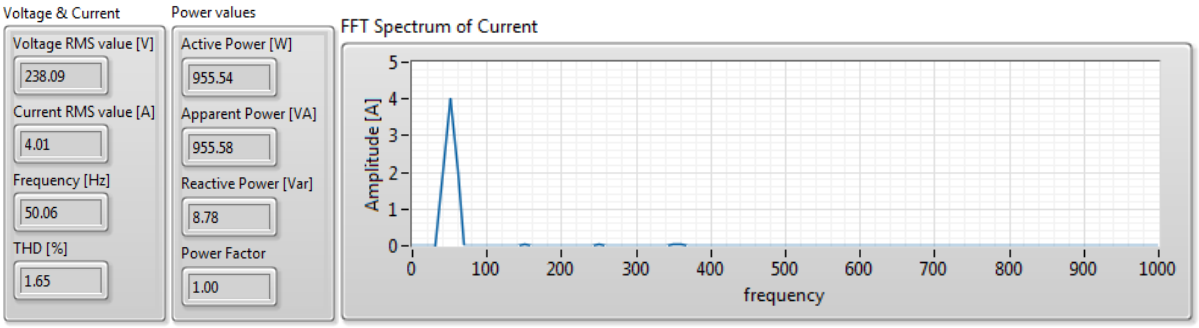

Figure 6.18 Voltage & current, power values and current harmonic content of heater mode 2

Instead of using traditional measurement mentioned earlier, appliances are classified by applying proposed signatures and new parameters namely HFR and FAD, which is calculated and demonstrated as follows:

$$A_{heater} = \begin{bmatrix} 4.09 & 0.04 & 0.03 & 0.04 & 0.02 \\ 0.35 & 2.25 & -1.41 & 0.57 & 5.04 \end{bmatrix}$$

$$HFR_{heater} = \frac{0.04}{4.09} = 1.0\% \text{ and } FAD_{heater} = 0.35$$

$$A_{incan\_light\_bulb} = \begin{bmatrix} 0.50 & 0.01 & 0.01 & 0.01 & 0.00 \\ 0.43 & 20.57 & 31.15 & 9.99 & -7.76 \end{bmatrix}$$

$$HFR_{incan\_light\_bulb} = \frac{0.01}{0.50} = 2.0\% \text{ and } FAD_{incan\_light\_bulb} = 0.43$$

As it shown above, the HFRs of these two loads are very small and lower than 5%, which means their current waveform are sinusoidal. On the other hand, the FADs of them are also close to 0. Therefore, it can be inferred that the current and voltage are in phase for this type of load. It demonstrates that a resistive load can be distinguished by only analysing the signature of it. In conclusion, an appliance with HFR lower than 30% and FAD smaller than 5 degree can be classified as a resistive load.

6.3.3 Inductive Load

This group consists of motor-driven, pump-operated and inductive loads such as refrigerators and fans. Most of them are driven by induction motor, which can be described by an equivalent circuit with inductive characteristics and results in a phase angle between its voltage and current. The most essential features of them is that they draw considerable reactive power. Due to its significant reactive power consumption, this type of loads does not normally operate at unity power factor. Its power factor may depend on its loads and typically from 0.85 to 0.95. They may also contain some harmonics but it is not as significant as nonlinear load. To show those features, the measurement of fan mode 1 is shown as Figure 6.19. As it shown in the figure, fan consumes 12Var reactive power and operates as 0.93 power factor, which is expected as an inductive load. Secondly, it can be noticed that its THD is 5.58% and higher than resistive load. The signature, HFR and FAD of fan mode 1 is shown as follows.

$$A_{fan\_mode1} = \begin{bmatrix} 0.14 & 0.01 & 0 & 0 & 0 \\ 20.70 & 76.71 & 0 & 0 & 0 \end{bmatrix}$$

$$HFR_{fan\_mode1} = \frac{0.01}{0.14} = 7.1\% \text{ and } FAD_{fan\_mode1} = 20.70$$

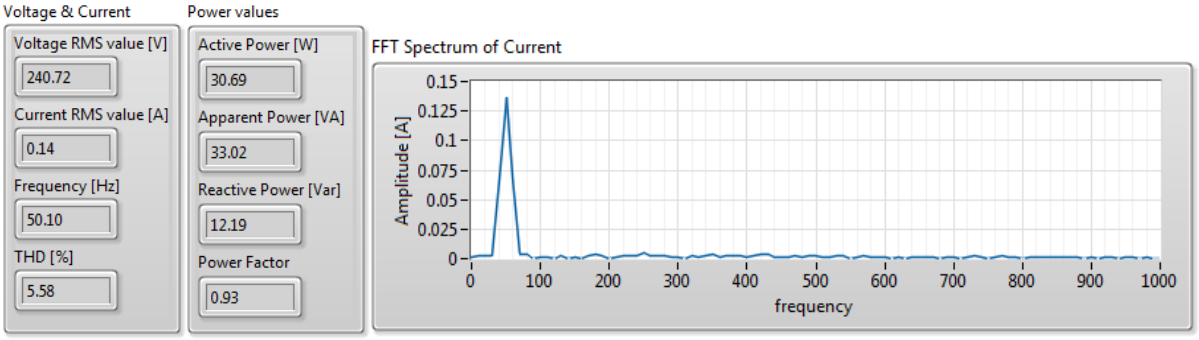

Figure 6.19 Voltage & current, power values and current harmonic content of fan mode 1

Compared with resistve load, inductive load tends to has large FAD, which means the angle difference of voltage and current for them cannot be negligible. Furthermore, the HFR of inductive load is also a little higher than resistive load but much smaller than nonlinear load. Therefore it can be concluded that an appliance with HFR smaller than 30% and FAD greater than 5 degree can be classified as an inductive load.

6.3.4 Non-linear Load

Generally, all modern electrical and electronic appliances involve some form of power control. Majority of modern electronic equipment apply switched-mode power supplies (SMPS) to convert the mains voltage to DC voltage or lower AC voltage as it required. The working principle of SMPS is different from traditional step-down transformer and rectifier plays essential part inside it. Instead of drawing continuous current from mains, SMPS only consumes pulses of current which includes large amounts of harmonic. Therefore, the current waveform it draws from the mains can be very distinct and distorted. However, SMPS demonstrates tremendous advantages on size, weight, cost and efficiency compared with traditional approaches, which also made it widely-used in powering electronic appliances.

Appliances such as laptop, monitor and energy saving light bulb belong to this category. The measurement and waveforms of laptop1 and energy saving light bulb are illustrated as follows:

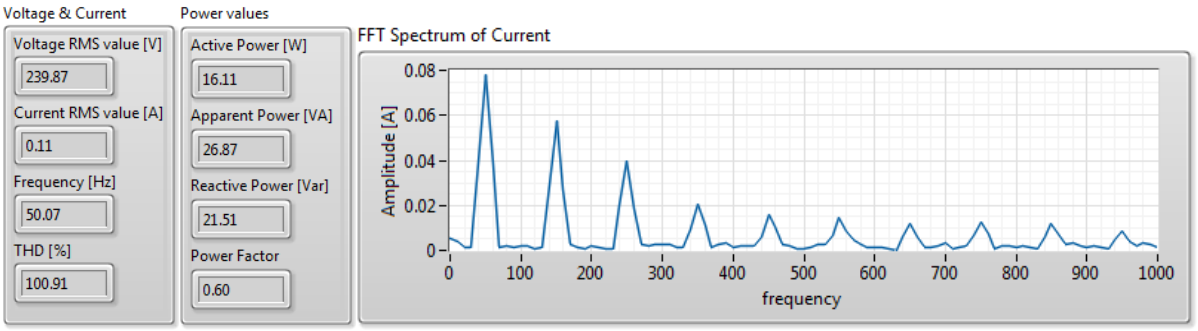

Figure 6.20 Voltage & current, power values and current harmonic content of ES light bulb

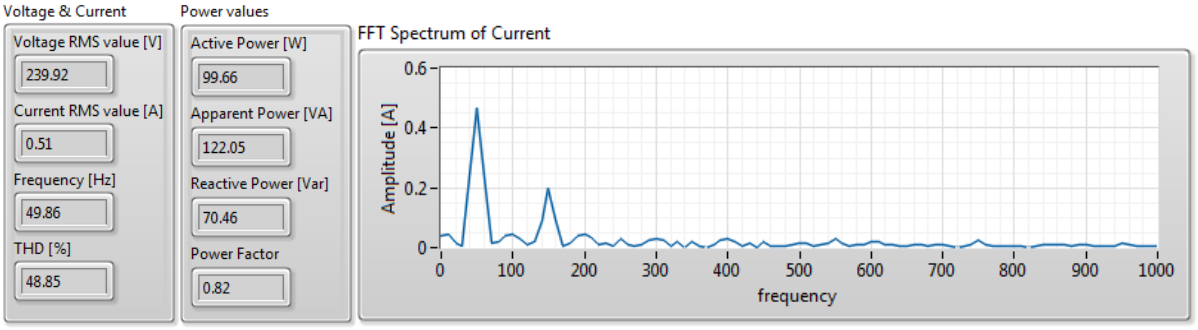

Figure 6.21 Voltage & current, power values and current harmonic content of laptop1

As they demonstrated in Figure 6.20 and Figure 6.21, these two appliances have significant levels of harmonic components. The THD (%) of energy saving light bulb and laptop1 are namely 100% and 48%. Moreover, the reactive power is relatively large and even exceeds the value of active power for energy saving light bulb. It can be also noticed that the power factors of them are far from unity as well.

Applying equation (6.20) and (6.21) to the corresponding signatures, the HFRs and FADs of two appliances mentioned above is shown as follows:

$$A_{ES\_light\_bulb} = \begin{bmatrix} 0.08 & 0.06 & 0.04 & 0.02 & 0.02 \\ 25.17 & 115.13 & -170.33 & 39.93 & 50.15 \end{bmatrix}$$

$$HFR_{ES\_light\_bulb} = \frac{0.06}{0.08} = 75\% \text{ and } FAD_{ES\_light\_bulb} = 25.17$$

$$A_{laptop1} = \begin{bmatrix} 0.45 & 0.21 & 0.04 & 0.04 & 0.04 \\ 23.33 & 93.81 & -32.27 & 95.99 & 30.95 \end{bmatrix}$$

$$HFR_{laptop1} = \frac{0.21}{0.45} = 46.7\% \text{ and } FAD_{laptop1} = 23.33$$

Since HFR is defined to describe the harmonic content in the current waveform, larger HFR value implies that the appliance contains more harmonic components and hence it is more likely to be a nonlinear load. Although HFR is similar to THD, it only considers the 3rd harmonic, which normally dominates among all harmonic contents apart from fundamental frequency. The advantage of using HFR to describe nonlinearity mainly is that it is capable of reflecting the harmonic ratio in a current waveform with simply computation. As the results shown above, the HFR of ES light bulb and laptop1 are 75% and 46.7% respectively. On the other hand, the FADs of nonlinear load are non-zero, which also makes it different from resistive load. Above all, an appliance with HFR higher than 30% is grouped as nonlinear loads in this work.

6.3.5 Classification using HFR & FAD

As the taxonomy describes previously, an appliance can be classified into resistive load, inductive load and nonlinear load, simply by using their signatures and calculating HFR along with FAD. The flow chart is shown Figure 6.22.

The process starts from calculating the HFR and FAD based on given signature by applying equation (6.20) and (6.21). Then, the HFR of an appliance is first compared with the nonlinearity threshold 30%. The appliance is grouped into nonlinear load if the HFR of it higher than the limit. Afterward, the FAD is compared with the threshold 5 degree. It can be concluded that an appliance with FAD higher than 5% and HFR lower than 30% is classified as inductive load. Finally, the rest of appliances, which has HFR and FAD both below their limits, are therefore considered as resistive load. This approach of classifying appliance has the same functionality as the one using tradition feature such as power factor, THD and reactive power. However, it is more consistent with the proposed signature, which means it can be easily obtained once the signature is known. The high compatibility makes this approach becoming a significant part in later stage of proposed load monitoring algorithm.

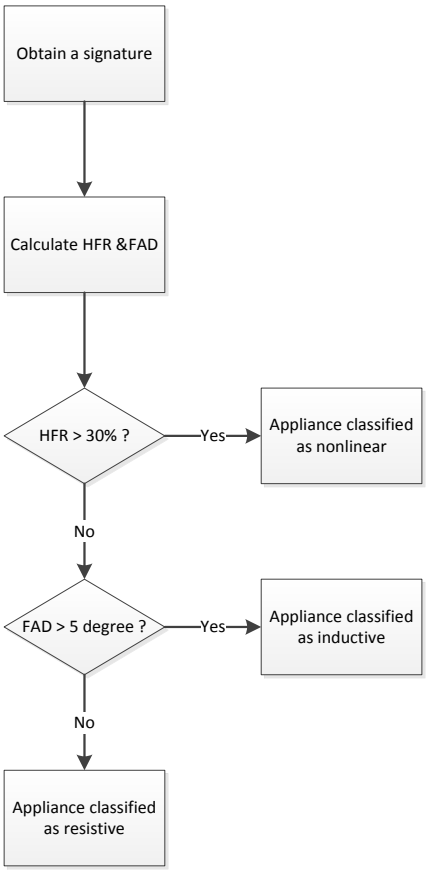

Figure 6.22 Flow chart of classifying appliances by using HFR and FAD

A classification of various appliances by using HFR and FAD is shown in Table 6-4:

Table 6-4 Classification of various appliances using HFR and FAD

	HFR (%)	FAD (Degree)	Type
fan mode 1	7.14	20.7	Inductive
fan mode 2	6.67	15.67	Inductive
fan mode 3	5.89	6.22	Inductive
heater mode 1	0.71	0.31	Resistive
heater mode 2	0.97	0.35	Resistive
fridge	12.5	27.15	Inductive
ES light bulb	75.00	25.17	Non-linear
light bulb	2.00	0.43	Resistive
Laptop 1	46.67	23.33	Non-linear

In addition to the load classification discussed above, there are other household appliance categories depending on other characteristics of appliances:

- Depending on the duration of on-off cycle: continuous (light bulbs, fans), long-cycle (fridge) and short-cycle (microwave)
- Depending on the modes: single-mode (light bulbs), multi-mode (fans, heaters)

Although they are the inherent features of appliances, they are not unique enough to be used to identify and classify appliance. Also, they are not easy to be associated with proposed signatures. Therefore, those taxonomies are not considered in the following work.

6.4 Summary

This chapter firstly explains the typical load features used to describe and distinguish an appliance. Those load features can somehow represent some characteristics of an appliance but is still incompetent to be used for identifying an appliance independently.

Therefore, a new load signature is proposed and defined. The detailed derivation process of this signature is also explained afterwards. It has been demonstrated that this signature can be applied to represent all the features mentioned previously. What's more, the addition and

subtraction between multiple signatures are also discussed. It forms the basis of conducting non-intrusive load monitoring by using proposed signatures.

Two parameters, namely HFR and FAD, are defined and derived based on the signature of an appliance. With this two parameters involved, a load classification mechanism is introduced and discussed. It takes advantage of known appliance signature to classify the appliance into different groups quickly and accurately with less calculation and inference.

Chapter 7 Development of Non-intrusive Load Monitoring Algorithm

This chapter introduces the non-intrusive load monitoring algorithm developed based on the proposed signature in Chapter 6, which consists of three stages: data acquisition & event detection, Error Computation & Signature Matching and Appliance Recognition & Classification. The implementation and experimental results of the proposed algorithm is also discussed in following sections.

7.1 Non-intrusive load Monitoring Algorithm

Basically, the algorithm developed for monitoring the on-off state of all appliances within household is an event-based algorithm. It is continuously monitoring the states of total current consumption and mains voltage. Once an event occurs, the algorithm applies signature operation to compute the signature of the event and then identify the event. Finally, the states of all appliances can be observed and recorded. The proposed non-intrusive load monitoring algorithm is divided into 3 stages, namely data acquisition & event detection, error computation & signature matching and appliance recognition & classification and explained in the following parts.

7.1.1 Data Acquisition & Event Detection

To start with, the voltage and current are sampled and acquired at relative high frequency (10 kHz) in real time. Meanwhile, Fast Fourier Transform is applied to both the acquired voltage and total current signals and hence the signature of aggregated load, which is defined as aggregated signature, can be obtained. Instead of monitoring the voltage and current directly, the algorithm focuses on the change of aggregated signature, which is updated and logged at 1 Hz frequency.

The most recent 5 samples of aggregated signatures are putted into a buffer and analysed in real time. The data in the buffer can be stored and also fetched anytime if necessary. It is mainly for appliance behaviour analysis and diagnoses purposes.

Applying the subtraction of signatures to consecutive values in the buffer, the derivative of aggregated signatures can be obtained. Normally, both the amplitude and phase angle of the derivative should be varied in a limit range if no appliance switched on or off. Either amplitude or phase angle of the derivative exceeding the set threshold results in an event being detected. The detailed flow chart of event detection can be shown as follows

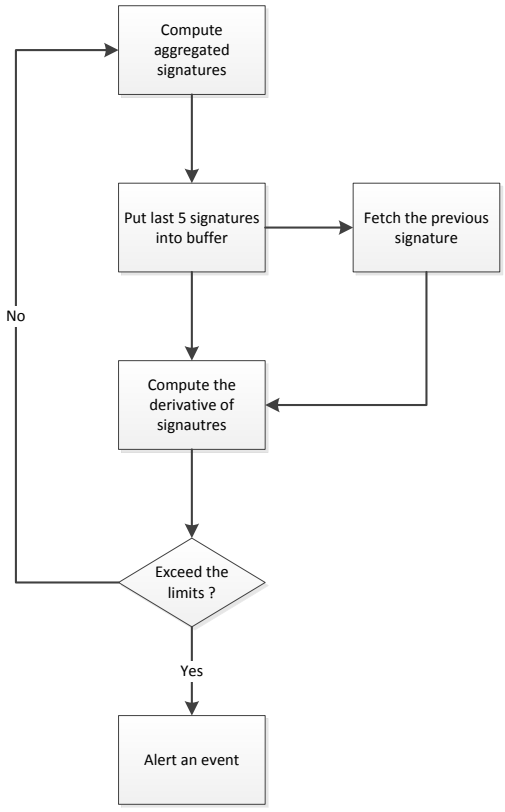

Figure 7.1Flow chart of event detection process

The threshold of amplitude and phase angle change is set as 0.05A and 5 degree respectively. Therefore any appliance with power consumption high than 10W can be detected when being either switched on or switched off.

Some appliances has very uncertain and significant transient at the beginning of start-up, therefore the derivative of signatures is not the same each time being switched on and tend to vary dramatically, for instance, fridge, laptop and TV. In this case, the previous values with more than 1 delay in the buffer instead of the consecutive values can be used to calculate the derivative and avoid the spike-shape transient.

7.1.2 Error Computation & Signature Matching

As long as the event is detected, the very first step is to obtain the sign of the current amplitude change and hence the event can be identified as either switch-on event or switch-off event. In another word, a positive current change results in a switch-on event and vice versa.

The **event signature** is computed by applying the subtraction of signatures as well. The result will be passed on to next stage and then compared with the signatures of all appliances one by one in the database. For each comparison, the relative error of every element is calculated and then formed into an **error signature** as follows:

$$E = \begin{bmatrix} e_{I\_1} & e_{I\_3} & e_{I\_5} & e_{I\_7} & e_{I\_9} \\ e_{\phi\_1} & e_{\phi\_3} & e_{\phi\_5} & e_{\phi\_7} & e_{\phi\_9} \end{bmatrix}$$

$$e_{\mathrm{I}\_k} = \frac{\left| I_k - I_k^{'} \right|}{I_k^{'}} \text{ and } e_{\phi\_k} = \frac{\left| \phi_k - \phi_k^{'} \right|}{\phi_k^{'}}$$

Where

E is the error signature

I_k and ϕ_k are the elements from event signature

$I_k^{'}$ and $\phi_k^{'}$ are the elements from signature in database

Considering 10 elements contained in error signature, a **weight factor matrix**, with 5 rows and 2 columns, is assigned to indicate the different significance of all the elements as follows:

$$E*W=\begin{bmatrix} e_{I\_1} & e_{I\_3} & e_{I\_5} & e_{I\_7} & e_{I\_9} \\ e_{\phi\_1} & e_{\phi\_3} & e_{\phi\_5} & e_{\phi\_7} & e_{\phi\_9} \end{bmatrix} * \begin{bmatrix} w_{11} & w_{12} \\ w_{21} & w_{22} \\ w_{31} & w_{32} \\ w_{41} & w_{42} \\ w_{51} & w_{52} \end{bmatrix} = \begin{bmatrix} e_{11} & e_{12} \\ e_{21} & e_{22} \end{bmatrix}$$

Where

W is the weight factor matrix and w_{ij} is the element of it.

Generally, the amplitude and phase angle of 1st and 3rd harmonic are much more significant than the rest of orders. Therefore, w_{1j} and w_{2j} are normally greater than others. In addition, the amplitude measurement is much more stable than phase angle measurement, so w_{i1} is set twice almost larger than w_{i2} .

Finally, a single value, named as **error index**, is defined and used to describe the similarity between the event signature and signature from database. Taking all ten elements in error signatures and weighting factor matrix into account, the definition of error index is shown as follows:

$$EI=\sum e_{I\_(2k-1)} * w_{k1} + \sum e_{\phi\_(2k-1)} * w_{k2} = e_{11} + e_{22} \quad , \quad k=1,2,3,4,5 \qquad (7.1)$$

Where EI is the error index.

Comparing the event signature with each appliance signature in the database, a series of error index can be computed. Among those error indexes, the minimum one indicates that event signature is closest to this appliance signature. Hence, the appliance is selected as **most possible appliance**. The overall flow chart of signature matching is illustrated as Figure 7.2 shows.

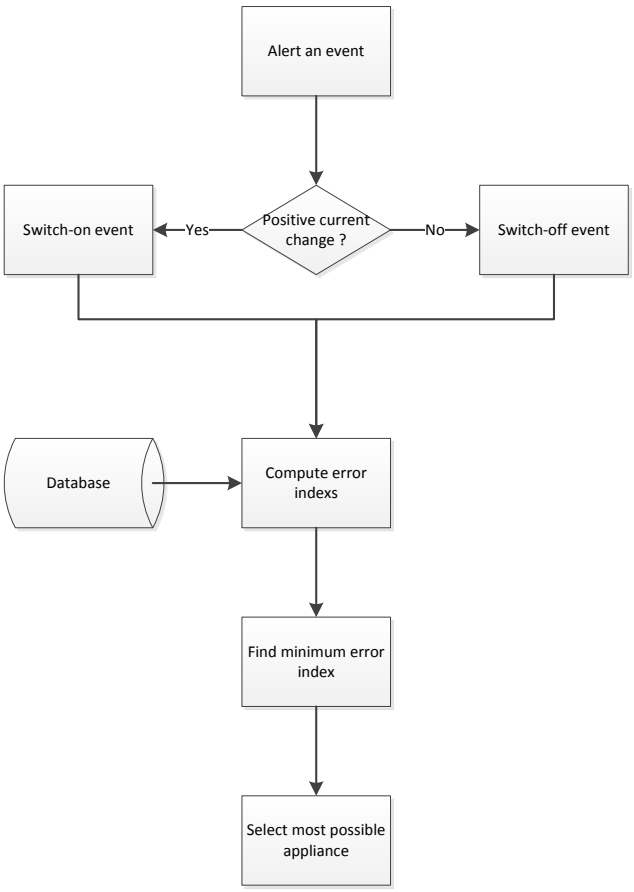

Figure 7.2 Flow chart of error computation & signature matching

7.1.3 Appliance Recognition & Classification

To begin with, the signature of most possible appliance from last stage is checked with event signature again. The error signature between them will be compared with tolerance of the most possible appliance. If the error is within the tolerance, the event is identified as the state change of the most possible appliance. The exact state change, either switch-on or switch-off,

has been decided in last stage already. Therefore, the on-off state change of whole residential load can be identified and monitored.

On the other hand, if the error signature between the signature of most possible appliance and event signature is greater than the tolerance, the appliance which changed state is considered as a **new appliance** and hence the event signature is regarded as the signature of the new appliance. In order to classify the new appliance, the HFR and FAD of this new appliance are then calculated by applying equation (6.20) and (6.21) as Figure 7.3 illustrates. Considering the two processes discussed above, the entire flow chart of appliance recognition & classification is shown as follows:

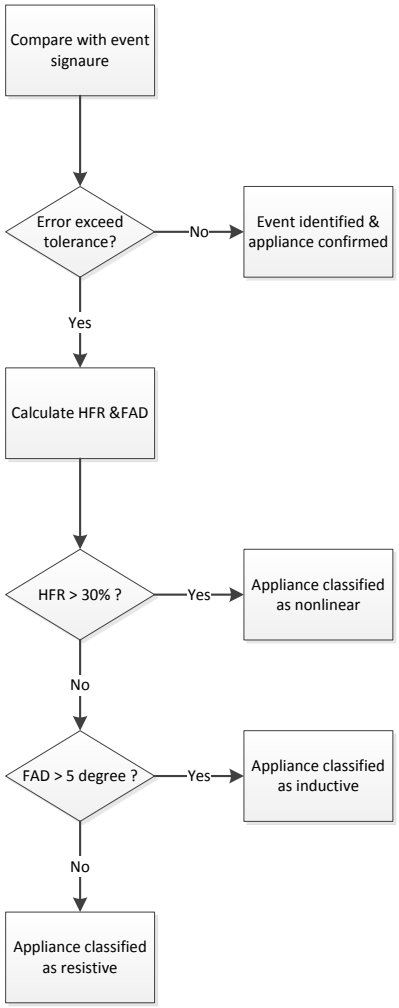

Figure 7.3 Flow chart of appliance recognition and classification

7.2 Implementation of Proposed Non-Intrusive Loading Monitoring Algorithm

A test rig is established based the proposed algorithm and it includes hardware design as well as the algorithm implemented in software. Hardware used in this test rigs mainly is to acquire voltage and current measurements and so it involves data acquisition system and sensors. The software includes not only the non-intrusive load monitoring algorithm itself but also the user interfaces.

7.2.1 Hardware

To obtain the load signatures and operate the proposed algorithm in real time, a data acquisition system is required to measure the voltage and current values in high sampling frequency and then implement the every steps of the proposed algorithm including load signature calculation, event detection, and error computation and so on. The selected DAQ is the same as the test rig in Chapter 4, which is is the PXIe-1082 chassis with PXle-6358 multifunction DAQ board from National Instruments (NI).

Since the voltage of this test ranges from 220-240V, the voltage transducer selected is LV 25-P manufactured by LEM due to its excellent flexibility, accuracy, linearity and reliability. As for the current measurement, it is required to have not only extremely good accuracy to acquire the harmonics but also relatively large range from 0-20A. The selected current transducer is LTS 6-NP from LEM and it is configured with 0-19.2A measuring range.

The sensors are mounted on an external circuit board and then connected with the mains power and NI DAQ system. A socket extension lead is modified to achieve the connection between sensors and mains power. The configuration is shown as Figure 7.4. The plug can be directly plugged into the socket to draw power from mains and the appliances can be connected on the sockets. The voltage and total current are then measured and converted to

isolated low voltage analogue inputs (AIs). Finally, the AIs are acquired by NI DAQ system and utilised by the software.

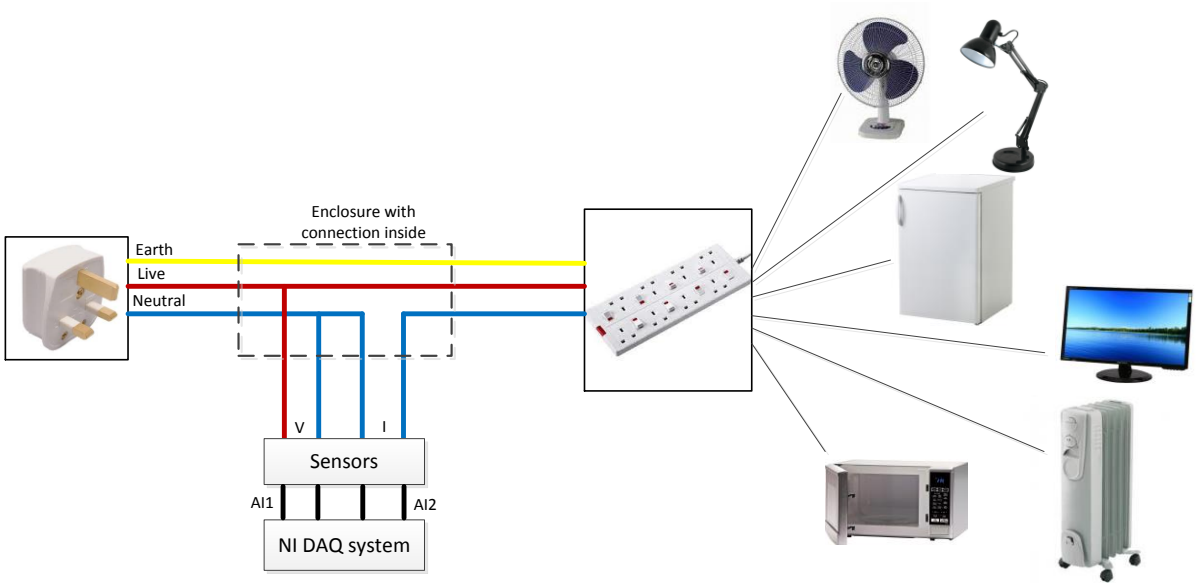

Figure 7.4 Connection of the test rig

7.2.2 Software

7.2.2.1 Programming in LabVIEW

LabVIEW, from NI, is selected as the software to implement the algorithm due to its full compatibility with NI data acquisition hardware. Firstly, the software follows every step of the flow charts discussed in last chapter to implement the major functionality of the algorithm. Secondly, it also sets up a user interface to display the plots and numerical numbers of all the involving parameters in real time, including raw voltage and current measurement, power values, harmonic contents and so on. Thirdly, it is able to save the measurement and the calculation of other important parameters at different frequency (10 kHz and 1 Hz) during processing. Fourthly, it illustrates the on-off states of all the appliances by using indicators and records all the events into an external file. Finally, it also involves a calibration control for user to tune the ratio of sensor if required.

The program is established based on a ‘Producer/Consumer Loops’ structure. It consists of one major producer loop and multiple consumer loops as it illustrated in Figure 7.5. Apart from those, the program also contains an initialisation process and its breakdown can be shown as follow:

- Initialisation: this part is out of all the loops. It basically initialises all the parameter, indexes and matrixes in the program and also involves the database of appliance signatures, tolerances, weight factor matrix and so on.
- Producer loop: this loop start with communicating and acquiring raw voltage and current measurement. On one hand, the program put all the raw measurement into a queue for data logging. On the other hand, it carries on processing the raw measurement. Power values calculation, FFT, harmonic analysis and signature computation are all executed and displayed in this loop. Finally, all the calculated results are again passed on another queue for load monitoring algorithm since the algorithm deals with signatures rather than raw measurement.
- Consumer loop 1: this part is set up purely for data logging purpose. It records the power values, signatures and voltage current RMS at 1 Hz different from the producer loop 10 kHz.
- Consumer loop 2: this loop receives the signatures of measured voltage and current in real time from produce loop and then implement the load monitoring algorithm, finally display the on-off states of all the appliances within the test rig.

7.2.2.2 User Interface

The user interface is designed to display the plots, values and necessary information and consists of three parts, namely controlled tabs, calibration & data logging control and numerical displays. The controlled tabs have four sub-tabs, which is described as follows:

- Display: this tab illustrates the date, time, on-off type and appliance of each event detected and the indicator for each appliance. Algorithm: this tab illustrates the intermediate values of algorithm, for instance, event signature, error signature, index of most possible appliance, database of signatures and signatures in buffer.

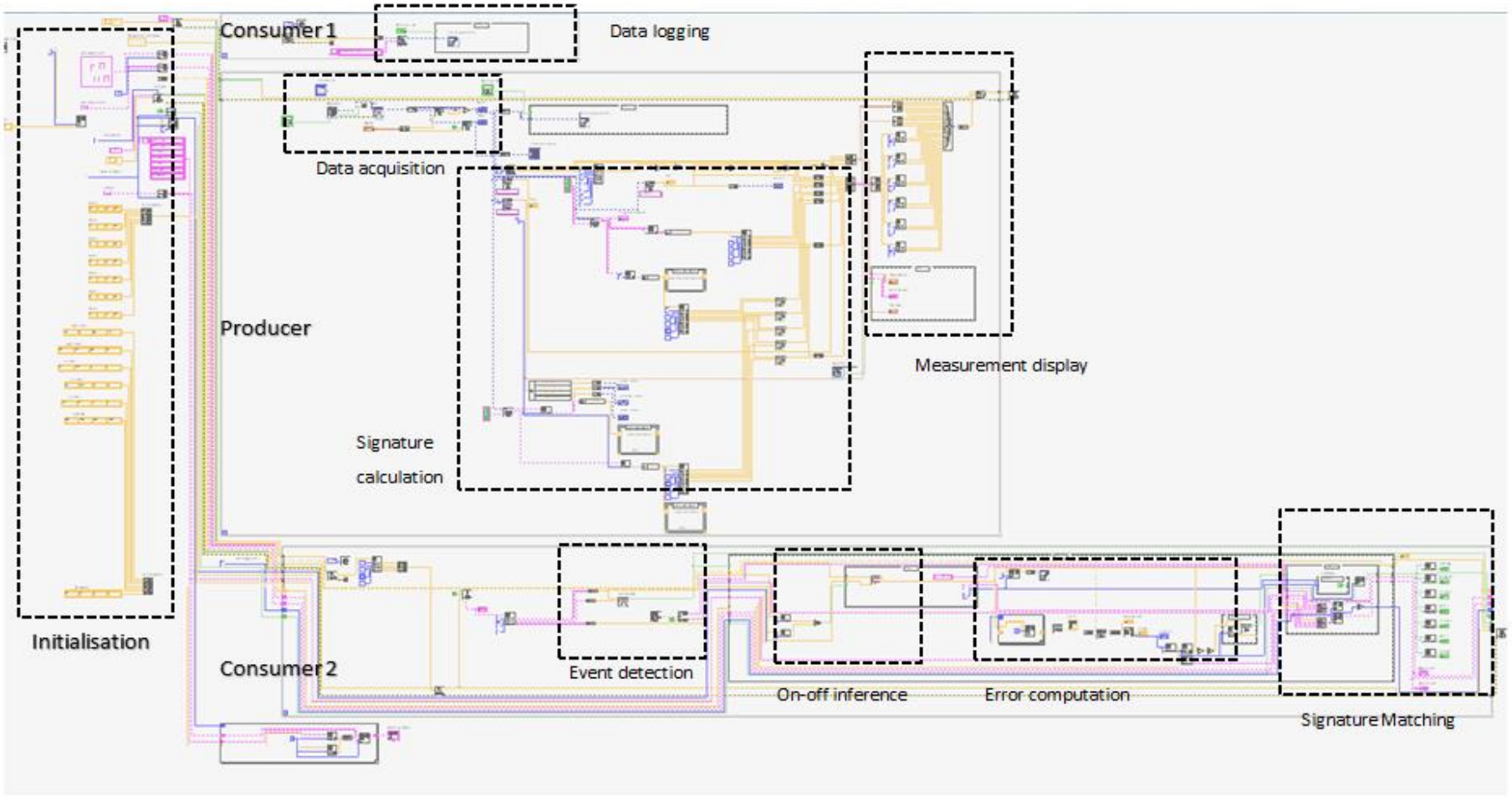

Figure 7.5 Program in Labview

- V&I waveforms: this tab illustrates the plots of voltage, current, current spectrum instantaneously.
- Power values: this tab illustrates the plots of active power, reactive power, and power factor against time.

The calibration & data logging part involves two numerical control for calibrating sensors and two buttons for data logging at different frequency. The numerical displays the V&I RMS values, power values, frequency and THD as well as the current harmonics. Figure 7.6 shows the user interface of the program.

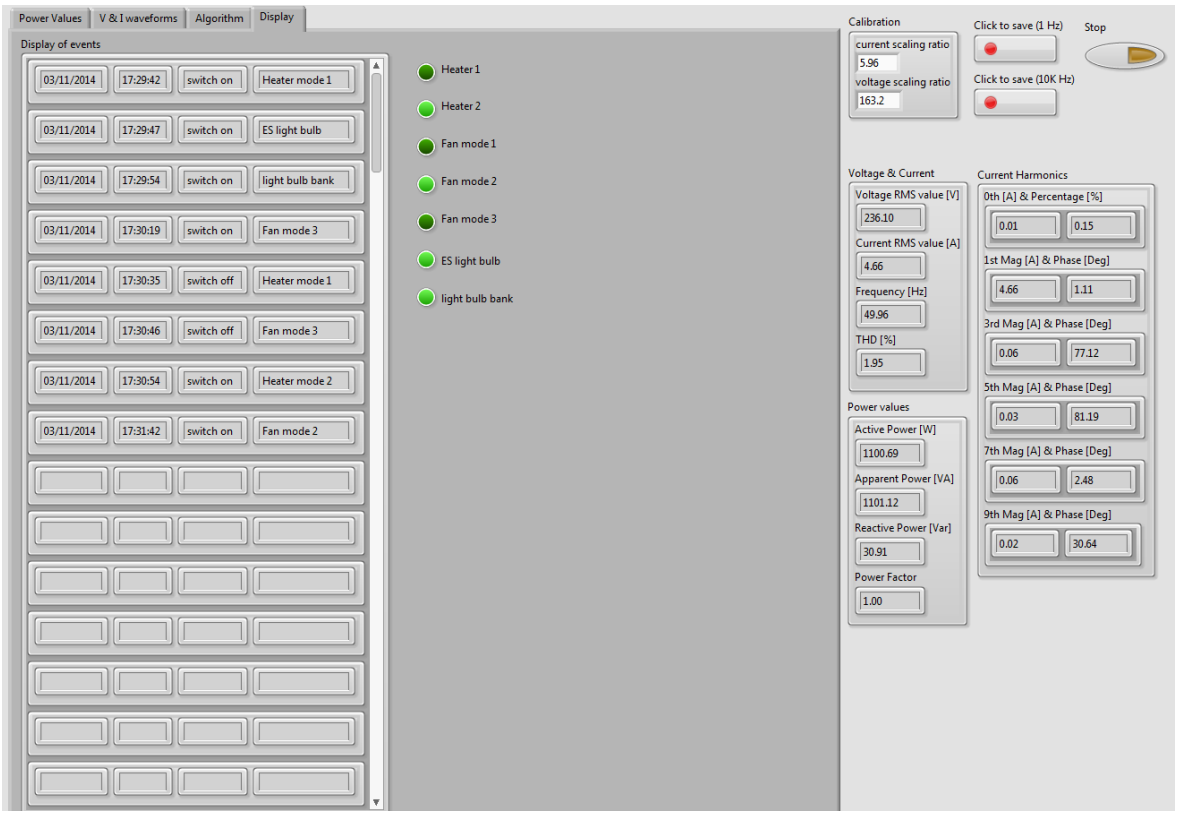

Figure 7.6 User interface with ‘display’ sub-tab shown

7.3 Algorithm Evaluation

In order to test the accuracy of the proposed algorithm, the whole system including both software and hardware is set up in the laboratory environment. For evaluation purpose, a set of appliance is selected to be monitored under the established system. The selected appliances are listed as Table7-1.

Table 7-1 List of appliances used for evaluation

Appliances	Mode	Power [W]	Type
Heater	Mode 1	657.1	Resistive
	Mode 2	971.1	Resistive
Fan	Mode 1	30.1	Inductive
	Mode 2	32.7	Inductive
	Mode 3	42.7	Inductive
ES light bulb	None	17.9	Non-linear
Fridge	Lighting	16.4	Resistive
	Operation	74.2	Inductive
Microwave	Lighting	24.7	Resistive
	Operation	1330.5	Non-linear
Monitor	None	25.7	Non-linear

As it shown in Table 7-1, 6 appliances with 11 working modes in total are included in the test environment. The selected appliances not only cover all typical types of loads, namely resistive, inductive and non-linear, but also drawn a wide range of power from 17.9W to 1330.5 W. It can be also noticed that some appliance consumes similar power, which could be problematic for traditional power value-based load monitoring algorithm.

The experiment is conducted during the day timing and all the appliances are expected to be switched on and operate at least once. As mentioned previously, the raw voltage and current measurement are sampled at 10 kHz and the other values, including RMS values, power values and load signatures are then calculated based on the measurement and recorded at 1 Hz. The software also logs the all events as well as the data and time of the events during the

operation. Finally, the event log is analysed and compared with the power plot to investigate the accuracy of algorithm.

One example of the event log created by the software is shown as Figure 7.7:

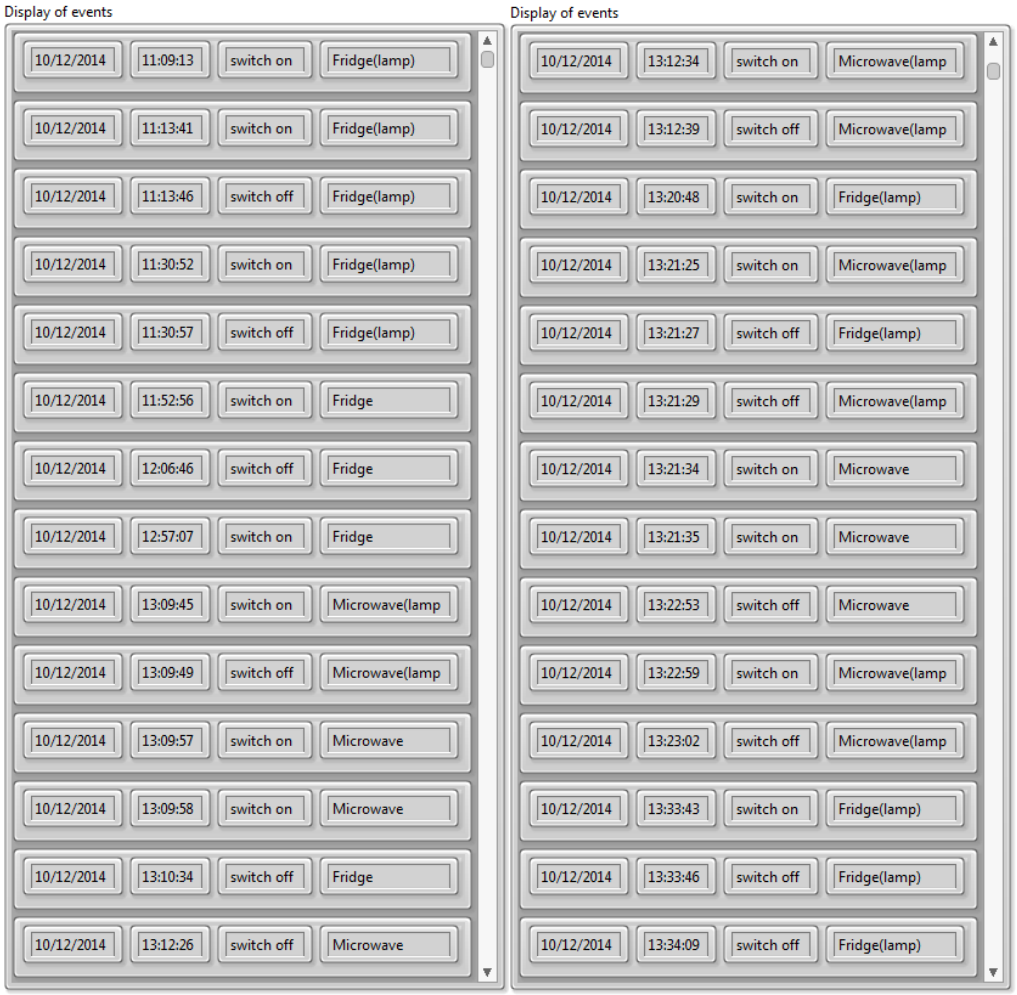

Figure 7.7 Event logs created by the software

As it shown in Figure 7.7, the data, time, identified event and appliances are recorded in sequence. Based on this record, the events on 10/12/2014 can be labelled on the power plot of the same day, which is shown as Figure 7.8. Although Figure 7.7 only displays the events in the morning, the power plot of both the morning and the afternoon are illustrated with the labels in Figure 7.8. The experiment results of individual appliance is shown in Table 7.2

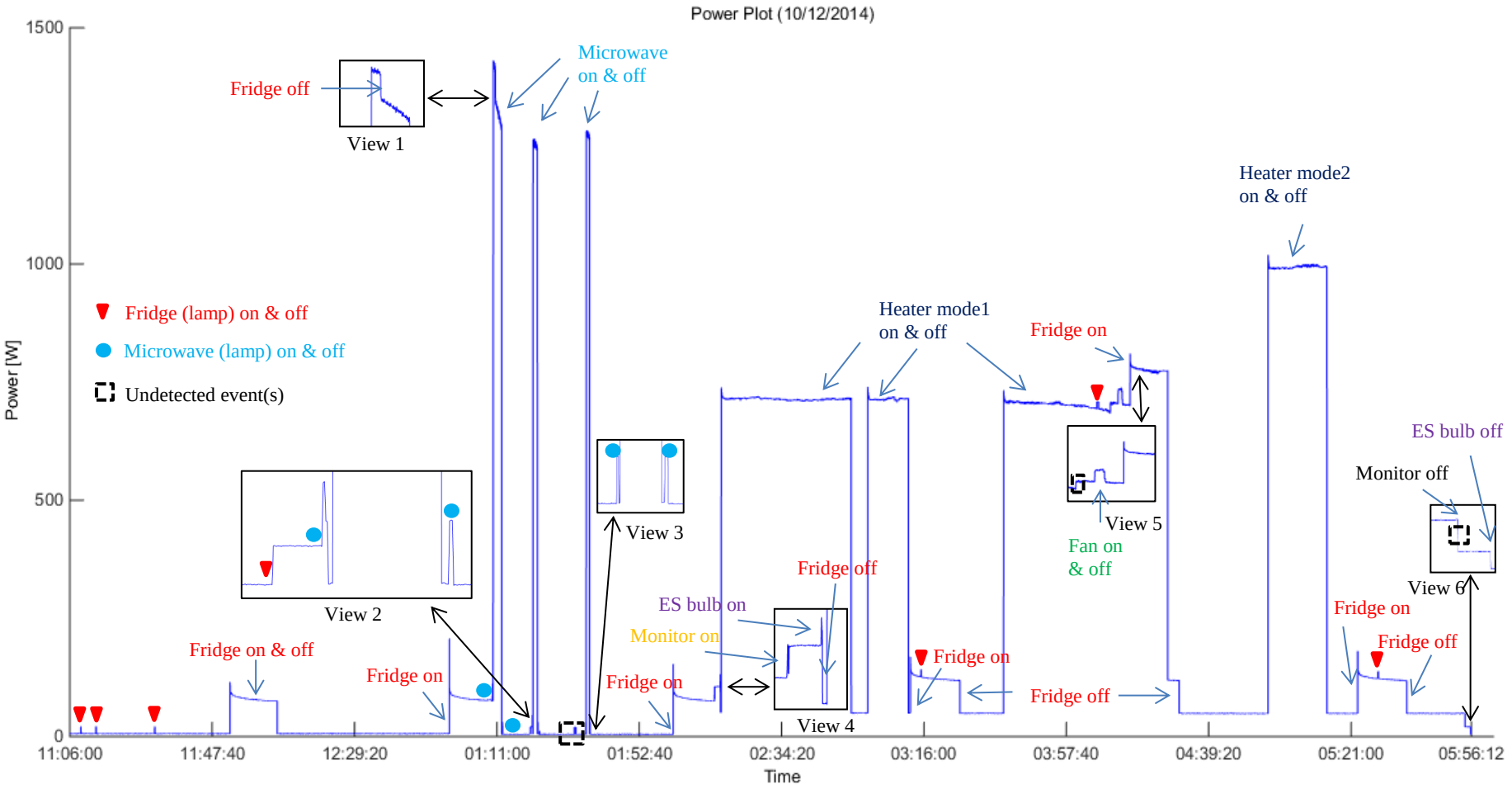

Figure 7.8 Power Plot with labelled events recorded by algorithm

Table 7-2 Experimental Results of Individual Appliances

Appliances	Mode	Total Events	Detected Events	Missed or Fault Events	Accuracy
Heater	Mode 1	6	6	0	100%
	Mode 2	2	2	0	100%
Fan	Mode 1	4	2	1	50%
ES light bulb	None	2	2	0	100%
Fridge	Lighting	14	13	1	92.8%
	Operation	12	12	0	100%
Microwave	Lighting	12	12	0	100%
	Operation	6	6	0	100%
Monitor	None	2	1	1	50%

As Figure 7.8 shows, the power plot starts from 11 am to 6 pm. To start with, the three events with high peak and very short time length which occurs around 1 pm can be noticed as events relating to microwave. It indicates that it is typically used around lunch time and the usage time of it is normally 1 min. Apart from that, the lamp in microwave is also associated with the operation of microwave. It is normally switched on and off for people to get food in and out shortly before and after the microwave operation. A typical of microwave cycle is shown in View 3 of Figure 7.8. It starts with an extremely short peak around 25 W (marked as blue circle), which represents the lamp switched on and off, then a one-minute operation of microwave is followed, finally another short peak indicates that the lamp is open and food is get out of the microwave.

Although it is also fitted with a lamp, the fridge doesn't work along with its lamp regularly as microwave because the compressing cycle of the fridge is independent with the lighting of the fridge. It can be noticed that the lamp of the fridge (small peak, marked as red triangle) is switched on and off randomly throughout the whole day while the compressing process starts periodically and lasts the same time length for each operation. View 2 is an interesting demonstration of activities relevant to both fridge and microwave. It can be noticed that the fridge is firstly open and then the microwave is open as well within several seconds, which

can be inferred that some food is taken out from fridge and put into the microwave. Both lamps of fridge and microwave are switched off shortly and then the microwave starts to heat the food. The results generated by the algorithm match the activities exactly in this scenario.

The monitor and ES light bulb are turned on around 2 pm in sequence and then turned off at the end of test around 6 pm. During this time period, the heater and fan are also switched on and operation from a while. In terms of the heater, there is a thermal protection mechanism to prevent from overheating, therefore it can be found that the operation of cannot last for long time, and a gap can be observed between two operations.

The 4 undetected events are marked as black rectangle in Figure 7.8 and they all consume power less than 30W. On the contrary, the appliances with large current draw can be identified perfectly. In real test, every appliance doesn't draw exactly same current all the time and the current variation range is different appliance from appliance. When multiple appliances in operation, the variation range becomes more unpredictable and the noise current may either cancel out or build up. When an event detected in this situation, the event signature is actually the combination of load signature and noise. It is possible that the event signature with this noise added exceeds the tolerance of the corresponding appliance, which fails the recognition. Compared to appliance with large current rating, the appliance drawing small current is much more likely to be affected by this noise build up by multiple appliances operation.

Above all, the evaluation of this algorithm is still very promising. 56 out of 60 events are successfully detected, which results in a 93.3% rate in this scenario. The same test also runs for another two days and it gives a 92.9% overall rate (92 out of 99). Considering the high accuracy and long running time, it can be concluded that the algorithm is able to monitor the loads in real time with high accuracy and robustness.

7.4 Case Studies

Some cases are studied to investigate the energy saving of different loads with and without voltage stabiliser (VS) through experiments. In the real experiments, the loads are assumed as fixed in one case and then different types and values of loads are looked into to demonstrate the energy saving can be made under different load conditions through installing a voltage stabiliser. One example of operation under a resistive load is shown as Figure 7.9.

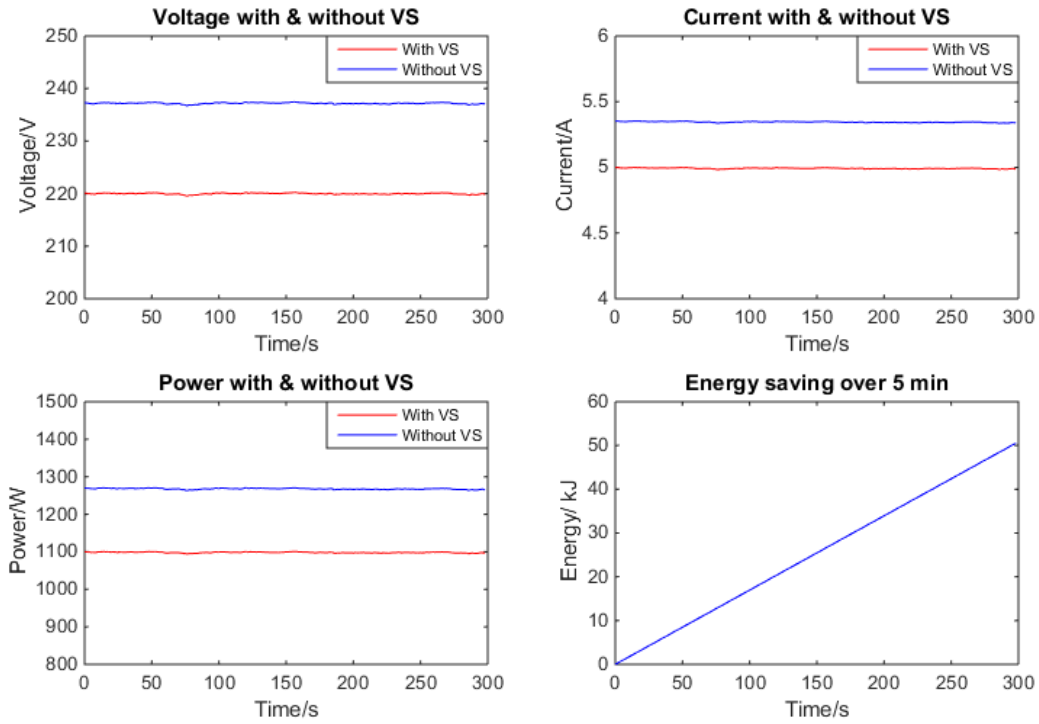

Figure 7.9 Experiment results of operation with and without voltage stabiliser under resistive load

It can be noticed that the voltage and current with voltage stabiliser both are lower than the situation without voltage stabiliser. Thus, the power is obviously smaller as well and it leads to energy saving as time accumulates. The amount of energy saving made varies as the load varies, basically the larger loads tends to results in more energy saving. In this particular case, the energy saving over 5 min is around 50.13KJ and the percentage energy saving is 13.3%, which is close to the simulation result 11.7%.

One example of operation under an inductive load is shown as Figure 7.10.

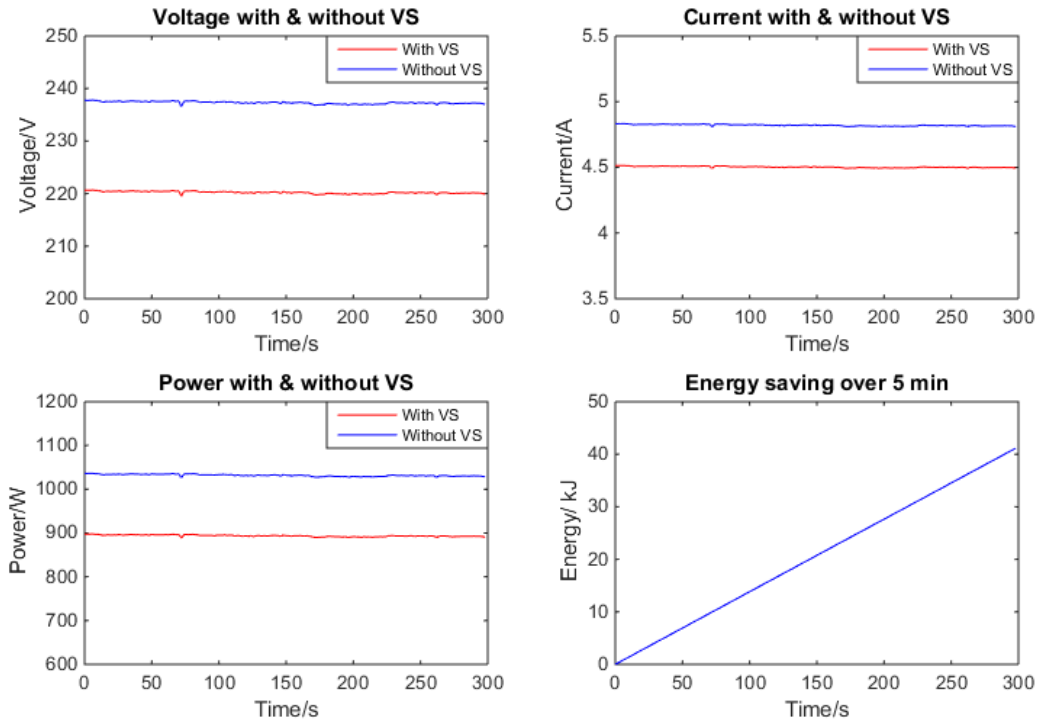

Figure 7.10 Experiment results of operation with and without voltage stabiliser under inductive load

In this case, the voltage, current and power of the operation with voltage stabiliser are all smaller as we expected. The total energy saving is 41.16KJ and the percentage saving is 13.4%.

One example of operation under a non-linear load is shown as Figure 7.11. As shown in the figure, the current with voltage stabiliser doesn't drop significantly although the voltage falls down to 220V. As a result, the power consumption of this operation with voltage stabiliser only slightly decreases compared with the power consumption without voltage stabiliser. The right bottom plot shows that there is only 6.85KJ energy saving during 5 min operation under non-linear load. The percentage energy saving in this operation is only 3.1% and is close to the simulation results which gives 5.90%. It can be concluded that the voltage stabiliser can make more energy savings for resistive load and inductive load over non-linear load.

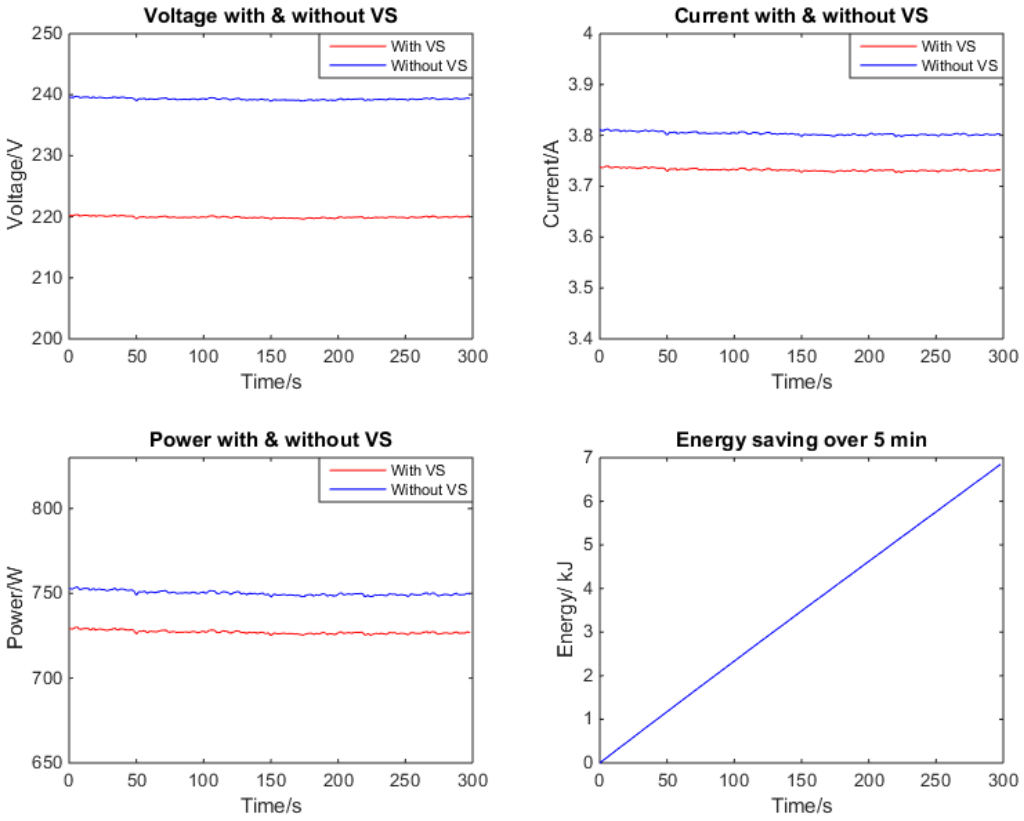

Figure 7.11 Experiment results of operation with and without voltage stabiliser under non-linear load

The observed, average annual electricity bill for all households monitored in Household Electricity Survey (2010-2011) was around £530 (Department of Energy & Climate Change 2013). The houses within the UK can be group as households without electric heating, with additional electric heating and with primary electrical heating. This three types of households has different electricity breakdown on different loads due to the different usage of electric heating. The relative contribution from the different loads is summarised in Figure 7.12 (Intertek 2012). In order to estimate the total energy saving can be made by voltage stabiliser, the different loads are grouped into three types of loads as we discussed in this work. Resistive loads include cooking, a part of lighting, heating and water heating, inductive loads include cold appliances, a part of lighting, washing, non-linear loads include audio-visual, ICT(Information and Communication Technology), a part of lighting. Therefore, resistive loads, inductive loads and non-linear loads account for approximately 46.1%, 32% and 21.9%

in a typical house with additional electric heating. Considering the different energy saving can be made with different type of loads, the expected energy saving of installing a voltage stabiliser is estimated as 11.09%.

	All households								
	Without electric heating			With additional electric heating			With primary electric heating		
	All days	Holidays	Workdays	All days	Holidays	Workdays	All days	Holidays	Workdays
Cold appliances	16.2%	15.9%	16.3%	13.4%	12.8%	13.6%	4.7%	5.0%	4.6%
Cooking	13.8%	14.1%	13.6%	11.7%	11.9%	11.5%	7.2%	8.3%	6.8%
Lighting	15.4%	14.3%	15.8%	10.0%	9.0%	10.3%	5.8%	6.4%	5.5%
Audiovisual	14.4%	14.5%	14.4%	10.4%	10.6%	10.2%	3.4%	3.2%	3.5%
ICT	6.1%	5.9%	6.1%	3.6%	3.5%	3.7%	2.6%	1.5%	3.0%
Washing/Drying	13.6%	14.7%	13.2%	10.7%	12.1%	10.0%	3.1%	3.1%	3.1%
Heating				22.5%	20.8%	23.0%	64.2%	59.1%	65.8%
Water heating	7.1%	7.0%	7.2%	4.0%	4.5%	3.8%	6.3%	7.6%	5.8%
Other	3.7%	3.6%	3.7%	5.8%	7.3%	5.1%	1.5%	1.0%	1.7%
Not known	9.7%	10.0%	9.8%	7.9%	7.4%	8.7%	1.2%	4.8%	0.2%

Figure 7.12 Relative contribution from the different loads in domestic house

The estimated energy saving is affected by several factors. As shown in Figure 7.12, the electricity breakdown of a house largely depends on the heating, which then lead to different proportion of resistive loads in it. Therefore, a house with more electrical heating may potentially make more savings through installation of voltage stabiliser. The mains voltage level also has effect on the energy saving. The higher mains voltage is the more energy saving can be made by voltage stabiliser.

On the other hand, non-intrusive load monitoring also can increase the chances of make potential saving in a house, it helps people making saving more easily. Ultimately, the saving is made via the change of behaviour, for instance, switch off the lighting when not used, switch off some standby appliances, and shift the usage of some appliance in off peak time.

The estimated saving by applying non-intrusive load monitoring is estimated as 12% in (Ehrhardt-martinez & Donnelly 2010).

7.5 Summary

To start with, the chapter explains the non-intrusive load monitoring algorithm in detail. This proposed algorithm takes advantages of the signatures introduced in chapter 5 to infer the on-off working states of individual appliances in real-time. It consists of several stages, namely data acquisition, event detection, error computation, signature matching, appliance recognition and classification.

Next, the algorithm is implemented in LabVIEW with the necessary data acquisition system as hardware. An interface is also established in LabVIEW to display the numeric measurement, voltage & current waveforms and the working states of the appliances involved. Apart from that, the measurement and output of the proposed algorithm are recorded for analysis in the future.

Finally, a series of experiment is carried out to evaluate the proposed algorithm. 6 appliances with 11 working modes are put into the test rig and tested for whole day time. The results are analysed in this chapter and it shows that the on-off working states of those appliances can be monitored by the proposed algorithm with accuracy higher than 92.9% and the algorithm is robust enough for long running time.

Chapter 8 Conclusion, Limitations and Future work

This chapter concludes the entire work of this thesis. It summaries both the new technology for voltage optimisation and non-intrusive load monitoring in household, point out the limitations of this work and then indicates directions for future work.

8.1 Conclusions

In this work, a topology of step-up and step-down AC voltage stabiliser is proposed. The mathematical model of the proposed voltage stabiliser is established and verified with the circuit model through simulation in MATLAB/Simulink and is proved to be accurate with error no greater than 1.12%. A control strategy based on PI controller is designed to stabilise the voltage level. The simulation results and experiment results shows that the proposed voltage stabiliser is able to stabilise the voltage in household with the disturbance from mains input and load current.

After introducing a fictive axis, dq transformation is applied to mathematical model of the proposed voltage stabiliser to linearize the model in dq rotating reference frame hence the controller can be design analytically. A LQR control with integral feedback is designed to regulate the voltage in the presence of input voltage variation and load disturbance. The control strategy is then simulated in Matlab/Simulink and the results concludes that the designed LQR has better performance in terms of response speed compared with PI controller in last chapter.

An algorithm to estimate the power saving by installing a voltage stabiliser in domestic house is presented and discussed based on theoretical analysis. Then the algorithm is verified through experiments with different types of loads. The experiments results shows that the

algorithm is able to estimate the saving accurately with less than 1% error over all range of tests up to 30A.

This work also introduce a new load signature for non-intrusive load monitoring. This proposed signature is not only unique and easy to be recognised but also reflects the features of the loads. Based on this new signature, an event driven algorithm is developed to monitor the operation of individual appliances by using mathematic operation between multiple load signatures. The algorithm is then implemented in LabVIEW and a test rig involving different appliances has been set up to evaluate it. The experiment results shows that the proposed algorithm is able to monitor the operation states of individual appliances involved in the test rig by using the aggregated measurement of voltage and current only with accuracy higher than 94.1%.

8.2 Limitations

Although the experiments results mentioned in previous section imply that the proposed step up/down voltage stabiliser, power saving algorithm and non-intrusive loading monitoring algorithm have been all deemed to be doable and successfully applied, it is still necessary to analyse the scenarios which are less successful. Therefore, several limitations are discussed in this section, which is also used to indicate the directions of the future work in the following part.

In terms of the proposed step up/down voltage stabiliser with close loop control, although both the simulation and experiment results shows that it works perfectly in both step up and step down mode with precise steady state value and rapid control, there still exists some scenario which cause problems in real application. When the input voltage varies around the default reference value, the proposed voltage stabiliser may change between step up and step

down modes quiet frequently. The operation mode is controlled by relay, typically an electromechanically relay with 5-15 ms switching time. The frequent mode switching of the voltage optimisation unit will cause the relay clicking on and off frequently as well, which will not only results in massive noises but also affect the operations of the appliances connected with the voltage optimisation unit.

As for the non-intrusive monitoring algorithm, one of the limitations is that the proposed algorithm is less effective for identifying appliances with multiple states consuming different power when being switched on and off. For instance, the monitor used in the test rig (Section 6.3) displays a default screen (showing the brand name) initially for around 1s and then starts the normal operation when switched on. The current drawn in this case normally experiences a small peak around 1s and then rises up again to maintain the normal operation level. Since the proposed algorithm is event-driven, multiple events will be detected in this switching on process, which would be problematic for appliance recognition. The current solution is that the most significant event among them is picked up as the sign of switching on the monitor. Although it can still achieve the accuracy of identifying monitor over 80%, it can be concluded that the proposed algorithm is less robust when recognising appliances with multiple states when being switched on and off.

Another potential limitation of the proposed non-intrusive load monitoring algorithm is that the accuracy of identifying appliances with low current consumptions (e.g. ES light bulb, fridge lighting) is compromised when several appliances with large current consumptions (e.g. heater, microwave) connected into the domestic house. The accuracy is getting worse if the current consumptions of those appliances varies significantly with long operating time (e.g. desktop PC, Laptop). An example of this scenario is that the accuracy of identifying an ES light bulb with a laptop is running is lower compared with it without the laptop running. The

current drawn by a laptop is always fluctuating within a certain range, which is around 0.04A for both fundamental and 3rd harmonic components. When turning on an ES light bulb under this condition, the event signature will have an error around 0.04A for the corresponding harmonic components. Since the ES light bulb only consumes 0.07 A as fundamental and 0.06A as 3rd harmonic, it is possible to mismatch or fail when the 0.04 A variation caused by the operation of laptop added together. The experiment results shows that the accuracy for identifying a same ES light bulb drops around 7% after a laptop connected in operation.

8.3 Future work

One of the potential future works on the proposed step up/down voltage stabiliser can be focused on advanced control strategy of the system, especially on how to control it switching between step up and step down modes. The limitation mentioned in previous section is mainly caused by the simple switching mechanism, which is comparing the input voltage with reference voltage to determine the operation mode. Therefore, the mode will change frequently if input voltage varies around reference voltage. One of the potential solutions is to set two reference values for different operation modes and take the crossing direction of input voltage with respect to the reference into consideration to determine if the mode should be changed. On the other hand, different relay can be selected to accomplish the task of switching between different modes. The default choice is electromechanical relay which has loud noise and long switching time and it somehow leads to bad performance of the whole system when input voltage varies around the reference voltage. Alternatively, solid state switches (e.g. MOSFET) can be a potential better choice as it has fast switching time and is suitable for low voltage appliance in this case. It is worth investigating the thermal performance, efficiency and reliability of the entire system with relay replaced by solid state switches in the future work.

In terms of the non-intrusive load monitoring algorithm, some limitations due to the event-based feature are discussed previously. It is possible to look into an algorithm combing proposed signature with other optimisation algorithm or statistical approach instead of event-based algorithm. Some mathematical optimisation method, such as integer programming (Suzuki et al. 2008), genetic algorithm (Leung et al. 2007) and dynamic programming (Baranski & Voss 2004a), can be applied to analyse the aggregated signature directly rather than the residue signature between two samples. It would be interesting to figure out how the proposed algorithm works along with sophisticated optimisation tools to monitor the on-off states of appliances. Another interesting challenge for extending this work would be apply the proposed signature to statistical modelling of each appliance, such as Hidden Markov Model (HMM)(Kim et al. 2011; Pattem 2012; Parson 2014), . HMM shows its strength on modelling appliance with multiple modes and is able to infer the working state sequence of appliance no matter how it changes its states during operation. Previously, only power values are modelled into HMM, which limits the accuracy of the algorithm. With the new signatures involving both current values and phase angles, it is very promising to improve the modelling work of difference appliances and hence increase the accuracy and robustness of the algorithm.

Reference

Akbar, M. & Khan, Z.A., 2007. Modified nonintrusive appliance load monitoring for nonlinear devices. In *INMIC2007 - 11th IEEE International Multitopic Conference*. Available at: http://ieeexplore.ieee.org/xpls/abs_all.jsp?arnumber=192069 [Accessed October 31, 2014].

Anderson, K. et al., 2012. BLUED : A Fully Labeled Public Dataset for Event-Based Non-Intrusive Load Monitoring Research. In *Proceedings of the 2nd KDD Workshop on Data Mining Applications in Sustainability (SustKDD)*. pp. 1 – 5. Available at: http://inferlab.org/wp-content/uploads/2012/08/2012_anderson_SustKDD.pdf [Accessed October 14, 2013].

Antoniewicz, P. & Kazmierkowski, M., 2006. Predictive direct power control of three phase boost rectifier. *Bull. Polisch Acad. Sci*, 54(3), pp.287–292. Available at: http://bulletin.pan.pl/(54-3)287.pdf?origin=publication_detail.

Arrillaga, J., Watson, N. & Chen, S., 2000. *Power system quality assessment*, New York: WILEY.

Baranski, M. & Voss, J., 2004a. Detecting patterns of appliances from total load data using a dynamic programming approach. In *Proceedings - Fourth IEEE International Conference on Data Mining, ICDM 2004*. Ieee, pp. 327–330. Available at: http://ieeexplore.ieee.org/lpdocs/epic03/wrapper.htm?arnumber=1410302 [Accessed January 5, 2015].

Baranski, M. & Voss, J., 2004b. Genetic algorithm for pattern detection in NIALM systems. *Conference Proceedings - IEEE International Conference on Systems, Man and Cybernetics*, 4(2), pp.3462–3468.

Baranski, M. & Voss, J., 2003. Non-intrusive appliance load monitoring based on an optical sensor. *2003 IEEE Bologna Power Tech Conference Proceedings,*, 4, pp.267–274.

Bijker, A.J., Xia, X. & Zhang, J., 2009. Active power residential non-intrusive appliance load monitoring system. In *IEEE AFRICON Conference*. pp. 1–6. Available at: http://ieeexplore.ieee.org/xpls/abs_all.jsp?arnumber=5308244 [Accessed October 14, 2013].

Burch, R. et al., 2003. Impact of aggregate linear load modeling on harmonic analysis: A comparison of common practice and analytical models. *IEEE Transactions on Power Delivery*, 18(2), pp.625–630. Available at: http://ieeexplore.ieee.org/xpls/abs_all.jsp?arnumber=1193887 [Accessed October 31, 2014].

Byun, J. et al., 2013. Intelligent household LED lighting system considering energy efficiency and user satisfaction. *IEEE Transactions on Consumer Electronics*, 59(1), pp.70–76.

Carmel, C., Shrimali, G. & Albert, A., 2013. *Is Disaggregation: the holy grail of energy efficiency*,

Chan, W.L., So, A.T.P. & Lai, L.L., 2000. Harmonics load signature recognition by wavelets transforms. *DRPT2000. International Conference on Electric Utility Deregulation and Restructuring and Power Technologies. Proceedings (Cat. No.00EX382)*, (April), pp.4–7.

Climate Change ACT, 2008. *Climate Change Act 2008*, Available at: http://www.legislation.gov.uk/ukpga/2008/27/contents.

Cole, a. & Albicki, A., 2000. Nonintrusive identification of electrical loads in a three-phase environment based on harmonic content. *Proceedings of the 17th IEEE Instrumentation and Measurement Technology Conference*, 1(7), pp.24–29.

Cole, a. I. & Albicki, A., 1998a. Algorithm for nonintrusive identification of residential appliances. *ISCAS '98. Proceedings of the 1998 IEEE International Symposium on Circuits and Systems*, 3, pp.338–341.

Cole, a. I. & Albicki, A., 1998b. Data extraction for effective non-intrusive identification of residential power loads. *IMTC/98 Conference Proceedings. IEEE Instrumentation and Measurement Technology Conference*, 2, pp.812–815.

Cook, P., 2002. *Commentary on IEE Wiring Regulations* 16th Editi., The Institution of Electrical Engineers.

Cortes, P. et al., 2008. Predictive Control in Power Electronics and Drives. *IEEE Transactions on Industrial Electronics*, 55(12), pp.4312–4324. Available at: http://ieeexplore.ieee.org/xpls/abs_all.jsp?arnumber=4663816 [Accessed March 25, 2014].

Department of Energy & Climate Change, 2013. housing energy fact file.

Djokić, S.Ž. et al., 2005. Sensitivity of personal computers to voltage sags and short interruptions. *IEEE Transactions on Power Delivery*, 20(1), pp.375–383. Available at: http://ieeexplore.ieee.org/xpls/abs_all.jsp?arnumber=1375117 [Accessed September 9, 2014].

Ehrhardt-martinez, A.K. & Donnelly, K. a, 2010. Advanced Metering Initiatives and Residential Feedback Programs : A Meta-Review for Household Electricity-Saving Opportunities. *Energy*, 123(6), p.128. Available at: http://scholar.google.com/scholar?hl=en&btnG=Search&q=intitle:Advanced+Metering+Initiatives+and+Residential+Feedback+Programs+:+A+Meta-Review+for+Household+Electricity-Saving+Opportunities#0.

Engelen, K. et al., 2006. The feasibility of small-scale residential DC distribution systems. *IECON Proceedings (Industrial Electronics Conference)*, pp.2618–2623.

Enjeti, P. & Choi, S., 1993. An approach to realize higher power PWM AC controller. *Proceedings Eighth Annual Applied Power Electronics Conference and Exposition,*,

pp.323–327. Available at: http://ieeexplore.ieee.org/xpls/abs_all.jsp?arnumber=290613 [Accessed October 14, 2013].

Farinaccio, L. & Zmeureany, R., 1999. Using a pattern recognition approach to disaggregate the toal electrical consumption in a house into the major end-uses. *Energy and Buildings*. Available at: http://www.sciencedirect.com/science/article/pii/S0378778899000079 [Accessed January 14, 2015].

Felce, A., Matas, G. & Silva, Y. Da, 2004. Voltage sag analysis and solution for an industrial plant with embedded induction motors. *Conference Record of the 2004 IEEE Industry Applications Conference, 2004. 39th IAS Annual Meeting.*, 4. Available at: http://ieeexplore.ieee.org/xpls/abs_all.jsp?arnumber=1348838 [Accessed September 9, 2014].

Figueiredo, M.B., De Almeida, A. & Ribeiro, B., 2011. An experimental study on electrical signature identification of non-intrusive load monitoring (NILM) systems. In *Lecture Notes in Computer Science*. pp. 31–40.

Garbesi, K. et al., 2011. Optimizing energy savings from“ Direct-DC” in US residential buildings. , (October). Available at: http://scholarworks.sjsu.edu/etd_theses/4078/.

Golestan, S. et al., 2011. A D-Q synchronous frame controller for single-phase inverters. *International Review on Modelling and Simulations*, 4(1), pp.42–54.

Gupta, S., Reynolds, M.S. & Patel, S.N., 2010. ElectriSense. In *Proceedings of the 12th ACM international conference on Ubiquitous computing*. p. 139. Available at: http://portal.acm.org/citation.cfm?id=1864375\nhttp://portal.acm.org/citation.cfm?doid=1864349.1864375.

H. Kim et al., 2011. Unsupervised Disaggregation of Low Frequency Power Measurements. In *Proceedings of the SIAM Conference on Data Mining*. pp. 747–758. Available at: http://www.cs.uiuc.edu/homes/hanj/pdf/sdm11_hkim.pdf.

Hart, G.W., 1992. Nonintrusive appliance load monitoring. *Proceedings of the IEEE*, 80(12), pp.1870–1891. Available at: http://ieeexplore.ieee.org/xpls/abs_all.jsp?arnumber=192069 [Accessed October 31, 2014].

Hart, G.W., Kern, J. & Edward, C., 1985. Digital AC Monitor.

Hassan, T., Javed, F. & Arshad, N., 2014. An Empirical Investigation of V-I Trajectory Based Load Signatures for Non-Intrusive Load Monitoring. *IEEE Transactions on Smart Grid*, 5(2), pp.870–878. Available at: http://ieeexplore.ieee.org/lpdocs/epic03/wrapper.htm?arnumber=6575197.

Hietpas, S.M. & Naden, M., 2000. Automatic voltage regulator using an AC voltage-voltage converter. *IEEE Transactions on Industry Applications*, 36(1), pp.33–38. Available at: http://ieeexplore.ieee.org/xpls/abs_all.jsp?arnumber=821793 [Accessed March 18, 2014].

Hunt, B.J., 2013. *Voltage optimisation*,

Intertek, 2012. *Household Electricity Survey A study of domestic electrical product usage*,

Ito, M. et al., 2004. A method of appliance detection based on features of power waveform. In *Proceedings - International Symposium on Applications and the Internet*. pp. 291–294. Available at: http://ieeexplore.ieee.org/xpls/abs_all.jsp?arnumber=1266131 [Accessed October 14, 2013].

Jang, D.H. & Choe, G.H., 1998. Step-up/down AC voltage regulator using transformer with tap changer and PWM AC chopper. *IEEE Transactions on Industrial Electronics*, 45(6), pp.905–911. Available at: http://ieeexplore.ieee.org/xpls/abs_all.jsp?arnumber=735334 [Accessed March 18, 2014].

Jie, Z. et al., 2008. Research on AC chopper power module with module parallel control. In *Conference Proceedings - IEEE Applied Power Electronics Conference and Exposition - APEC*. pp. 1324–1327. Available at: http://ieeexplore.ieee.org/xpls/abs_all.jsp?arnumber=4522894 [Accessed October 15, 2013].

Jin, N. et al., 2009. Analysis and control of buck-boost chopper type AC voltage regulator. In *2009 IEEE 6th International Power Electronics and Motion Control Conference, IPEMC '09*. Ieee, pp. 1019–1023. Available at: http://ieeexplore.ieee.org/lpdocs/epic03/wrapper.htm?arnumber=5157534.

Jin, N., Jiang, S.X. & Cui, G.Z., 2012. AC chopper dynamic voltage swells restorer design. In *Conference Proceedings - 2012 IEEE 7th International Power Electronics and Motion Control Conference - ECCE Asia, IPEMC 2012*. pp. 269–273.

Kato, T. et al., 2009. Appliance recognition from electric current signals for information-energy integrated network in home environments. In *Lecture Notes in Computer Science*. pp. 150–157. Available at: http://link.springer.com/chapter/10.1007/978-3-642-02868-7_19 [Accessed October 14, 2013].

Khoei, A; Yuvarajan, S., 1988. Single-phase AC-AC converters using power MOSFETs. *Industrial Electronics, IEEE Transactions on*, 35(3), pp.442–443. Available at: http://scholar.google.com/scholar?hl=en&btnG=Search&q=intitle:No+Title#0 [Accessed September 27, 2014].

Kim, H. et al., 2011. Unsupervised Disaggregation of Low Frequency Power Measurements. *Proceedings of the 11th SIAM International Conference on Data Mining*, pp.747–758. Available at: http://epubs.siam.org/doi/abs/10.1137/1.9781611972818.64 [Accessed January 5, 2015].

Kim, J.H. et al., 1998. A PWM buck-boost ac chopper solving the commutation problem. *IEEE Transactions on Industrial Electronics*, 45(5), pp.832–835. Available at: http://www.ncbi.nlm.nih.gov/pubmed/24649985.

Kolter, J.Z. & Johnson, M.J., 2011. REDD : A Public Data Set for Energy Disaggregation Research. In *SustKDD workshop*. pp. 1–6. Available at:

http://users.cis.fiu.edu/~lzhen001/activities/KDD2011Program/workshops/WKS10/doc/SustKDD3.pdf [Accessed October 14, 2013].

Kouro, S. et al., 2009. Model Predictive Control-A Simple and Powerful Method to Control Power Converters. *Industrial Electronics, IEEE Transactions on*, 56(6), pp.1826–1838. Available at: http://ieeexplore.ieee.org/xpls/abs_all.jsp?arnumber=4682711 [Accessed April 1, 2014].

Kwon, B., Min, B. & Kim, J., 1996. Novel topologies of AC choppers. *IEE Proceedings - Electric Power Applications*, 143(4), p.323. Available at: http://digital-library.theiet.org/content/journals/10.1049/ip-epa_19960374 [Accessed October 17, 2013].

Kwon, B.H. et al., 2002. Novel line conditioner with voltage up/down capability. *IEEE Transactions on Industrial Electronics*, 49(5), pp.1110–1119.

Lam, H.Y., Fung, G.S.K. & Lee, W.K., 2007. A novel method to construct taxonomy electrical appliances based on load signatures. *IEEE Transactions on Consumer Electronics*, 53(2), pp.653–660. Available at: http://ieeexplore.ieee.org/xpls/abs_all.jsp?arnumber=4266955 [Accessed October 31, 2014].

Laughman, C. et al., 2003. Power signature analysis. *IEEE Power and Energy Magazine*, 1(2), pp.56–63. Available at: http://ieeexplore.ieee.org/xpls/abs_all.jsp?arnumber=1192027 [Accessed October 14, 2013].

Lee, W.K. et al., 2004. Exploration on Load Signatures. In *International Conference on Electrical Engineering (ICEE)*. pp. 1–5. Available at: http://www.icee-con.org/papers/2004/725.pdf [Accessed October 14, 2013].

Leeb, S.B., Shaw, S.R. & Kirtley, J.L., 1995. Transient event detection in spectral envelope estimates for nonintrusive load monitoring. *IEEE Transactions on Power Delivery*, 10(3), pp.1200–1210.

Leung, S., Ng, S. & Cheng, W., 2007. Identifying appliances using load signatures and genetic algorithms. *International Conference on Electrical Engineering*, pp.1–5. Available at: http://www.icee-con.org/papers/2007/Oral_Poster Papers/01/ICEE-031.pdf [Accessed October 8, 2013].

Li, J., West, S. & Platt, G., 2012. Power decomposition based on SVM regression. *Modelling, Identification Control (ICMIC), 2012 Proceedings of International Conference on*, pp.1195–1199.

Liang, J. et al., 2010. Load Signature Study—Part I: Basic Concept, Structure, and Methodology. *IEEE Transactions on Power Delivery*, 25(2), pp.551–560. Available at: http://ieeexplore.ieee.org/lpdocs/epic03/wrapper.htm?arnumber=5337912.

Liu, H. & Wang, J., 2012. Analysis and control of a single phase AC chopper in series connection with an auto-transformer. *International Conference on Automation and Computing (ICAC)*, (September), pp.2–7. Available at:

http://ieeexplore.ieee.org/xpls/abs_all.jsp?arnumber=6330531 [Accessed October 14, 2013].

Makonin, S. et al., 2013. AMPds: A public dataset for load disaggregation and eco-feedback research. In *2013 IEEE Electrical Power and Energy Conference, EPEC 2013*. pp. 1–6. Available at: http://ampds.org/makonin2013ampds.pdf [Accessed January 14, 2014].

Marceau, M.L. & Zmeureanu, R., 2000. Nonintrusive load disaggregation computer program to estimate the energy consumption of major end uses in residential buildings. *Energy Conversion and Management*, 41(13), pp.1389–1403. Available at: http://linkinghub.elsevier.com/retrieve/pii/S0196890499001739.

Matthews, H.S. et al., 2008. Automatically Disaggregating the Total Electrical Load in Residential Buildings: a Profile of the Required Solution. *International Workshop on Intelligent Computing in Engineering*, pp.381–389. Available at: http://www.marioberges.com/pubs/2008_matthews_eg-ice.pdf.

Miranda, H. et al., 2009. Predictive Torque Control of Induction Machines Based on State-Space Models. *IEEE Transactions on Industrial Electronics*, 56(6), pp.1916–1924.

Miranda, U. a., Rolim, L.G.B. & Aredes, M., 2005. A DQ Synchronous Reference Frame Current Control for Single-Phase Converters. *IEEE 36th Conference on Power Electronics Specialists, 2005.*, pp.1377–1381.

Mueller, J. a. et al., 2014. Hidden Markov models for nonintrusive appliance load monitoring. *2014 North American Power Symposium (NAPS)*, pp.1–6. Available at: http://ieeexplore.ieee.org/lpdocs/epic03/wrapper.htm?arnumber=6965464.

Nan, J. et al., 2010. Analysis and control of two switches AC chopper voltage regulator. *WSEAS Transactions on Circuits and Systems*, 9(4), pp.208–217. Available at: http://www.wseas.us/e-library/transactions/circuits/2010/42-297.pdf [Accessed October 14, 2013].

Norford, L.K. & Leeb, S.B., 1996. Non-intrusive electrical load monitoring in commercial buildings based on steady-state and transient load-detection algorithms. *Energy and Buildings*, 24(1), pp.51–64. Available at: http://linkinghub.elsevier.com/retrieve/pii/0378778895009582.

Oliveria, T.R. de, Bolzon, A.S. & Donoso-Garcia, P.F., 2014. Grounding and safety considerations for residential DC microgrids. In *Industrial Electronics Society, IECON 2014*. pp. 5526 – 5532.

Park, S. et al., 2010. Concurrent simulation platform for energy-aware smart metering systems. *IEEE Transactions on Consumer Electronics*, 56(3), pp.1918–1926.

Parson, O., 2014. *Unsupervised Training Methods for Non-intrusive Appliance Load Monitoring from Smart Meter Data*. Available at: http://eprints.soton.ac.uk/364263/ [Accessed May 9, 2014].

Patel, S.N. et al., 2007. At the Flick of a Switch : Detecting and Classifying Unique Electrical Events on the Residential Power Line. In *UbiComp Computing*. pp. 271–288. Available at: http://link.springer.com/chapter/10.1007/978-3-540-74853-3_16 [Accessed October 8, 2013].

Pattem, S., 2012. Unsupervised Disaggregation for Non-intrusive Load Monitoring. *2012 11th International Conference on Machine Learning and Applications*, pp.515–520. Available at: http://ieeexplore.ieee.org/lpdocs/epic03/wrapper.htm?arnumber=6406788 [Accessed December 18, 2014].

Perez, M. a. et al., 2012. Predictive Control of AC–AC Modular Multilevel Converters. *IEEE Transactions on Industrial Electronics*, 59(7), pp.2832–2839. Available at: http://ieeexplore.ieee.org/lpdocs/epic03/wrapper.htm?arnumber=5875882.

Polmai, S. & Sugprajun, E., 2007. Experiment on Instantaneous Value Voltage Control of a Single-Phase AC Chopper. *2007 Power Conversion Conference - Nagoya*, (1), pp.77–82. Available at: http://ieeexplore.ieee.org/lpdocs/epic03/wrapper.htm?arnumber=4239141.

Powers, J.T., Margossian, B. & Smith, B. a., 1991. Using a rule-based algorithm to disaggregate end-use load profiles from premise-level data. *IEEE Computer Applications in Power*, 4(2), pp.42–47.

Preiss, R.F. & Warnock, V.J., 1978. Impact of Voltage Reduction on Energy and Demand. *IEEE Transactions on Power Apparatus and Systems*, (5), pp.1665 – 1671. Available at: http://ieeexplore.ieee.org/xpls/abs_all.jsp?arnumber=4181606 [Accessed January 14, 2015].

Rodríguez, J. et al., 2004. Predictive control of three-phase inverter. *Electronics Letters*, 40(9), p.561. Available at: http://discovery.ucl.ac.uk/45673/.

Rufer, a. et al., 2009. Vector control of single-phase voltage source converters based on Fictive Axis Emulation. *2009 IEEE Energy Conversion Congress and Exposition*, pp.2689–2695.

Ruzzelli, a. G. et al., 2010. Real-time recognition and profiling of appliances through a single electricity sensor. In *SECON 2010 - 2010 7th Annual IEEE Communications Society Conference on Sensor, Mesh and Ad Hoc Communications and Networks*.

Ryoo, H.S. et al., 2003. A Study on the Series Compensated AC Voltage Regulator using AC Chopper with Auxiliary Transformer. In *IECON Proceedings (Industrial Electronics Conference)*. pp. 2628–2633. Available at: http://ieeexplore.ieee.org/xpls/abs_all.jsp?arnumber=1280662 [Accessed October 14, 2013].

Saritha, B. & Jankiraman, P. a., 2006. Observer based current control of single-phase inverter in DQ rotating frame. *Power Electronic, Drives and Energy Systems*, 00, pp.1–5. Available at: http://ieeexplore.ieee.org/lpdocs/epic03/wrapper.htm?arnumber=4147922.

Shaw, S.R. et al., 2008. Nonintrusive Load Monitoring and Diagnostics in Power Systems. *Ieee Transactions On Instrumentation And Measurement*, 57(7), pp.1445–1454. Available at: http://ieeexplore.ieee.org/lpdocs/epic03/wrapper.htm?arnumber=4463663.

Soeiro, T.B. et al., 2012. High-efficiency line conditioners with enhanced performance for operation with non-linear loads. *IEEE Transactions on Industrial Electronics*, 59(1), pp.412–421. Available at: http://ieeexplore.ieee.org/xpls/abs_all.jsp?arnumber=5742695 [Accessed November 24, 2014].

Srinivasan, D., Ng, W.S. & Liew, a. C., 2006. Neural-network-based signature recognition for harmonic source identification. *IEEE Transactions on Power Delivery*, 21(1), pp.398–405.

Sultanem, F., 1991. Using appliance signatures for monitoring residential loads at meter panel level. *Power Delivery, IEEE Transactions on*, 6(4), pp.1380–1385. Available at: http://scholar.google.com/scholar?hl=en&btnG=Search&q=intitle:No+Title#0 [Accessed October 31, 2014].

Suzuki, K. et al., 2008. Nonintrusive appliance load monitoring based on integer programming. *2008 SICE Annual Conference*, pp.2742–2747. Available at: http://ieeexplore.ieee.org/lpdocs/epic03/wrapper.htm?arnumber=4655131.

Tomlinson, M. et al., 2011. Model predictive control of an AC-to-AC converter with input and output LC filter. *2011 6th IEEE Conference on Industrial Electronics and Applications*, pp.1233–1238. Available at: http://ieeexplore.ieee.org/lpdocs/epic03/wrapper.htm?arnumber=5975774.

Wang, X. et al., 2013. An online load identification algorithm for non-intrusive load monitoring in homes. *2013 IEEE Eighth International Conference on Intelligent Sensors, Sensor Networks and Information Processing*, pp.1–6. Available at: http://ieeexplore.ieee.org/lpdocs/epic03/wrapper.htm?arnumber=6529753.

Wang, Z. & Zheng, G., 2012. Residential appliances identification and monitoring by a nonintrusive method. *Smart Grid, IEEE Transactions on*, 3(1), pp.80–92. Available at: http://ieeexplore.ieee.org/xpls/abs_all.jsp?arnumber=6032723 [Accessed October 31, 2014].

Wong, Y.F. et al., 2013. Recent approaches to non-intrusive load monitoring techniques in residential settings. *2013 IEEE Computational Intelligence Applications in Smart Grid (CIASG)*, pp.73–79. Available at: http://ieeexplore.ieee.org/lpdocs/epic03/wrapper.htm?arnumber=6611501.

World Energy Council, 2013. *Word Energy Perspective: Energy Efficiency Techologies*,

Yabe, M., Sakanobe, K. & Kawakubo, M., 2005. High efficient motor drive technology for refrigerator. In *Proceedings - Fourth International Symposium on Environmentally Conscious Design and Inverse Manufacturing, Eco Design 2005*. pp. 708–709.

Yusoff, S. & Lillo, L. De, 2012. Predictive control of a direct AC/AC matrix converter for power supply applications. *6th IET International Conference on Power Electrionics*,

Machines and Drives (PEMD 2012), pp.1–6. Available at: http://ieeexplore.ieee.org/xpls/abs_all.jsp?arnumber=6242078 [Accessed March 30, 2014].

Zhang, R. et al., 2002. A grid simulator with control of single-phase power converters in D-Q rotating frame. *2002 IEEE 33rd Annual IEEE Power Electronics Specialists Conference*, 3(1431-1436).

Zia, T., Bruckner, D. & Zaidi, A., 2011. A hidden Markov model based procedure for identifying household electric loads. In *IECON Proceedings (Industrial Electronics Conference)*. pp. 3218–3223. Available at: http://ieeexplore.ieee.org/xpls/abs_all.jsp?arnumber=6119826 [Accessed November 7, 2013].

Zoha, A. et al., 2013. Low-power appliance monitoring using Factorial Hidden Markov Models. *2013 IEEE Eighth International Conference on Intelligent Sensors, Sensor Networks and Information Processing*, pp.527–532. Available at: http://ieeexplore.ieee.org/lpdocs/epic03/wrapper.htm?arnumber=6529845.